Department of Geomatics Engineering

Performance Evaluation of Sensor Combinations for Mobile Platoon Control

(URL: http://www.geomatics.ucalgary.ca/links/GradTheses.html)

by

Scott Alan Crawford

April 2005

UNIVERSITY OF
CALGARY

UNIVERSITY OF CALGARY

Performance Evaluation of Sensor Combinations for Mobile Platoon Control

by

Scott Alan Crawford

A THESIS

SUBMITTED TO THE FACULTY OF GRADUATE STUDIES

IN PARTIAL FULFILMENT OF THE REQUIREMENTS FOR THE

DEGREE OF MASTER OF SCIENCE

DEPARTMENT OF GEOMATICS ENGINEERING

CALGARY, ALBERTA

APRIL, 2005

Abstract

Autonomous relative navigation of vehicles may soon be feasible. The concept of Collaborative Driving Systems (CDS) involves linking several vehicles together in a platoon. This will have many benefits, including increasing road capacity, improving safety, and reducing driver fatigue and stress. This thesis is focused on examining various positioning sensors for potential use in a CDS. Firstly, the use of GPS as a relative positioning sensor is examined. Tests were conducted using four instrumented vehicles, each equipped with a precise GPS position and heading determination system. This enabled the relative position and velocity estimation between vehicles as well as between antennas with a constant inter-antenna baseline, using carrier phase and Doppler observations. Relative position accuracy was shown to be within a few centimetres, while relative velocity was accurate to a few centimetres per second. Secondly, various sensors were mounted on mobile robots. The lead robot was manually controlled, while another robot was left to autonomously follow. The sensors on the robots include GPS, a digital camera, and a laser scanner. Results show that GPS gives very high accuracy distance measurements but can not consistently or accurately provide angle. The digital camera provides continuous distance and angle measurements, though with less distance accuracy than GPS. The laser scanner provides distance and angle measurements of high accuracy, except often has difficulty identifying the target. Combining GPS with either auxiliary sensor resulted in superior performance, by reducing time to fixing ambiguities, and improving accuracy during GPS data outage and float ambiguity positioning.

Acknowledgements

Table of Contents

List of Tables

List of Figures

List of Nomenclature

Abbreviations

ABS	…	Anti-locking Braking System
CCIT	…	Calgary Centre for Innovative Technology
CDS	…	Collaborative Driving Systems
CPU	…	Central Processing Unit
DGPS	…	Differential GPS
DoT	…	Department of Transportation
GPS	…	Global Positioning System
IGS	…	International GPS Service
IMU	…	Inertial Measurement Unit
L1	…	Primary GPS Frequency (1575.42 MHz)
L2	…	Secondary GPS Frequency (1227.60 MHz)
LABORIUS	…	Laboratoire de Recherche en Robotique Mobile et Systèmes Intelligents
LAMBDA	…	Least-Squares Ambiguity Decorrelation Adjustment
MBS	…	Moving Base Station
MDB	…	Minimum Detectible Blunder
NDL	…	Navigation Development Library
PATH	…	Partners for Advanced Transit and Highways
PL	…	Protection Level
PLAN	…	Positioning, Location, and Navigation
PRN	…	Pseudorandom Noise
RMS	…	Root Mean Squared
SBS	…	Static Base Station

Symbols

δ_0 … Non-centrality parameter

ΔN … Change in northing from station 1 to station 2

ΔE … Change in easting from station 1 to station 2

ΔU … Change in height from station 1 to station 2

$\Delta\rho$ … Difference in range

$\Delta\hat{x}_{ki}$ … The effect of the ith blunder on the parameters at epoch k

$\nabla\Delta$ … Double difference operator

∇_{ki} … Minimum detectible blunder in observation i at epoch k

∇_k … Column vector of all minimum detectible blunders at epoch k

ε_P … Pseudorange noise and multipath (m)

ε_Φ … Carrier phase noise and multipath (m)

$\dot{\varepsilon}_\Phi$ … Doppler noise and rate of change of multipath (m/s)

λ … Geodetic longitude

λ … Wavelength (m/cycle)

λ_{L1} … Wavelength of L1 (0.190 metres)

λ_{L2} … Wavelength of L2 (0.244 metres)

ρ … Geometric range between satellite and antenna (m)

$\dot{\rho}$ … Rate of change of geometric range (m/s)

ϕ … Geodetic latitude

φ … True fractional cycle (cycles)

Φ … Carrier phase measurement (m)

$\dot{\Phi}$ … Doppler measurement (m/s)

$\Phi_{k,k-1}$ … Transition matrix from epoch k-1 to epoch k

a … Azimuth from station 1 to station 2

a_{image} … Angle to the target in the image

a_{total} … Total angle from the follower to the leader

a_{pan} … Camera pan angle

a_H … Calibrated constant for use of height observations

a_W ... Calibrated constant for use of width observations

$\bar{b}_{12}$ ... Baseline vector from station 1 to station 2 in the local level frame

c ... Speed of light (m/s)

C_{vk} ... Variance-covariance matrix of the innovation sequence

d ... Distance from station 1 to station 2

D ... Distance from the camera lens to the object

$d\rho$ ... Orbital error (m)

$d\dot{\rho}$ ... Rate of change of the orbital error (m/s)

d_{iono} ... Ionospheric error (m)

$\dot{d}_{iono}$ ... Rate of change of ionospheric error (m/s)

d_{trop} ... Tropospheric error (m)

$\dot{d}_{trop}$ ... Rate of change of tropospheric error (m/s)

dt ... Satellite clock error (s)

$d\dot{t}$ ... Satellite clock drift (s/s)

dT ... Receiver clock error (s)

$d\dot{T}$ ... Receiver clock drift (s/s)

dx ... X-offset of the centre of the object in the camera image

... X-offset observation

f ... Camera focal length

f_W ... Camera focal length in the width domain (pixels)

h ... Height of the object in the camera image

... Height observation

H ... Object height

H_k ... Design matrix at epoch k

I_{L1} ... Ionospheric effect on L1 (metres)

I_{L2} ... Ionospheric effect on L2 (metres)

K_k ... Kalman gain matrix for the epoch k

m_i ... Column vector of zeroes, with a 1 in the ith row

N ... Ambiguity (cycles)

p ... Pitch from station 1 to station 2

P	...	Pseudorange measurement (m)
P_k	...	Covariance of the parameters
$P_k^{(-)}$	...	Predicted covariance of the parameters prior to use of current observations
Q_k	...	Variance-covariance associated with input noise (Process noise matrix)
R_k	...	Variance-covariance matrix associated with measurement noise
R_A	...	Absolute position vector of antenna A
R_{AB}	...	Inter-antenna position vector between antennas A and B
$\vec{r}_{12}$	...	Vector between stations 1 and 2
T	...	Rotational transform matrix
$\vec{u}_j^i$	...	Unit vector to a satellite
V_A	...	Absolute velocity of antenna A
V_{AB}	...	Inter-antenna velocity vector between antennas A and B
v_k	...	Measurement noise, assumed to be white noise
w_k	...	Input noise, assumed to be white noise
w	...	Width observation
W	...	True width of the target, the diameter of the cylinder
x_k	...	Parameters at epoch k
$\hat{x}_k$	...	Optimal estimate of parameters at epoch k
$\hat{x}_k^{(-)}$	...	Predicted parameters prior to use of current observations
x_{k-1}	...	Parameters at epoch k-1
z_k	...	Observations at epoch k

1 Introduction

Automated driving is a task that has received increasing attention in recent years. While absolute positioning of vehicles is one complex task that is being investigated, a somewhat simpler, yet complementary, task of relative positioning of vehicles is also being examined. Using a relative positioning system, a platoon of vehicles on a highway could be formed whereby all vehicles would automatically follow the leader. This concept is known as a Collaborative Driving System (CDS) (Auto21 2003). The benefits of such a system are quite compelling.

However, no system concept has been accepted so far by experts and by society as being the leading choice among several. For this reason, this thesis examines one idea of how automated driving may be facilitated. Several sensors are evaluated, as will the advantages of combinations of these sensors.

1.1 Collaborative Driving Systems

A CDS is a system in which several vehicles on a highway autonomously follow a lead vehicle. Such a system requires a relative positioning system between vehicles, a communication system, an intelligent decision-making algorithm, and a means of implementing these decisions.

1.1.1 Requirements

Each component of a CDS must meet some strict requirements. The requirements of each component depend greatly on the performance of other components.

First and foremost, all systems require a high level of reliability. The positioning system must provide consistent accuracy, and consistent estimates of accuracy. The

communication system can not be jammed, and must have continuous availability. The decision-making algorithm must not make any mistakes, and the means of implementing these decisions must not break down. A CDS controlling multiple vehicles weighing several hundred kilograms each and travelling at high velocities has virtually no room for system failures. If any failures do occur, corrective measures such as alarms must take place immediately.

The relative positioning system must be highly accurate. Exactly how accurate depends on what is to be achieved. A minimum accuracy could be considered to be one or two decimetres, in order to keep vehicles in the correct lanes. Longitudinally, accuracy can be somewhat lower, though this would result in higher distances between vehicles being required to maintain safety, thereby reducing one of the prime advantages of a CDS.

The communication system will depend upon the sensors used for relative positioning. The amount of data that the system must be able to transmit depends upon the amount of data that must be communicated between vehicles to position them.

1.1.2 Benefits

There are several benefits to a CDS. The three most prominent are an increase in roadway capacity, an increase in driver safety, and a reduction in driver stress and fatigue.

A CDS improves the performance of existing road infrastructure by allowing vehicles to travel more closely together without decreasing safety (Hallé et al 2003). Currently, the amount of space between vehicles is based on the human decision-making perception and reaction process (US DOT 2002), as well as the time it physically takes for the vehicle to slow down. A CDS, with near instantaneous automated perception and response, virtually eliminates the perception and response time. Therefore vehicles will not have traveled as far before corrective action is taken. Vehicles can travel more closely

together without reducing safety, and therefore an increased number of vehicles may fit on existing infrastructure. This is a major economical and environmental benefit.

Safety is improved, again by removing the human component in the perception and reaction process. This results in quicker and more frequently correct actions. Also, there will be less "driver error" style collisions with a CDS. Another phenomenon known as asymptotic stability is improved by a CDS (US DOT 2002). If a lead vehicle suddenly slows down, then by the time the following vehicle notices that it has to slow down, it must slow down at a greater rate to avoid a collision. By the time a third vehicle notices the second vehicle slow down, it must slow down at an even greater rate. There is a continuous growth in magnitude of the required deceleration rate towards the rear of the platoon, until vehicles are physically unable to stop in time. A CDS, with quicker perception and reaction, reduces this growth in magnitude. Additionally, a CDS may link a vehicle farther back in the platoon directly to the lead vehicle, rather than solely to the vehicle directly in front of it.

Thirdly, a CDS reduces driver fatigue and stress. Many collisions occur because the driver is tired and not paying close attention to the surroundings, or not immediately capable of making the decisions and actions necessary to correct a situation. A CDS reduces this responsibility. Once a system is developed that is proven to be safe, the driver can relax more. Also, road rage should be greatly reduced, partly because the drivers are more relaxed, and partly because actions of other vehicles are not the fault of the drivers (Smart et al 2004). The need for driver interaction in the case of an emergency, or at the start or end of platooning sessions, must be addressed.

Other possible benefits include lower greenhouse gases, due to a more stable and controlled driving situation.

1.1.3   Stages of System Development

There are three major levels of testing that can be performed in the creation of a CDS. Firstly, software simulation can be performed. In this situation, sensor data and roadway conditions are simulated, and vehicle reactions are also simulated. This is very useful to begin designing decision-making algorithms, especially for manoeuvres such as merging into a platoon and leaving a platoon (Hallé et al 2003). One of the main problems is the difficulty with which sensor data can accurately be simulated.

A second stage of testing involves using real sensors on low cost test beds, such as mobile robots. This way, the output of real sensors can be used, along with all real issues that those sensors encounter. Meanwhile, if errors in action take place, such as collisions, the results are not catastrophic. The main disadvantage with this level of testing is that it does not always represent the dynamics of real vehicles.

The final stage of testing is in essence the final product. Real vehicles with real sensors must be driven on roads, with navigation of the following vehicles being completely autonomous. This is necessary as the final proving ground for the system before it can be released into public use. However, it is also a very expensive step, and can not be afforded until confidence has been built in the system through the first two stages.

1.2   Overview of Collaborative Driving System Sensors

Several concepts for automated driving have been explored by various groups in the past, and these will be briefly discussed in the following paragraphs. In general, all systems require sensors that can give highly accurate positions and often orientations, at a high data rate.

1.2.1 Global Positioning System

The core of many positioning sensor systems is the Global Positioning System (GPS). GPS is a series of 28 satellites orbiting Earth, broadcasting signals that can be received by a user. Range and range-rate measurements from the satellites to the receiver are made, and based on assumed known positions of the satellites, a user position and velocity can be computed. GPS is versatile in that it is an all weather system; the signal is only minimally attenuated by rain and snow. GPS provides different types of measurements that can be processed in different ways; accuracy increases with cost and processing complexity. Kato et al (2002) demonstrated some of the capabilities of GPS in vehicle platoon control with the Demo 2000 cooperative driving demonstration. In this demo, the lead vehicle was positioned using differential GPS with a reference station, to create a series of positions over time. Following vehicles positioned themselves using differential GPS with the reference station, and attempted to pass through the points determined by the lead vehicle. Speed was controlled based on the GPS velocities of each vehicle and the distance between vehicles. Laser ranging was used for obstacle detection. This approach was successfully demonstrated, as vehicles were able to drive in a platoon, and perform merging and leaving manoeuvres. Researchers at the University of Minnesota have also used GPS for positioning vehicles (Bajikar et al 1997). Systems for assisting bus drivers and snow plow drivers in poor weather conditions were successfully tested (Lim et al 1999).

However, GPS has several drawbacks. The most prominent of these is that it is a "line-of-sight" system. This means that the path from the receiver to the satellites must not be obstructed by buildings, trees, or other solid matter. For vehicular applications, signal blockage may or may not frequently occur, depending on the environment. Another drawback is that to use the highest accuracy measurements, some initialisation must take place, and this can take some time.

1.2.2 Inertial Sensors

A system that is often used to augment GPS is known as an Inertial Measurement Unit (IMU). An IMU consists of triads of gyroscopes and accelerometers. These can be used in combination as a dead reckoning device to determine a current position relative to the original position, as well as platform orientation (Petovello 2003). However, accelerometers and gyros drift over time with the extent of this drift depending on the quality of the sensor. In general, a unit costing upwards of one hundred thousand dollars will yield decimetre-level errors in less than a minute (Petovello 2003). A lower cost IMU costing several thousand dollars can lead to 30 metres of error in 20 seconds or so (Nayak 2000). Price is therefore a major limiting factor in using an IMU for navigation.

By integrating GPS with an IMU, GPS can provide position estimates and help to calibrate the IMU continuously. When the GPS incurs signal blockage, the IMU can be used to maintain position updates until the GPS becomes available again. This method works reasonably well as long as the GPS becomes available again quite soon. This is a very commonly researched sensor integration approach, shown in Wei & Schwarz (1990), Da (1997), and Salychev et al (2000).

1.2.3 Differential Odometry

By tracking the distance that the right and left wheel have moved on a vehicle, distance driven and heading changes can be computed. This technique has been used by Bétaille & Bonnifait (2002) and Stephen & Lachapelle (2000) amongst others. Generally the amount of distance travelled by each wheel is measured, based on the number of rotations and the wheel circumference. Number of rotations can be accurately measured by anti-locking braking systems (ABS). The primary problem with this system is caused by wheel slippage. When the wheel slips, it appears to have travelled farther or shorter than it really has. Overall the accuracy of this system is not very high, but can be quite useful

as an augmentation to GPS and other sensors. Stephen & Lachapelle (2000) found that during a 100 second period, the error in ABS-derived position grew to nearly 20 metres (RMS) and nearly 30 metres (RMS) during a 200 second gap. Of course, these errors depend on the vehicle dynamics during the tests.

1.2.4 Magnetic Sensors

The California Partners for Advanced Transit and Highways (PATH) project has performed extensive research into the use of magnetic sensors (Farrel & Barth, 2001). Essentially, magnets would be imbedded into the road, and magnetometers on the vehicle would sense these and create measurements of off-trajectory distances. This information can be used to help guide the vehicle. The major drawback with this method is that it is heavily infrastructure-based. Automated driving could only take place on roads that have had the magnets built in. Therefore, this would take a long time to implement, and would be very expensive. In adverse climates where roads frequently need repairing, this would be even more expensive and unfeasible. Magnetic sensors in roads have the advantage that they can be used as a stand-alone driving system rather than just a collaborative driving system.

1.2.5 Magnetic Compass

A magnetic compass is an inexpensive way to provide heading data (El-Sheimy et al 2001). The primary drawback of such a system is the variable error of unknown magnitude due to the existence of external magnetic fields. These can be caused by a wide variety of phenomena, including the presence of magnetic objects in the vicinity. Obviously, there would be many magnetic objects nearby in a driving situation. Harvey (1998) found that even seemingly benign acts such as opening a car door or turning on the rear window defroster could significantly change the magnetic field detected by a

magnetic compass mounted above the car roof. Nonetheless, the information provided by a magnetic compass could still be useful.

1.2.6 Laser Ranging

Laser scanners have not received a great deal of attention for the purposes of vehicle navigation. Generally laser ranging is used to acquire an accurate distance measurement, while another sensor gives an angular measurement to tell where the laser is pointing, and a GPS receiver gives the position of the laser. Many military targeting systems use this approach (Boggs 2001). However, lasers also exist as scanners, where the laser turns back and forth across a certain angular range, making distance measurements at small angular increments. This is commonly used for obstruction avoidance (Buchberger et al 1993) but if a target can be identified in the resultant pattern, an approximate angle and an accurate distance to that target can be obtained. However, this depends on the ability to identify the target in the laser profile. Roberts & Vallot (1990) use this technique with a horizontal + vertical scanner.

1.2.7 Camera Vision

Cameras have received a great deal of attention in mobile mapping applications (El-Sheimy 1996). By driving a vehicle which has accurately known position and orientation, and taking multiple photographs along the way, features appearing in these images can be positioned by photogrammetric means. However, this requires a lot of processing, and generally user interaction to identify common points in multiple images.

Another technique of camera vision is to have a well defined object appear in an image (Michaud et al 2002). If this object can be isolated, an approximate angle and distance can be determined based on the position and size of the object in the image compared to its known true size. Unfortunately, in a real automated driving situation, it is not very likely that an easily identifiable object of known proportions will be visibly in place on

all vehicles on the road. If an error is made and an incorrect target is tracked, the vehicle could easily end up in a collision.

Another application is to have the camera detect a road centreline. Wu (1996) detects a line that is then followed by the robot. Grejner-Brzezinska et al (2000) detects the road centreline, but is actually trying to position the centreline, and uses other sensors to determine the vehicle position. Some roads however either do not have centrelines, or have centrelines that are faded. Also, if the road is obscured by snow or dirt, this method would fail.

1.2.8 Sonar

Sonar is another distance measurement device. Sonars emit sound wave pulses, and the time required for these to travel and meet their target then return to the sensor is measured (Vexilar 2003). Based on the speed of sound, this time can be converted into a distance. In the case of multiple sonars, they must be decoupled either spatially or temporally so that the waves from one sonar are not detected erroneously by another sonar. Three major problems with sonar include specularity, beamwidth, and frequent misreadings (Buchberger et al 1993). The beamwidth is a major problem in real-time navigation, as it is difficult to know where, in an angular sense, the object being sensed by the sonar is. It is generally used only to maintain a safety bubble around the vehicle. If the position and orientation of the vehicle is known, the sonar measurements collected over time may be combined to form a map of the surroundings of the robot (Buchberger et al 1993).

1.2.9 Millimetre Wave Radar

Millimetre wave radar systems can be used to determine both distance and relative velocity. Distance is computed based on the time taken for a signal to reach a target and return, and relative velocity is computed via a Doppler shift in the return signal (Honma

& Uehara 2001). However, this technology has two major limitations. The first is maximum range, which may be near 120 metres, and the other is accuracy, which may be only 1 metre in the distance domain (Honma & Uehara 2001). While this could be useful for adaptive cruise control, it is not sufficient for manoeuvres such as passing and merging into a platoon.

1.3 Collaborative Driving System Architecture

A CDS requires more than just sensor information. A communication system must exist as well as a detailed decision-making procedure. Frankel et al (1994) discusses the overall architecture of vehicle platoons in detail as a part of the research done at the California PATH program.

Depending on the sensors used, the communication system may be simple or complex. In the case of sensors such as vision or laser ranging, the following vehicle already has the spatial data linking it to the vehicle in front of it. It may still require information from the leader such as its status, the actions it is performing, and any other ancillary data that may be sensed by the leader such as road conditions. In turn, the follower may inform the leader of its own status. If a sensor system such as differential GPS is used, observations must be transmitted between the vehicles such that the differential processing may be performed. The transmission of this information requires a communication system. The required speed of the system depends on the amount of data to be transferred. A large amount of information being shared at a high data rate will require a relatively high bandwidth. Possible communication systems include conventional radio systems or a form of wireless Ethernet onboard the vehicle computers. Michaud et al (2002) have used Ethernet, while Kato et al (2002) have used 5.8 GHz dedicated short range communication. Many wide area GPS services broadcast corrections on L-band signals from geostationary satellites (Cannon et al 2002).

Vehicles must decide what actions to take based on the available sensor data in an automated way. These decisions include whether to speed up or slow down, how much of a turn to make, how to deal with adverse road conditions, and whether to alert the driver to a situation. These decisions could be simply for maintaining several vehicles following each other in a platoon, or they could be expanded to handle manoeuvres such as merging and passing of other vehicles. Research into these decision-making processes is being performed at various institutes using various methods. Simulators are one of the most time- and cost-effective methods of evaluating decision-making procedures (Hallé et al 2003). However, real-world conditions are still only approximated by simulators, and therefore tests using actual vehicles must be performed. At a low level, mobile robots can be used, as this limits the risks that would be present in navigating full size vehicles. Again, this only approximates real conditions, as the dynamics of robots is different than the dynamics of full size vehicles. Eventually tests would need to be performed using real vehicles on regular roads.

1.4 Thesis Objectives

The first objective of this thesis is to investigate the use of GPS as a sensor system for a CDS. In order to do this, a field test was performed, using several vehicles equipped with GPS, travelling on a highway. Data was post-processed using various methods in order to evaluate the accuracy of GPS in the position and velocity domain. One of the important goals that has not frequently been done was to process GPS data between antennas on different moving vehicles without the need for a static reference station. Other advantages of GPS compared to other sensor systems were also investigated.

The second objective is to test the use of GPS with other sensors on a low cost platform. Researchers at the University of Sherbrooke have several mobile robots which have previously been designed to follow each other automatically using a digital camera seeing

a coloured tube on another robot (Michaud et al 2002). In a general sense, this research will add GPS and a laser scanner on to the robots as additional sensors, and evaluate the accuracies achievable by each sensor alone and by combinations of sensors. The sensors were assessed to give an estimate of the quality of each of them. The filter to process the data had to be developed in such a way as to flexibly combine the observations from each of the sensors. One particularly important point was the need to process between moving platforms without the use of a static base station. Sensors were processed alone and in combination to evaluate obtainable accuracy, speed of ambiguity resolution, and reliability.

1.5 Outline

Chapter 2 of this thesis gives additional background information relevant to this thesis, including detailed descriptions of the sensors used as well as estimation theory. Chapter 3 involves the evaluation of GPS as a sensor for collaborative driving systems, by describing the field test performed, the processing techniques used, and giving single vehicle and inter-vehicle results. Chapter 4 involves the use of GPS and other sensors on mobile robots, alone and in combinations, by firstly describing the equipment used, the field tests performed, how the data was processed, and the numerous tests performed and their results. Chapter 5 summarises the conclusions reached, and gives recommendations for future research.

2   Sensor Fundamentals

GPS is a complex system with many types of observations and methods of processing. An overview is given here. In addition, details of the other sensors that were used on the mobile robots are given. An overview of estimation theory using Kalman filters is included.

2.1   GPS

GPS is a series of 24 satellites including four active spares orbiting Earth at an orbital radius of 26600 km (Kaplan 1996). Because of their configuration, signals can be received at any point on Earth. Originally developed by the United States Department of Defense, GPS has become quite useful to the civilian community as well. However, some signals are still reserved for military use only. There are three different types of observables, several sources of error, and a few different processing formulations.

2.1.1   GPS Observables

GPS measurements can be broken into three categories: pseudorange measurements, also known as code measurements, carrier phase measurements, and Doppler measurements (Hofmann-Wellenhof et al 2001).

Pseudorange measurements are direct measurements of the ranges between the receiver and the satellites. Each satellite signal has a pseudorandom noise (PRN) code modulated onto it and the receiver generates an identical code. By determining the time offset required to align the satellite generated code with the receiver generated code, and multiplying by the speed of light, a distance between the satellite and the receiver can be computed. However, due to the presence of several sources of error, this measurement commonly has accuracies of several metres. Equation 2.1 gives the formula for a

pseudorange measurement. Details about the errors and how they may be dealt with are given in section 2.1.2.

$$P = \rho + d\rho + c(dt - dT) + d_{trop} + d_{iono} + \varepsilon_P \qquad (2.1)$$

where

P represents the pseudorange measurement (m),

ρ represents the geometric range between satellite and antenna (m),

$d\rho$ represents the orbital error (m),

c represents the speed of light (m/s),

dt represents the satellite clock error (s),

dT represents the receiver clock error (s),

d_{trop} represents the tropospheric error (m),

d_{iono} represents the ionospheric error (m), and

ε_P represents the pseudorange noise and multipath (m).

Carrier phase measurements are a more accurate measurement of distance between the antenna and satellite, but are more difficult to use. A fractional portion of a cycle is measured, and continuously tracked by the GPS receiver. However, on top of this fraction of a cycle, an integer number of full cycles exist between the receiver and the satellite. This integer number of cycles is known as the ambiguity. The integer ambiguity must be correctly determined in order to make full use of this highly accurate measurement. This can be difficult, and generally takes time, although a great deal of research has been performed to improve the speed and accuracy of this process. Processing methods to determine the ambiguity are briefly discussed in section 2.1.3. The accuracy of the fractional cycle measured is generally near a millimetre, though other

errors, if not dealt with, are much higher. Equation 2.2 gives the formula for a carrier phase measurement.

$$\Phi = \lambda\varphi + d\rho + c(dt - dT) + d_{trop} - d_{iono} + \lambda N + \varepsilon_\Phi \qquad (2.2)$$

where

Φ represents the carrier phase measurement (m),

φ represents the true fractional cycle (cycles),

λ represents the signal wavelength (m/cycle),

$d\rho$ represents the orbital error (m),

c   represents the speed of light (m/s),

dt   represents the satellite clock error (s),

dT   represents the receiver clock error (s),

d_{trop} represents the tropospheric error (m),

d_{iono} represents the ionospheric error (m),

N   represents the ambiguity (cycles), and

ε_Φ represents the carrier phase noise and multipath (m).

Doppler measurements are instantaneous range-rate measurements. When an emitter and receiver are moving relative to each other, a shift in the received frequency occurs with respect to the transmitted frequency (Hanks 1985). They can generally be used to compute a receiver's velocity. Equation 2.3 gives the formula for a Doppler measurement.

$$\dot{\Phi} = \dot{\rho} + d\dot{\rho} + c(d\dot{t} - d\dot{T}) + \dot{d}_{trop} - \dot{d}_{iono} + \dot{\varepsilon}_{\Phi} \qquad (2.3)$$

where

$\dot{\Phi}$ represents the Doppler measurement (m/s),

$\dot{\rho}$ represents the rate of change of the geometric range (m/s),

$d\dot{\rho}$ represents the rate of change of the orbital error (m/s),

c   represents the speed of light (m/s),

$d\dot{t}$ represents the satellite clock drift (m/s^2),

$d\dot{T}$ represents the receiver clock drift (m/s^2),

$\dot{d}_{trop}$ represents the rate of change of tropospheric error (m/s),

$\dot{d}_{iono}$ represents the rate of change of ionospheric error (m/s), and

$\dot{\varepsilon}_{\Phi}$ represents the Doppler noise and rate of change of multipath (m/s).

2.1.2 GPS Errors

Here the individual GPS errors will be discussed for a single GPS measurement. Discussion of errors for combinations of measurements will be discussed in sections 2.1.3 and 2.1.4, along with processing techniques.

The orbital error, $d\rho$, exists because there is no perfect data regarding the location of the GPS satellite. The amount of error introduced into the pseudorange and carrier phase measurements depends upon the geometry of the situation. For real-time applications, the available orbital information comes from a navigation message modulated onto the GPS signal, giving Keplerian parameters. These are estimated beforehand (predicted), and therefore an error of about 2 metres could result in the computed satellite position

(IGS 2004). For post-processing, precise orbits are available from the International GPS Service (IGS) a few weeks after the data collection, computed from a series of precisely known reference stations around the globe. These have accuracies of fewer than 5 centimetres (IGS 2004). Other orbital products are available from the IGS, with lower accuracies but less delay.

The satellite clock error, dt, exists because the satellite clock is not perfectly synchronised with GPS time. However, parameters for the computation of this satellite clock error are included in the navigation message. The clocks onboard GPS satellites are very stable, in that the error can be well modelled. Thus the computed satellite clock errors are very close to the true clock errors even after some time has passed. As a result, this error can be greatly reduced to several nanoseconds, corresponding to about 2 metres. Again, for post-mission analysis, precise satellite clock data is available from the IGS at accuracies of less than 0.1 nanoseconds (IGS 2004).

The receiver clock error, dT, exists because the receiver clock is not perfectly synchronised with GPS time. In general, receiver clocks are not highly stable, in that the error can vary a great amount in an unpredictable manner, and thus this value can be quite large and varies greatly over time. The actual receiver clock error is also a function of the receiver firmware as some receivers will constantly slew the clock to maintain alignment to GPS time to with 20-30 nanoseconds, though this is still a large error. As a result, this parameter is estimated along with the three-dimensional position of the receiver, which is why four satellites are required for GPS positioning.

The tropospheric error, d_{trop}, exists because electromagnetic radiation travels slower than the speed of light when it is not in a vacuum. Additionally, the path of the signal bends slightly as it passes through the atmosphere, though this is a much smaller effect (Hoyle et al 2004). The change in speed of light in the atmosphere is related to the temperature, pressure, and presence of water vapour. Many models have been developed which

estimate the magnitude of the tropospheric error. The modified Hopfield model (Goad & Goodman 1974) and the Saastamoinen model (Saastamoinen 1973) are among the most popular. These can reliably reduce the tropospheric error by about 90%.

The ionospheric error, d_{iono}, exists because of the effect of ionized particles and free electrons on electromagnetic radiation (Olynik 2002). Ionized particles and free electrons are present in Earth's ionosphere, which GPS signals must travel through. Group delay and phase advance are the two primary effects. The group delay slows down the propagation of the pseudorange observable, while phase advance has the effect of increasing the speed of the carrier phase observable. The magnitude of these is the same, thus there is simply a change in sign in the observation equations. The ionospheric effect varies diurnally, and thus a model can be used to reduce the magnitude by about 50% (Klobuchar 1987). Alternately, since the ionospheric effect depends on frequency, if dual frequency GPS data is available the ionospheric effect can be removed (Olynik 2002).

Multipath exists because a signal can reach the antenna via a direct path, or via a path that involves reflections from nearby objects. As a result, when the multipath and direct signals are mixed in the receiver, an error in the measurements occurs (Ray 2000). Multipath error is very difficult to model, and therefore it is joined with noise in the observation equations and treated as random. Most multipath reduction work is currently done in the receiver, rather than in data processing. Pseudorange multipath is limited by the code chipping rate, while carrier phase multipath is limited by the wavelength. As a result, pseudorange multipath can have a magnitude of more than 100 metres while carrier phase multipath remains within a few centimetres (Ray 2000). However, the actual maximum magnitude of multipath depends on the strength of the direct and reflected signals, and the processing performed in the receiver. For example, a narrow correlator spacing can easily reduce code multipath to under 10 metres, and other more recent technologies can reduce this further (Ray 2000).

Noise is generated by the receiver, and includes any other errors not mentioned above. It is generally considered white noise, and thus can not be deterministically modelled. It is left to be averaged out in the estimation process, through stochastic modelling. The noise for pseudorange measurements is traditionally about 3 metres, though it has been shown to actually be sub-metre, while the noise for carrier phase measurements is under 2 millimetres (Hofmann-Wellenhof et al 2001).

Errors in the Doppler measurements are generally not dealt with as rigorously as those in the pseudorange and carrier phase measurements. This is because many errors are temporally correlated, or are too difficult to model. For example, the orbital error is not changing at a large rate, and therefore the orbital error rate is near zero. Similarly, the troposphere is not rapidly changing, so its rate is also near zero. Finally, the rate of change of multipath is usually near zero. The satellite clock drift is fairly stable because of the high quality clocks used, and a correction is broadcast in the navigation message. The receiver clock error may be much larger, and is therefore usually modelled along with the three-dimensional velocity parameters. Olynik (2002) showed the ionospheric error to change by less than half a centimetre per second.

2.1.3 Single Frequency Processing Techniques

GPS positioning can be broken up into two common modes: single point positioning and differential positioning (DGPS). Single point positioning simply uses one receiver: the one who's position is to be determined. In DGPS, the idea is that many large errors are strongly spatially correlated (Parkinson & Enge 1995). Therefore, by differencing measurements from two receivers that are near to each other, these errors are greatly reduced. The result of processing these differenced measurements is the vector between the two receivers. If one receiver's position is accurately known, then the absolute position of the other receiver can be determined. DGPS can be performed using single differenced observations, which involves differencing between two receivers, or double

differenced observations, which involves differencing between two receivers and two satellites (Hofmann-Wellenhof et al 2001).

Single point positioning using code measurements is the simplest positioning mode. The measurement equations are used as given in Equation 2.1. This gives positions accurate to several metres with the primary error components being the ionosphere and satellite orbit/noise (Cannon 2001). Carrier phase measurements are less frequently used in single point mode, since errors are too large for the integer ambiguity to be correctly determined. Precise point positioning is a technique that has been developed for use with a single receiver's GPS data, processed post-mission using satellite and orbit products created by the IGS (Gao & Shen 2001). This leads to positions accurate to less than a decimetre, but still takes a long time to resolve ambiguities.

Single differencing between receivers has several effects. Firstly, the satellite clock offsets are completely eliminated. Secondly, many of the other errors are spatially correlated. If the two receivers are relatively close together, the signal from a satellite to each of them will pass through approximately the same ionosphere and troposphere, and thus the atmospheric errors will be greatly reduced. Also, any errors in the satellite positions will have a similar effect for both receivers, and this error will be mostly differenced out. This leaves receiver clock errors and noise and multipath. The receiver clock errors can be estimated as a single differential receiver clock error. The noise and multipath are completely uncorrelated between receivers. As a result, noise and multipath actually increase in magnitude by a factor of $\sqrt{2}$.

Use of single differenced code measurements can generally give position accuracies of 0.5 to 2 metres (RMS) (Kaplan 1996). The primary remaining error sources are code noise and multipath. Single differencing of carrier phase observations is less useful, since the differential ambiguity and the differential receiver clock offset are highly correlated, and thus the correct integer ambiguities are difficult to determine.

Double differencing between receivers and satellites has all the benefits of single differencing plus some additional effects. Most importantly, the receiver clock offsets are completely eliminated. This leads to one less parameter, however four satellites are still needed to form the three double differenced observations to estimate a three-dimensional position difference. As in the case of single differencing, noise and multipath are uncorrelated between measurements, and so the error from these sources will be 2 times higher than for undifferenced observations.

Use of double differenced code measurements is not particularly useful as the noise is increased while other errors are not significantly reduced. Double differencing is more useful for carrier phase measurements since the ambiguities are more easily determined without the influence of the receiver clock offsets. This leads to accuracies of a centimetre once ambiguities are resolved (Kaplan 1996).

It is clear that for an automated driving task, the carrier phase measurements in differential mode with correctly determined integer ambiguity values must be used to provide sufficient accuracy since a metre of error could be disastrous. Integer ambiguities are generally determined by being among the unknown parameters in a least-squares adjustment (Liu 2003a). These unknown values are floating point values. A search is then performed by choosing nearby integer combinations of ambiguities. A variance factor is produced for each integer combination, and the combination of ambiguities that produces the lowest variance is chosen as the best choice. If this best choice is sufficiently better than the second best choice, it is chosen and used until either it is shown to be incorrect, or a loss of lock occurs on the signal. If loss of lock occurs, the ambiguity must be determined anew. The most common search technique is known as the least-squares ambiguity decorrelation adjustment (LAMBDA) method (de Jonge & Tiberius 1996). This attempts to decorrelate the ambiguities, resulting in a smaller search space, resulting in a quicker ambiguity determination procedure.

2.1.4   Dual Frequency Processing Techniques

Additionally, since GPS signals are available on two frequencies, L1 and L2, more processing techniques have been developed. There is no civilian code on the second frequency, so only phase measurements are available. Measurements on the L2 are not as accurate as those on L1, but linear combinations of the measurements can be quite useful. The most common linear combinations are widelane, narrowlane, and ionosphere-free combinations (Liu 2003a).

The most basic technique is to simply process the additional L2 observations as well as the L1 observations.   This results in additional observations which increase the redundancy.

The widelane combination results from subtracting the L2 observation from the L1 observation. This effectively produces an observation with a much higher wavelength. The noise is higher on this new observation, and the ionospheric effect is somewhat increased, but with a longer wavelength, it is easier to compute the correct integer ambiguity (Liu 2003a).

The narrowlane combination results from addition of the measurement on each frequency. This produces an observation with a much shorter wavelength. The noise is lower on this new observation, but the ionospheric effect is somewhat increased, and it is more difficult to determine the ambiguity (Liu 2003a).

The ionosphere-free combination results from a combination of measurements based on the frequencies of the signals. Since the ionosphere is dispersive, it has a different effect on signals on different frequencies, as given in Equation 2.4.

$$I_{L2} = \frac{\lambda_{L2}^2}{\lambda_{L1}^2} * I_{L1} \tag{2.4}$$

where

I_{L1} represents the ionospheric effect on L1 (m),

I_{L2} represents the ionospheric effect on L2 (m),

λ_{L1} represents the wavelength of L1 (m), and

λ_{L2} represents the wavelength of L2 (m).

Therefore these signals may be linearly combined to eliminate the effect of the ionosphere. This is quite useful as the ionosphere is a major error. However, the non-integer linear combination results in non-integer ambiguity, and therefore the ambiguity must be left in float mode (Liu 2003a). One technique to create fixed-ambiguity ionosphere-free observations is to fix the integers on the individual frequencies first, and then combine these in the new observation.

2.2 Camera

In this thesis, use of a camera is limited to observing a well defined object in the image collected by the camera. In this case, the observables include the x and y position of the center of the object in the image, as well as the x and y dimensions of the object in the image. It is intuitive that if the object is in the right half of the image, the robot should turn right, while if the object is in the left half of the image, the robot should turn left. It is also intuitive that if the object appears large, the object is near, while if the object appears small, the object is farther away. In a more detailed sense, when the target has constant dimensions, the distance and angle can be mathematically computed. Figures 2.1 and 2.2 show the relationship between a real-world object and the image of it in a camera. Equations 2.5 and 2.6 show the relationships mathematically.
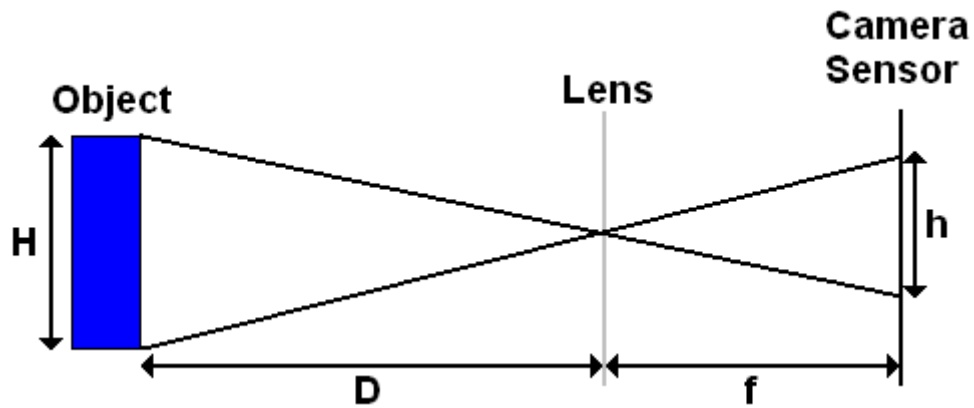
Figure 2.1: **Relationship** **Between** **Real-World** **and** **Image** **for** **Distance** **Computation**

$$\frac{H}{D} = \frac{h}{f}$$

$$D = H * \frac{f}{h}$$

(2.5)

where

  H   represents the object height,

  D   represents the distance from the camera lens to the object,

  h   represents the height of the object in the camera image, and

  f   represents the camera focal length.
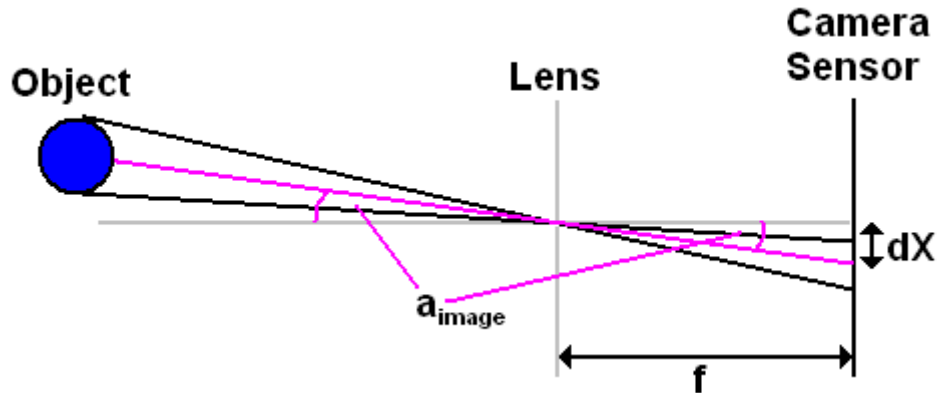
Figure 2.2: **Relationship Between Real-World and Image for Angle Computation**

$$\frac{dx}{f} = \tan(a_{image})$$

$$a_{image} = \tan^{-1}\left(\frac{dx}{f}\right) \hspace{4cm} (2.6)$$

$$a_{total} = a_{image} + a_{pan}$$

where

    dx   represents the x-offset of the centre of the object in the camera image

    f   represents the camera focal length,

    a_{image} represents the angle to the target in the image,

    a_{total} represents the total angle from the follower to the leader, and

    a_{pan} represents the camera pan angle.

Equation 2.5 shows that distance to the target is a function of the target height, camera focal length, and image height. The target height and camera focal length are constant, while the image height is measured by the camera. Therefore, distance can easily be computed. In a similar way, distance could be computed using the known and measured

target width instead of the height, if there is reason to believe the height observation is not correct. Equation 2.6 shows that the angle in the image is a function of the x-offset and the focal length. The focal length is constant, while the x-offset is measured by the camera. Therefore the angle in the image is easily calculated. This must be combined with the pan of the camera, which is also measured, to give a total estimate of the angle to the target.

Accuracies attainable will depend upon a few factors. One is the resolution of the camera. If the camera has a low resolution, then one pixel of measurement error will correspond to a large error in the computed result. If a high resolution camera is used, then a single pixel of error has a much smaller influence on the computed result. Another factor is the target to be identified. It must be a target that can be identified by an automated process. An example of this would be an object of a colour that is not expected to occur in the rest of the image. The size of the target must be chosen based on the application. A target may be too large if it fills the camera's image, therefore preventing a measurement of the full width or height. A target may be too small if it only takes up a few pixels in the image, and therefore a single pixel of error will have a major effect on the output result.

2.3   Laser

In this thesis, a laser refers to a linear laser scanner. This instrument fires a laser, and based on the time it takes for the laser to reach a target and return, a distance can be computed using the speed of light as a multiplier. The laser scanner rotates across a range of angles, making laser range measurements at small angular increments. If there is a well defined object in the range of angles, this might be identified in the profile of distances over the range of angles. The angle at which this target is identified directly

gives the angle to the target, while the distance measured by the laser at this angle directly gives the distance. Figure 2.3 shows how this works.
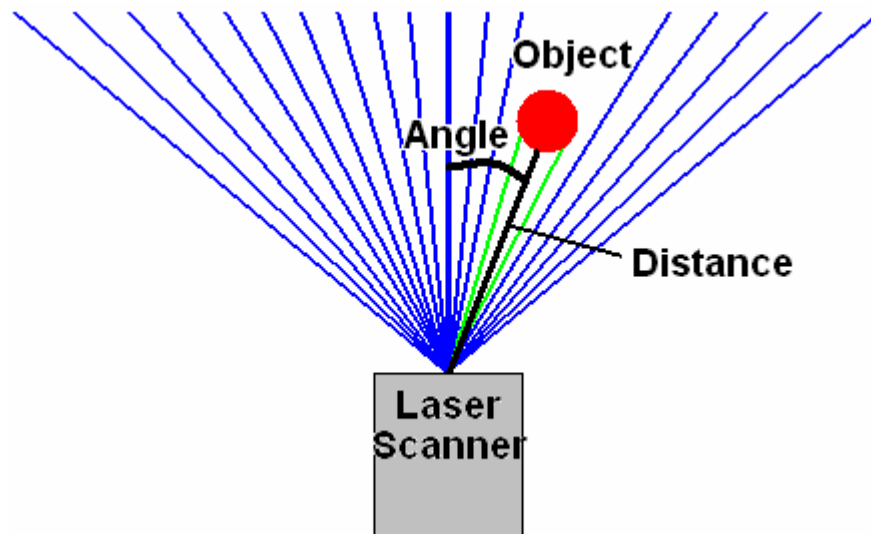
Figure 2.3:   **Laser Scanner Detecting an Object to Measure Distance and Angle**

2.4   Estimation Theory – Kalman Filters

The most common estimators for geomatics applications are least-squares estimation and Kalman filtering. Kalman filtering is a recursive process of estimation using a dynamic model and updating the estimate using a measurement model (Gelb 1974, Brown & Hwang 1992). Kalman filtering seeks to use all available information from past epochs and the current epoch to create an optimal estimate, by minimizing the mean square estimation error, while least-squares estimation simply uses measurements from the current epoch. There has been a lot of research into these estimators and many references give the derivations (Gelb 1974, Brown & Hwang 1992) and therefore only an overview of the discrete case will be given here.

The measurement model can be represented by Equation 2.7. This equation gives the relationship between the measurements at an epoch and the parameters that we wish to estimate at that epoch. A stochastic model is assumed, in that all systematic errors have been modelled out and only a white noise component remains.

$$z_k = H_k x_k + v_k \qquad\qquad (2.7)$$

where

z_k represents the observations at epoch k,

H_k represents the design matrix at epoch k,

x_k represents the parameters at epoch k, and

v_k represents measurement noise, assumed to be white noise, with associated variance-covariance R_k.

In the creation of the dynamic model, the relationship between parameters at a current epoch and those at a previous epoch must be determined. There are three common types of processes used: the random constant, random walk, and Gauss-Markov, also known as an exponentially correlated random variable. For a random constant, the time derivative of the parameter is zero. For a random constant, the time derivative of the parameter is simply white noise. For a Gauss-Markov process, the time derivative of the parameter is a function of the parameter plus white noise. The most common is the random walk process, which will be used in this thesis, as described in section 4.3. The dynamic model for the random walk can be described by Equation 2.8. This equation gives the relationship between the parameters at the current epoch and parameters at the previous epoch.

$$x_k = \Phi_{k,k-1} x_{k-1} + w_k \qquad (2.8)$$

where

x_k represents the parameters at epoch k,

$\Phi_{k,k-1}$ represents the transition matrix from epoch k-1 to epoch k,

x_{k-1} represents the parameters at epoch k-1, and

w_k represents the input noise, assumed to be white noise, with associated variance-covariance Q_k.

A flow chart view of the Kalman filtering algorithm is given in Figure 2.4. The following list explains the symbols used in the equations.

Prediction

$$\hat{x}_k^{(-)} = \Phi_{k,k-1} \hat{x}_{k-1}$$

$$P_k^{(-)} = \Phi_{k,k-1} P_{k-1} \Phi_{k,k-1}^{-1} + Q_k$$

Kalman Gain

$$K_k = P_k^{(-)} H_k^T (H_k P_k^{(-)} H_k^T + R_k)^{-1}$$

$$k \longrightarrow k\text{-}1$$

Final Estimate

$$\hat{x}_k = \hat{x}_k^{(-)} + K_k (z_k - H_k \hat{x}_k^{(-)})$$

$$P_k = (I - K_k H_k) P_k^{(-)}$$
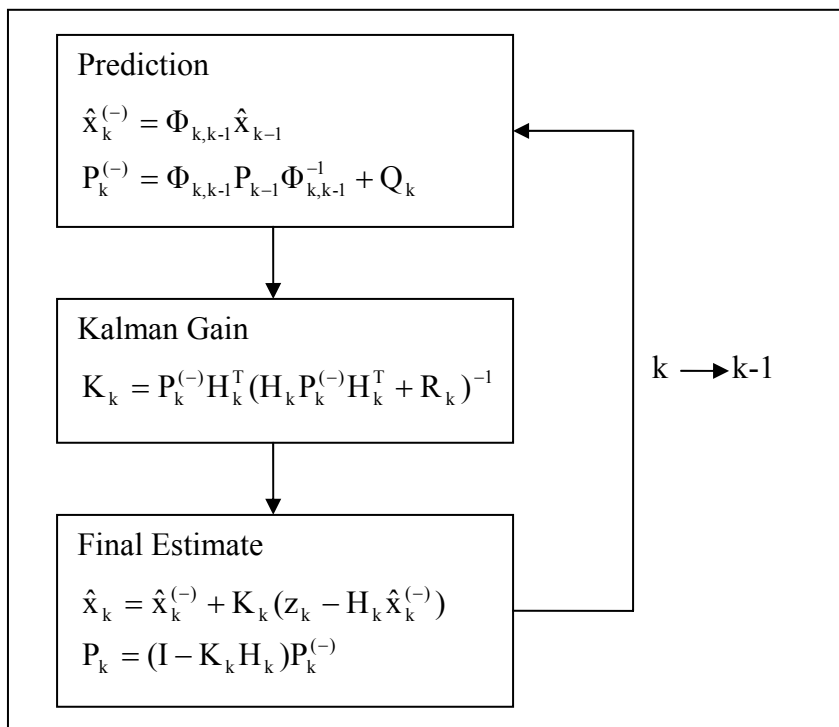
Figure 2.4:   **Flow Chart of Kalman Filtering**

$\hat{x}_k$ represents the optimal estimate of parameters at epoch k.

P_k represents the covariance of the parameters.

$\hat{x}_k^{(-)}$ represents the predicted parameters, prior to use of current observations.

$P_k^{(-)}$ represents the predicted covariance of the parameters, prior to the use of current observations.

$\Phi_{k,k-1}$ represents the transition matrix from epoch k-1 to epoch k.

Q_k represents the variance-covariance associated with the input noise (process noise matrix).

K_k represents the Kalman gain matrix for the kth epoch.

H_k represents the design matrix at epoch k.

R_k represents the variance-covariance matrix associated with the measurements.

z_k represents the observations at epoch k.

One of the useful properties of the Kalman filter for sensor integration is that when different observations are not correlated, the Kalman filter can process them sequentially. The loop can perform all the steps in the sequence for each observation set, except that since the observations are for the same time epoch, the time between epochs is zero and therefore the transition matrix is identity and the process noise matrix is zero.

Section 4.3 describes the Kalman filtering scheme developed to process data from two robots using differential GPS, a digital camera, and a laser scanner.

2.4.1   Statistical Reliability in Kalman Filters

Reliability as it is used here refers to the ability of the Kalman filter to detect faulty observations and reject them, and how much effect any faulty observations that are not

detected will have on the filter output. Petovello (2003) gives an excellent description of the concept of reliability as it relates to Kalman filters. Additionally, it describes how processing uncorrelated observations sequentially effects the results.

Initially, the probability of committing each of two types of error must be chosen. The first type of error results from rejecting a good observation. The second type of error results from not rejecting a bad observation. A quantity known as the non-centrality parameter can be determined based on the probability of committing each of these types of errors. Commonly used values are a 0.1 % chance of committing the first type of error, and a 20% chance of committing the second type of error, leading to a non-centrality value of 4.12.

The Minimum Detectible Blunder (MDB) for the ith observation on the kth epoch can then be determined using Equation 2.9.

$$\nabla_{ki} = \frac{\delta_0}{\sqrt{(C_{vk}^{-1})_{ii}}} \qquad (2.9)$$

where

∇_{ki} represents the MDB,

δ_0 represents the non-centrality parameter, and

C_{vk} represents the variance-covariance matrix of the innovation sequence.

Since $C_{vk} = H_k P_k^{(-)} H_k^T + R_k$, C_v and C_v^{-1} are actually produced in the Kalman filter without additional processing, as seen in Figure 2.4.

When uncorrelated observations are processed sequentially in order to improve processing efficiency, some changes to the MDB occur. C_{vk} is proportional to the variance-covariance of the estimated parameters, P_k. The first observation set improves

P_k, which is used to form the C_{vk} for the first observation set. Then the second observation set is used to further improve P_k, which is used to form an improved C_{vk} for the second observation set. It is clear that the first observation set is useful for improving (decreasing) the MDB of the observations of the second observation set, however, the second observation set has not improved the MDB for the first observation set. This is the disadvantage of processing uncorrelated observations sequentially. Generally, however, the efficiency improvement is worth this sacrifice.

The effect of an undetected blunder is also very important. A blunder in the ith observation can be mapped directly into the resulting parameters using Equation 2.10.

$$\Delta \hat{x}_{ki} = K_k m_i \nabla_{ki} \qquad (2.10)$$

where

$\Delta \hat{x}_{ki}$ represents the effect of the ith blunder on the parameters,

K_k represents the Kalman gain matrix for the kth epoch,

m_i represents a column vector of zeroes, with a 1 in the ith row, and

∇_{ki} represents the MDB.

Equation 2.10 can be rewritten as

$$\Delta \hat{x}_{ki} = K_k m_i m_i^{T} \nabla_k \qquad (2.11)$$

where

∇_k represents a column vector of all MDBs.

This shows us the biggest effect that an undetected blunder could have on the parameters. It is commonly referred to as the Protection Level (PL).

3   Evaluation of GPS as a CDS Sensor

In order to be a useful sensor for a CDS, GPS must be shown to provide highly accurate positions and velocities in a vehicular application. GPS must also be shown to have some benefits over other available sensors. The following sections describe the field test that was performed, discuss the various methods of processing the data, and present results verifying the system accuracy and demonstrating the other useful outputs that can be produced. Cannon et al (2003) presents many of these results.

3.1   Field Test

In order to evaluate GPS, a vehicular field test was performed. Field testing took place on March 19, 2003, on a stretch of open road near Calgary, Alberta, as illustrated in Figure 3.1. Four vehicles were coordinated in a simulated platoon. Each vehicle was outfitted with two GPS antennas and receivers to provide redundancy and also the capability of heading determination.

Figure 3.1:   Map of Test Area West of Calgary

The test track began with a coarse gravel pavement, and then runs east-west about 12 kilometres to intersect Highway 22. The road is mostly straight with an undulating profile. There is a slight swerve in the road at about 5 kilometres from the start of the road and there is a stop sign at about 4 kilometres from the start. A pillar was present beside the road approximately 5 kilometres along the track, which was used to set up a GPS reference station. This pillar was part of the Calgary Electronic Distance Measurement Calibration Baseline and coordinates are known to within a few centimetres. Figure 3.2 shows the test track. Note the extreme difference in the scales of the horizontal and vertical axes.
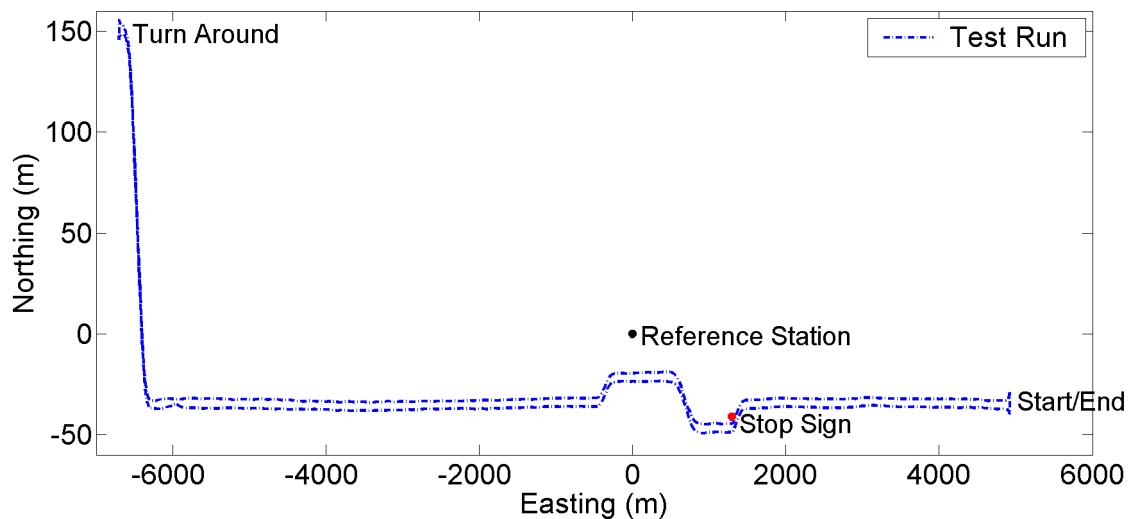
Figure 3.2:   Trajectory of a Vehicle on One Run

GPS code and carrier phase measurements were logged using NovAtel Beeline and OEM4 receivers connected to NovAtel 600 and 501 antennas as per Figure 3.3. The SiRF receiver was incorporated into the test setup to support another set of experiments and will not be further discussed. Figures 3.4 and 3.5 show one test vehicle with the typical instrument setup. The reference station consisted of a NovAtel 600 antenna and

OEM4 receiver. A second reference station was also set up at the University of Calgary Calgary Centre for Innovative Technology (CCIT) building using a NovAtel 600 antenna and OEM4 receiver. Data was logged at various rates, but was processed at 1 Hz.
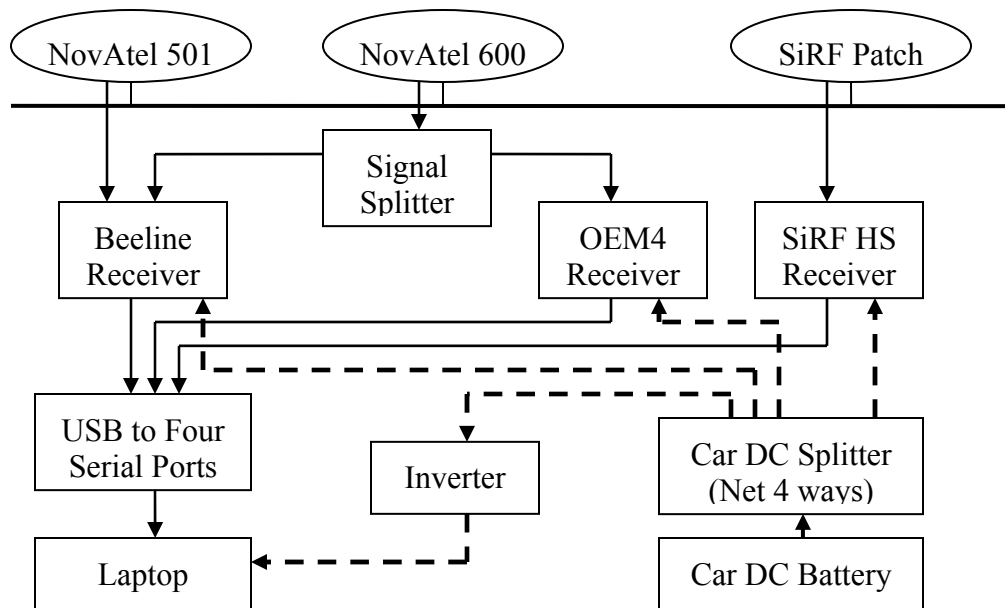
Figure 3.3: **Vehicle Equipment Setup**

Figure 3.4:   **Instrumented Test Van**

Figure 3.5:   Equipment inside Test Van

The test was carried out under different dynamic conditions. A total of three runs of the trajectory were made in the field. A static initialization of 15 minutes was performed at the start of each trip to make sure carrier phase ambiguities could be resolved before movement. In each test trip, three vehicles started from the beginning of the pavement and followed each other in a straight line on the test track. A fourth vehicle simulated different scenarios of joining, leaving, and passing the platoon.   The speed was maintained constant at different speeds ranging from 20 km/h to 90 km/h for various lengths of time.   The vehicles followed each other while maintaining a safe driving distance of approximately 2 seconds.

In the first trip, Vehicle 4 joined the platoon at the stop sign, about 4 kilometres from the start of the pavement, into the third position in the group, and left the platoon at about 6 kilometres from the start of the pavement. This is demonstrated in Figure 3.6. In the

second and third runs, Vehicle 4 joined at the stop sign, into the fourth position in the group. Vehicle 4 passed the entire group then soon slowed down allowing the entire group to pass it. This is demonstrated in Figure 3.7.
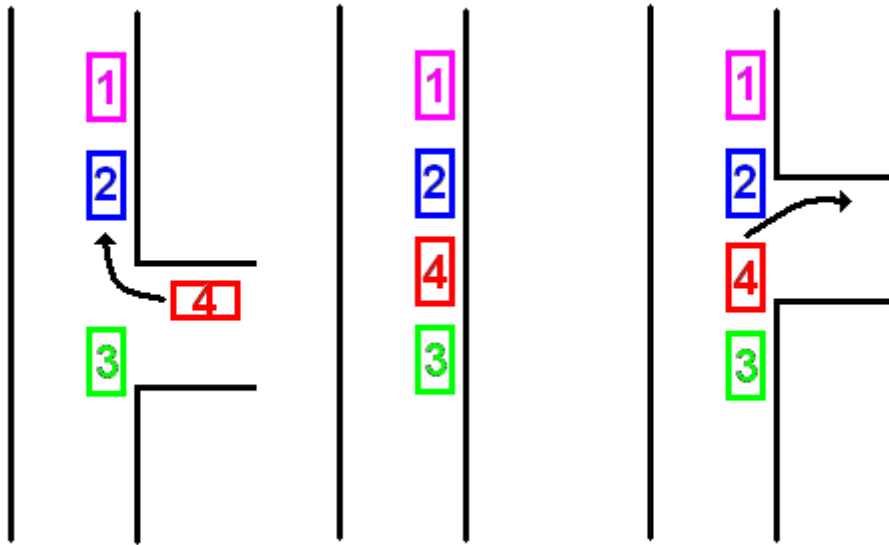
Figure 3.6: **Vehicle 4 Joins the Platoon then Leaves the Platoon**
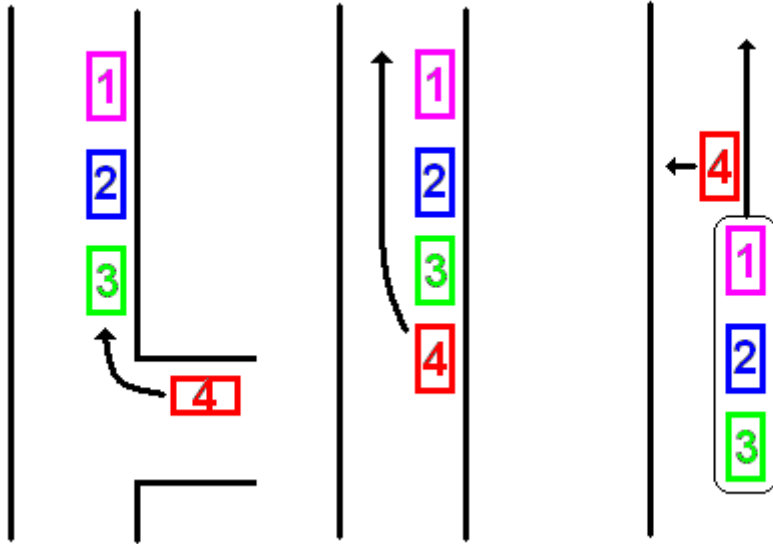
Figure 3.7: **Vehicle 4 Joins the Platoon, Passes the Platoon, and Lets the Platoon Pass**

3.2 Processing Techniques

Three different techniques were used in post-processing. Figure 3.8 illustrates these techniques.

In the first technique, processing was performed using the FLYKIN+^{TM} software developed by the University of Calgary. FLYKIN+^{TM} processes GPS data differentially using a Kalman filter, incorporating a wide variety of processing options (Liu 2003b). L1 only was used in this case since the distances to the field reference station were relatively short, along with a Hopfield tropospheric model, a 10 degree elevation mask, and an ambiguity fixing ratio threshold of 3. The field reference station was used as the reference station to compute positions and velocities of each antenna on each car. The inter-antenna vectors were then computed by differencing the positions. The relative

velocities were computed by differencing the velocities. These results will be referred to as the FLYKIN+^{TM} Static Base Station (SBS) results.

In the second technique, FLYKIN+^{TM} was modified to use a moving base station. In this way, relative position and velocity vectors between antennas could be directly computed without the need for a static reference station. This is likely how inter-vehicle positioning would be performed in a real application, since it circumvents the need for an extensive infrastructure of reference stations. These results will be referred to as the FLYKIN+^{TM} Moving Base Station (MBS) results. Again, L1 only was used.

The third technique uses the HEADRT+^{TM} software and was primarily used to confirm other results using a different software package. HEADRT+^{TM} is designed to compute the position vector and orientation parameters between two or more antennas on a rigid platform. This software uses sequential least-squares, attempting to compute fixed-ambiguity carrier phase positions (Lachapelle & Cannon 2002). A constraint of the approximate baseline between antennas is required, and was obtained by measuring the inter-antenna distance with a tape. Since a rigid platform is required, this software can not be used to compute inter-vehicle positions and velocities.

FLYKIN+™ SBS	FLYKIN+™ MBS	HEADRT+™
Positions and velocities of A, B, C, and D directly computed using static base station X. Inter-antenna position and velocity vectors B-A, B-C, and B-D computed as $R_{BA} = R_B - R_A$ $V_{BA} = V_B - V_A$	Inter-antenna position and velocity vectors B-A, B-C, and B-D directly computed using moving base station B.	Rigid platform position vector B-A (distance and attitude parameters) directly computed.

Figure 3.8:   Graphical Representation of Three Processing Techniques

Luo (2001) similarly performed SBS and MBS processing applied to moving vehicles. Approximately 5 to 7 centimetres of difference were found between the SBS and MBS positions.

All three techniques are usable in a real-time environment. For the static reference station approach, a smaller amount of information needs to be transferred from the reference station to the rover, since corrections to observations based on the reference stations known positions could be first computed and then transmitted. These corrections are fairly simply applied to the rovers observations. However, computations must be performed for both antennas, and then the difference computed. In the moving base station approach, a higher amount of information must be communicated, since the entire observation from the reference station should be transmitted. Alternately, an assumed position as well as corrections based on this assumed position could be transmitted. However, compared to the static base station approach, less processing must be performed, since only one baseline is being computed.

3.3   Single Vehicle Inter-Antenna Results

The system accuracy must be demonstrated in the position domain as well as the velocity domain. In order to do this, processing between two antennas on the same vehicle needs to be performed, as is discussed below. Besides position and velocity, another useful output is the vehicle attitude parameters, as discussed in section 3.3.3.

3.3.1   Inter-Antenna Position Accuracy

For this experiment, "truth" data is not available. Therefore, in order to assure positional accuracy, the relative position between the two antennas on each vehicle is examined. Since the antennas are not moving on the vehicle (a rigid platform), the magnitude of the three-dimensional vector between them is constant. Firstly, Figure 3.9 shows the components of the inter-antenna vector for one vehicle, clearly showing that the vehicle was oriented east-west with minimal northward and upward components, and that 180 degree turns periodically took place throughout the test. Figures 3.10 to 3.12 show

differences between the GPS-determined inter-antenna distance and the tape-measured distance using each of the three approaches for one representative vehicle.
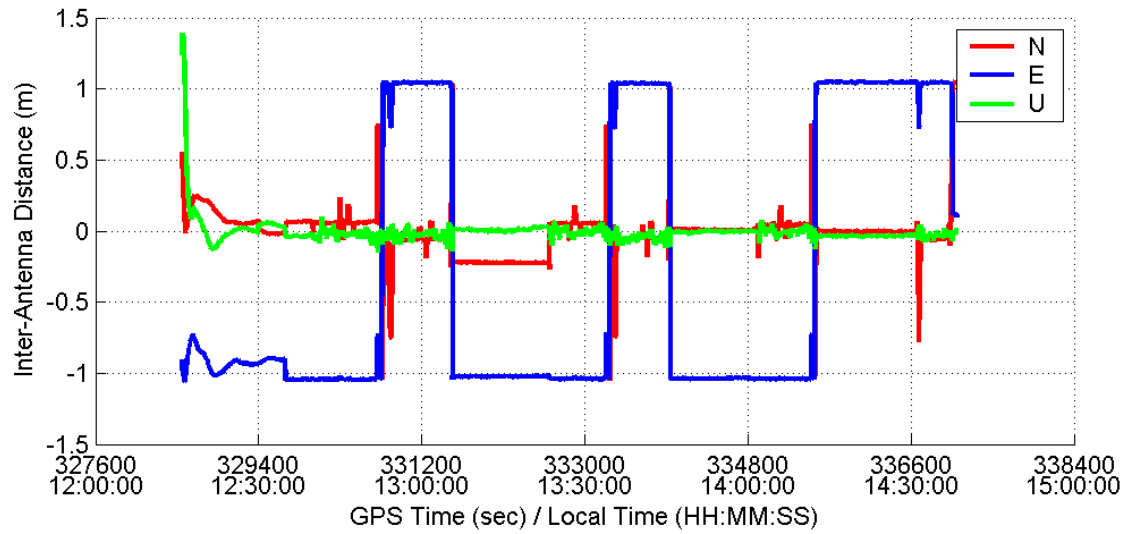
Figure 3.9: **Components of Inter-Antenna Vector for Vehicle 2 Using FLYKIN+**[TM] **SBS Approach**

Figure 3.10:   Magnitude of Inter-Antenna Vector for Vehicle 2 Using FLYKIN+™ SBS Approach Relative to Tape Measured Distance
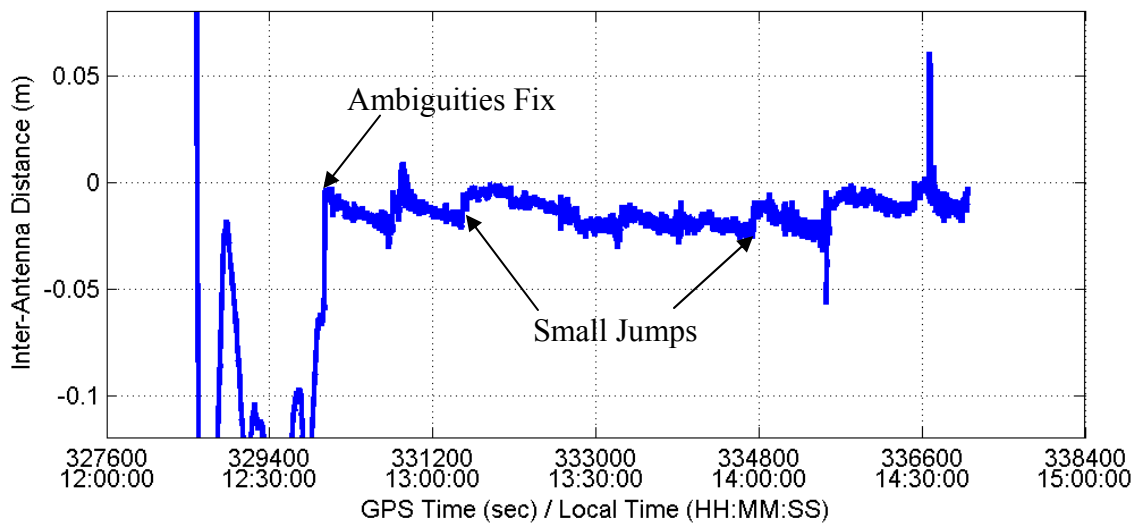
Figure 3.11:   Magnitude of Inter-Antenna Vector for Vehicle 2 Using FLYKIN+™ MBS Approach Relative to Tape Measured Distance
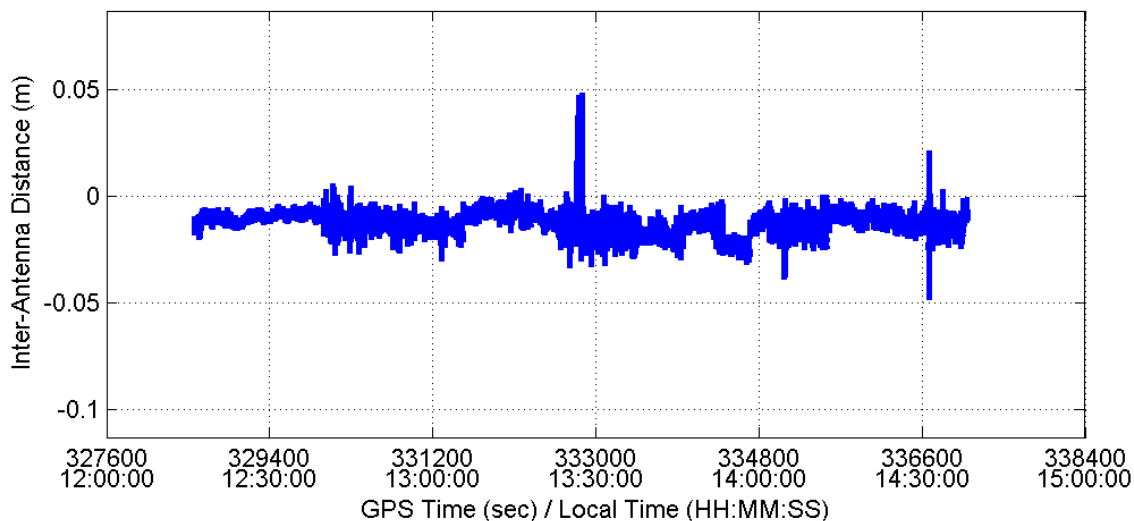
Figure 3.12:   Magnitude of Inter-Antenna Vector for Vehicle 2 Using HEADRT+^{TM} Approach Relative to Tape Measured Distance

It can clearly be seen in the figures that once the ambiguities are fixed, the inter-antenna position stays constant to within a few centimetres, using all three methods. The time taken to fix ambiguities is not necessarily representative, since the receivers underwent a full reset at different initial times, and plots begin as soon as any solution is available, even though the receiver is still trying to acquire satellites. Any bias from zero is likely due to the inaccuracy of the tape-measured distance. Less care was taken in the creation of this measurement than should have. The SBS approach appears more constant than the MBS approach. Examination of the small jumps in the MBS approach showed them to generally correspond with the vehicle turning around. For the MBS approach, the three components of the position difference between antennas are being estimated using a random walk process. This functions well when the vehicle is driving smoothly along the road, as each component of the position difference is changing only slightly. However, when the vehicle turns around, the northing and easting component of the relative position between antennas changes quite quickly. This is not well modelled by the

random walk process, and thus some estimation errors occur. These do not occur in the SBS approach, because the positions of each antenna relative to the base station are being computed. During the turns, these relative positions are not changing in a significantly different way than during the rest of the test. During a platooning session, manoeuvres such as 180 degree turns are unlikely to occur, so these small jumps should not be a problem for a CDS. The HEADRT+^{TM} results are slightly noisier than the other approaches. This is likely because a Kalman filter is not employed. The Kalman filter used in the FLYKIN+^{TM} approaches helps smooth the data by using information from previous epochs. Table 3.1 shows statistics on the plots above. A common time period of 13:00 to 14:00 local time was chosen for producing the statistics, during which ambiguities were fixed.

Table 3.1:   Statistics on Inter-Antenna Distance

Vehicle	Technique	Minimum (mm)	Maximum (mm)	Mean (mm)	Standard Deviation (mm)
1	SBS	-18	3	-8	2
1	MBS	-23	12	-3	5
1	HEADRT+™	-25	12	-8	4
2	SBS	-30	-7	-18	4
2	MBS	-31	0	-15	6
2	HEADRT+™	-33	49	-13	7
3	SBS	-26	-4	-13	2
3	MBS	-32	3	-9	5
3	HEADRT+™	-29	37	-12	3
4	SBS	-16	10	0	2
4	MBS	-19	18	2	6
4	HEADRT+™	-49	17	0	4

3.3.2   Inter-Antenna Velocity Accuracy

In a similar manner, since truth velocities are not available, the relative velocity between two antennas on each vehicle is examined. In this case, as long as the vehicle is not changing its orientation (turning or changing pitch), the velocity of each antenna should be identical. When the vehicle turns, the front antenna will have a higher velocity than the rear antenna. If the vehicle drives over a bump, or starts or finishes climbing a hill, the velocity of each antenna will be slightly different. Figures 3.13 to 3.15 show the

relative velocity between antennas determined from GPS. The magnitudes were formed as the square root of the sum of squared components of the velocity difference. Results are shown for one representative vehicle, using the FLYKIN+^{TM} SBS and MBS approach. HEADRT+^{TM} does not produce velocity results.
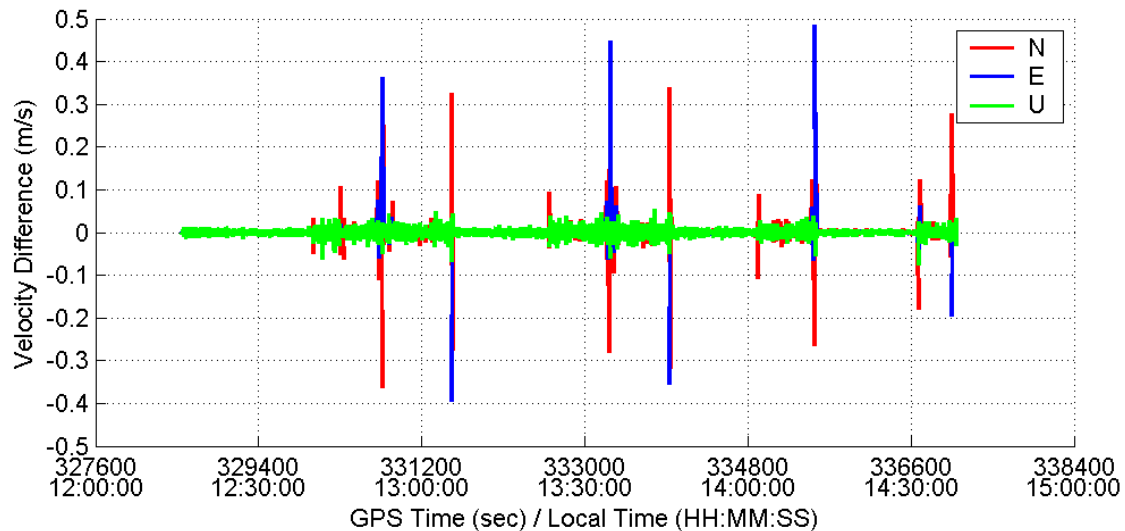

Figure 3.13: Components of Inter-Antenna Velocity for Vehicle 2 Using FLYKIN+^{TM} SBS Approach
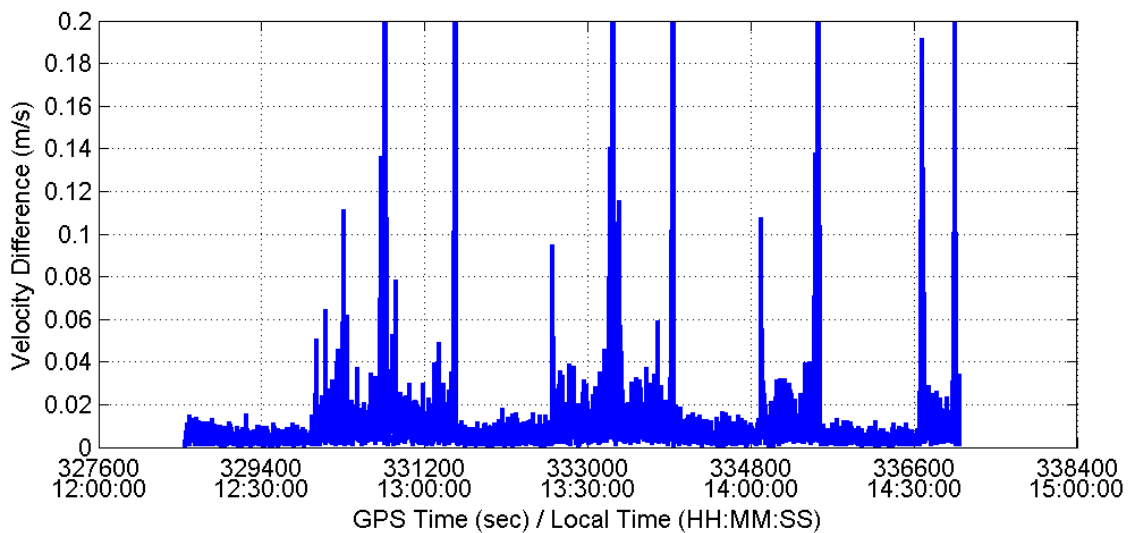
Figure 3.14: **Magnitude of Inter-Antenna Velocity Difference for Vehicle 2 Using FLYKIN+**[TM] **SBS Approach**
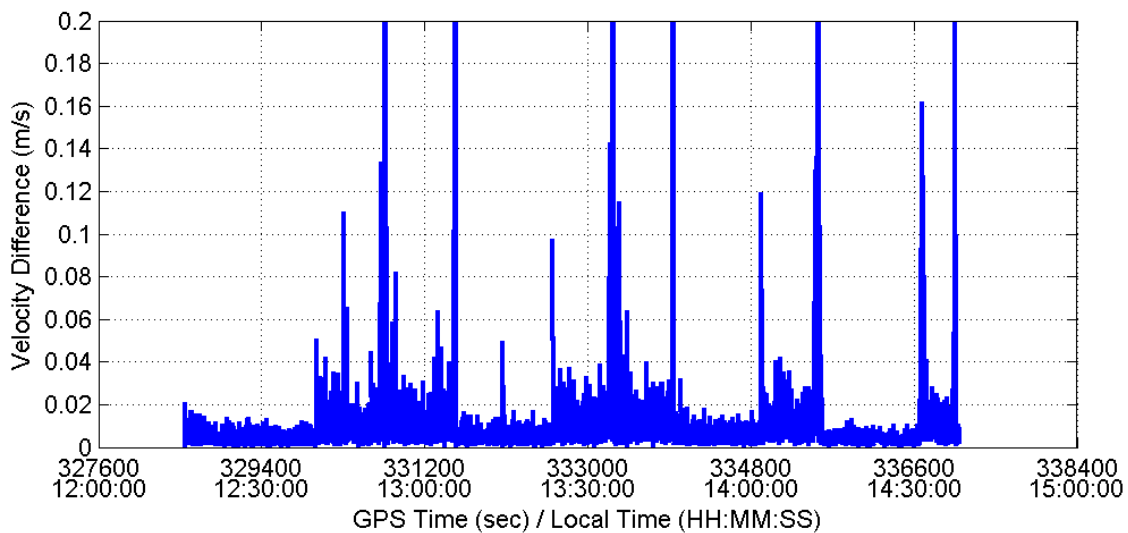
Figure 3.15: **Magnitude of Inter-Antenna Velocity Difference for Vehicle 2 Using FLYKIN+**[TM] **MBS Approach**

The plots of relative velocity demonstrate a few interesting results. First, the relative velocity is near zero for the majority of the plot. This is what should occur when the vehicle is not changing orientation, and demonstrates the accuracy with which GPS can determine velocity. The relative velocity is extremely close to zero during those periods of time when the vehicle is not moving, since the orientation is guaranteed to not change. During motion, the trajectory is roughly constant east-west, but there will always be small bumps, dips or turns encountered by the vehicle, and as a result the relative velocity is above zero. Statistics will not be presented, since they would not be representing the accuracy of GPS velocity estimation. From the plots, it is safe to say that the accuracy is within one or two centimetres per second. Large spikes can be seen in the plots at the times that the vehicles turned around at the start and end of the test trajectory. These are fully expected, as during turns the front and rear antennas will move at different speeds. Also noteworthy is the fact that the FLYKIN+^{TM} SBS and FLYKIN+^{TM} MBS approach provide very similar results.

3.3.3   Vehicle Attitude Determination

Attitude determination is important in platoon control as the azimuth of the vehicle gives the direction in which the platoon, or an individual vehicle, is traveling. If a vehicle leaves or intends to leave, the relative heading between the individual vehicle and the majority of other vehicles in the platoon starts to change. Similarly, pitch information is useful in supplying the terrain information to the trailing vehicles if the platoon length is long. Also the time lag between the vehicles can be estimated by examining the attitude trends of the different vehicles in a platoon.

At least two GPS receivers are required to determine pitch and azimuth (or heading) accurately. Over a baseline of just a few metres, code measurements do not provide sufficient accuracy for attitude determination. Carrier phase measurements can be used in estimating attitude because of their centimetre-level measurement accuracy. The use

of carrier phase measurements results in the ambiguity problem of carrier phase integer cycles. Most attitude determination techniques based on GPS carrier phase measurements involve two sequential steps, ambiguity resolution and attitude estimation (Wang 2003). The accuracy of GPS-derived attitude components is a function of many factors, the major ones being the accuracy of the carrier phase observable, the magnitude of multipath, and the distance between the antennas (Lachapelle et al 1996).

The attitude computation was done using the HEADRT+™ software. The NovAtel 600 antenna mounted on the front of the vehicle was used as the primary antenna and the NovAtel 501 antenna mounted on the rear of the vehicle was used as the secondary antenna in computations. The L1 data collected by the Beeline receiver (two antenna inputs) was used for the attitude determination.

Figure 3.16 shows the variation of heading with time. The horizontal section of the curve shows the vehicle traveling on the highway. The vertical jump in the heading curve is due to a U-turn taken by the vehicle. Other variations from a straight line are due to small curves on the road. There is a change of 180 degrees in the heading when the car moves in the opposite direction after the U-turn. The curve repeats itself periodically due to multiple test runs on the same road. The small jump before the U-turn is due to a curve in the road.
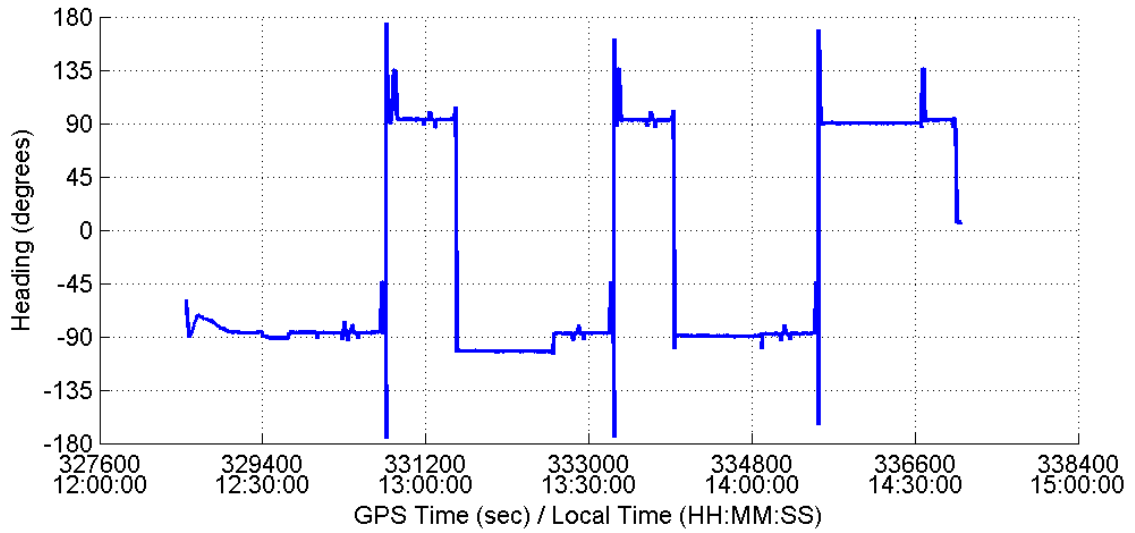
Figure 3.16:   Variation of Vehicle Heading with Time

The pitch of the vehicle as shown in Figure 3.17 is close to zero with small variations due to undulation on the roads. Again there is a periodicity in the curve due to the repetition of the road terrain. This information can be used effectively as a means to prepare for uphill and other terrain variations.
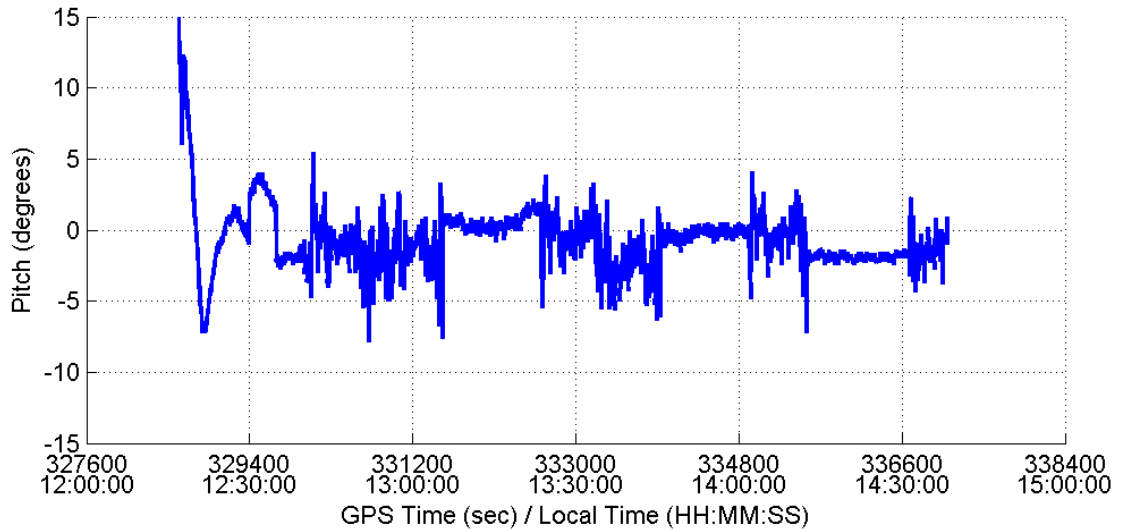
Figure 3.17:   Variation of Vehicle Pitch with Time

Figure 3.18 shows the time lag between the vehicles following each other by showing a lag in the heading curves. Biases exist between the curves because of the local orientation of the antennas on the car body. The two antennas were approximately in-line with the vehicle heading, but were not perfectly so. Since Vehicle 1, the test van, had a roof rack, there is a minimal bias in heading as they are travelling due west. It is clear that firstly Vehicle 1 makes a manoeuvre, and this same manoeuvre is soon performed by Vehicle 2, then Vehicle 3, and finally Vehicle 4.
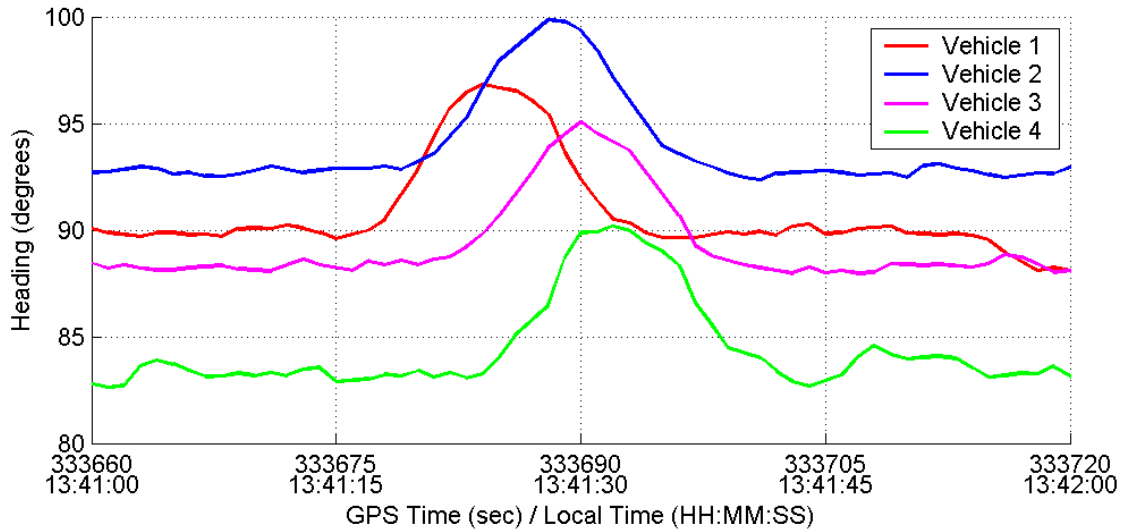
Figure 3.18: Time Lags in Heading Curves of Vehicles in a Platoon

3.4 Inter-Vehicle Results

The manoeuvres performed by the vehicles show many interesting results as discussed below.

3.4.1 Positioning Vehicles in a Platoon

Positioning each vehicle with respect to all other vehicles in a platoon is essential for successful implementation of the CDS concept. In this section, a simple driving scenario from the third test run (shown in Figure 3.7) is presented and the GPS data is analysed. The third vehicle is considered the host vehicle for the analysis and FLYKIN+[TM] MBS output is used. The scenario involves all vehicles traveling westward on a straight road with approximately east-west orientation. Vehicles reduced their speed to be close to zero at a stop sign where Vehicle 4 joined, as shown in the speed profile in Figure 3.19.

Figure 3.19 shows a plot of Vehicle Speed (km/h) on the y-axis versus GPS Time (sec) / Local Time (HH:MM:SS) on the x-axis. An annotation reads: "Vehicles reduce speed near stop sign where Vehicle 4 joins the platoon"
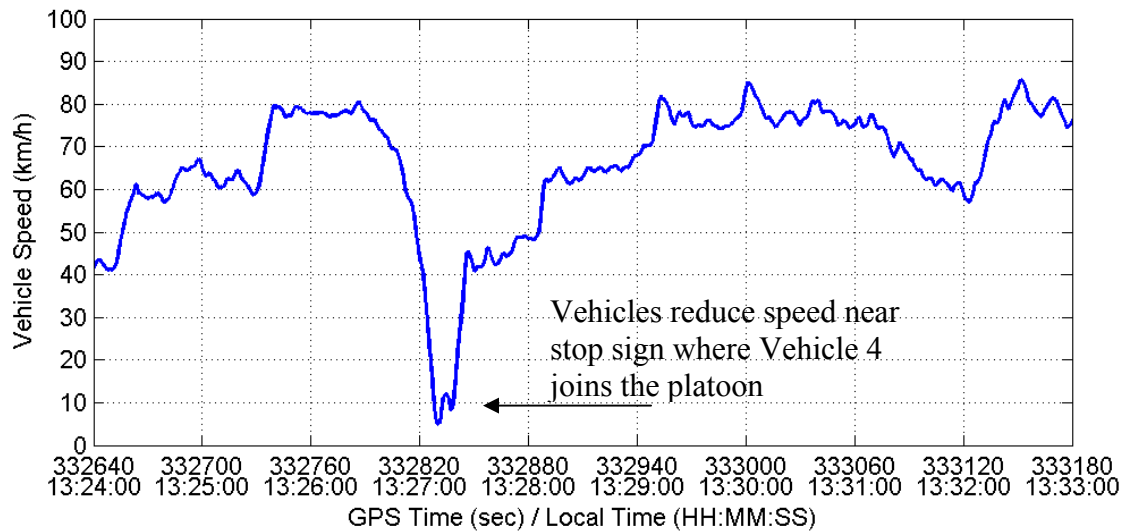
Figure 3.19:   Speed of Vehicle 3 during One Run

Based on the east component of relative distance shown in Figure 3.20, the host vehicle can position Vehicles 1 and 2 in front of it throughout the scenario. Based on the relative distance observed in the north direction in Figure 3.21, these two vehicles can be positioned in the same east-west roadway as the host vehicle. According to the relative velocity data provided in Figures 3.22 and 3.23, Vehicles 1 and 2 travel in the same platoon of vehicles with the host vehicle. Data in Figures 3.20 to 3.23 can provide the host vehicle with all the data necessary to position it safely in the three-vehicle platoon.

Observations made by the host vehicle to Vehicle 4 provide similar data to safely integrate Vehicle 4 into the platoon and later switch back to a three-vehicle formation. As a first step of this manoeuvre, the three-vehicle platoon approaches Vehicle 4 which is waiting beside the road at a stop sign, approximately 10 metres south of the road, at a high relative velocity as shown in Figures 3.21 and 3.22, respectively. The three-vehicle platoon is then joined by Vehicle 4, indicated by positive relative eastward distance in Figure 3.20. Vehicle 4 then passes all three vehicles as indicated by westward relative

distance in Figure 3.20. Vehicle 4 acts as the platoon leader for approximately 3 minutes. All three vehicles pass Vehicle 4 concluding the manoeuvre towards the end.
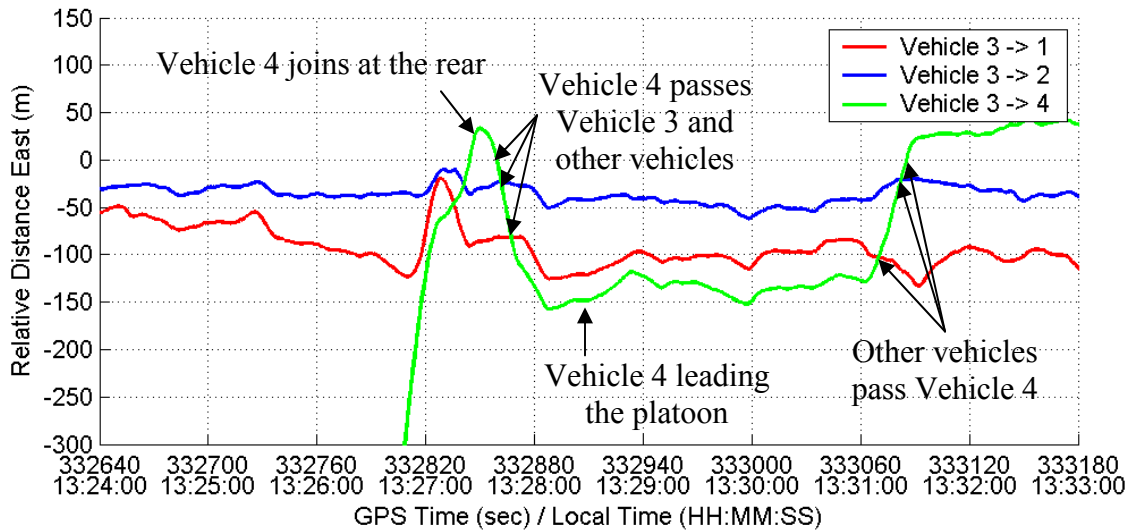
Figure 3.20:   Relative Distances East
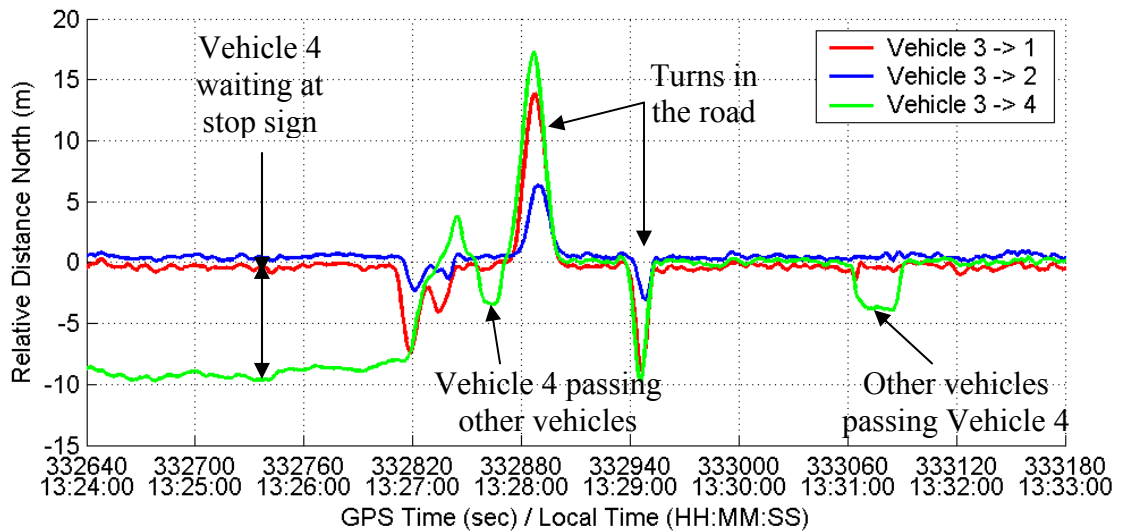
Figure 3.21:   Relative Distances North
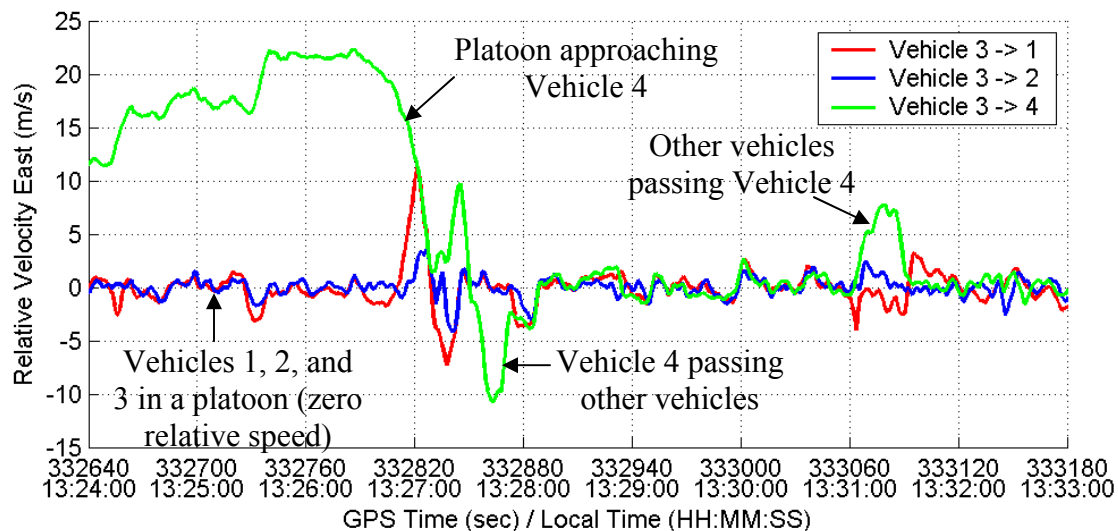
Figure 3.22: Relative Velocity East
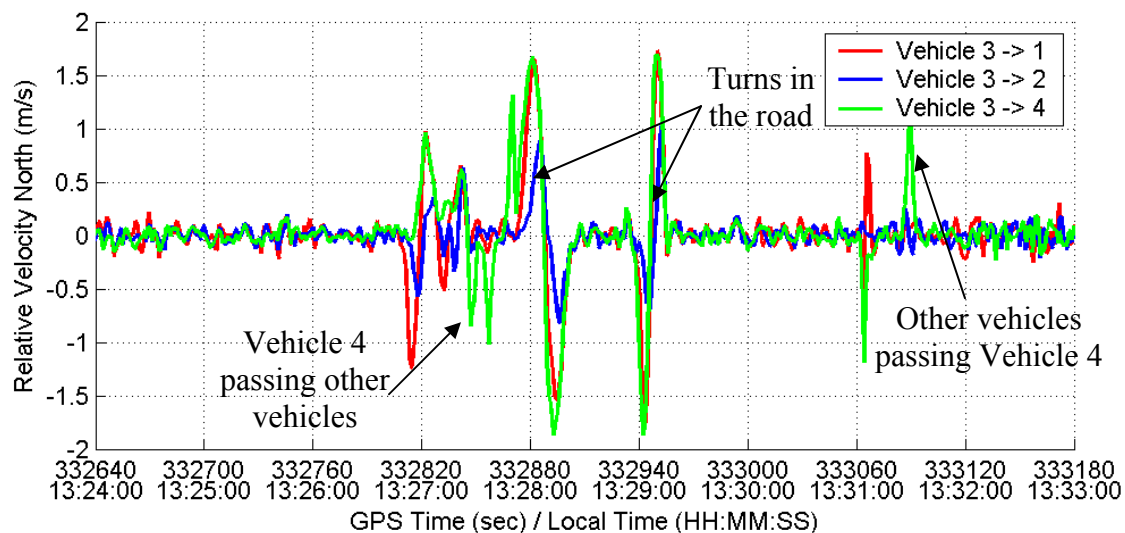
Figure 3.23: Relative Velocity North

3.4.2 Passing Vehicles in a Platoon

Driving in a platoon involves passing and changing lanes, as well as joining and leaving platoons. A passing manoeuvre requires very accurate measurement of distances and

velocities of all vehicles involved in the manoeuvre. A typical scenario is presented in this section with measurements provided by the GPS subsystem of the passing vehicle. The third component of the manoeuvre shown in Figure 3.7 is analysed. Vehicles are traveling westbound. Vehicle 4 begins in the lead position, then changes lanes, slows down while the entire platoon passes, and then rejoins the platoon in the rear position. The path followed by the vehicle in the passing manoeuvre is illustrated in Figure 3.24 and the path is segmented to three sections, which will be illustrated with heading observations from the passing vehicle. In a CDS, the decision to pass will be made based on relative speeds and distances of other vehicles in the platoon. Onboard systems in the passing vehicle will assess the measurements and make a decision to pass other vehicles using its control systems.
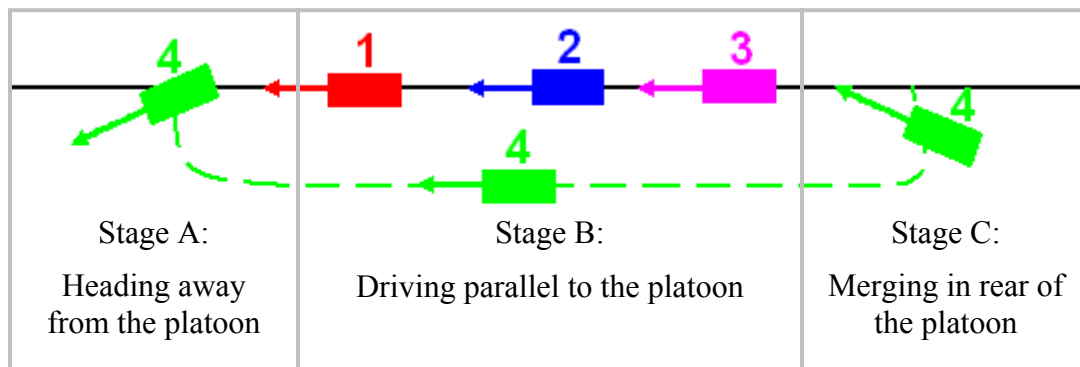
Figure 3.24: Stages in the Passing Manoeuvre

Figure 3.25 illustrates the heading observations of each vehicle during the manoeuvre, as determined by HEADRT+^{TM}. Correspondence is shown with the stages of the manoeuvre shown in Figure 3.24. Observations for Vehicles 1, 2 and 3 show approximately constant values throughout the manoeuvre. However, they all have biases unique to individual vehicles as a result of local frame orientation differences. The heading of Vehicle 4 shows two spikes of approximately 3 degrees around 20 seconds apart. These correspond to the start and the end of a passing manoeuvre as Vehicle 4

deviated in and out of the constant heading direction. From a CDS point of view, Vehicles 1, 2 and 3 can sense the passing manoeuvre using heading data from the subsystem of Vehicle 4 if this is communicated between vehicles, giving them a vision of activities in the platoon.
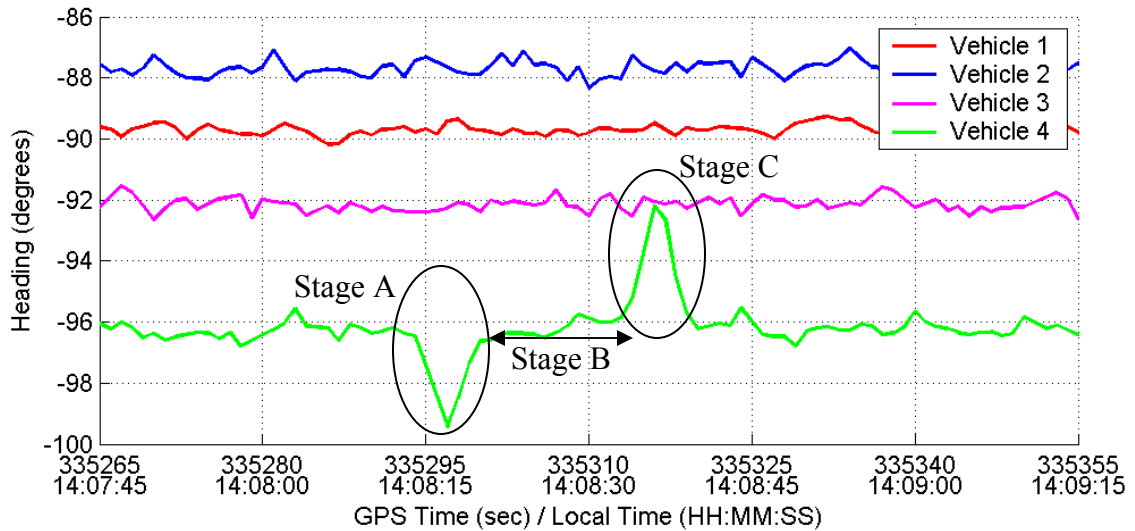
Figure 3.25:   Vehicle Headings during a Passing Manoeuvre

The relative position measurements from the sensor subsystem in Vehicle 4 are illustrated in Figures 3.26 and 3.27. Once the decision is made by Vehicle 4 to pass other vehicles, monitoring relative distances and velocities during the manoeuvre is critical for a successful execution of the manoeuvre. In this case vehicles were heading due west, therefore eastward measurements may be considered along-track, while northward distance measurements may be considered across-track. Figures 3.26 and 3.27 illustrate across-track (north) and along-track (east) relative distances from Vehicle 4 to Vehicles 1, 2 and 3 during the manoeuvre, as determined by the FLYKIN+^{TM} MBS output.
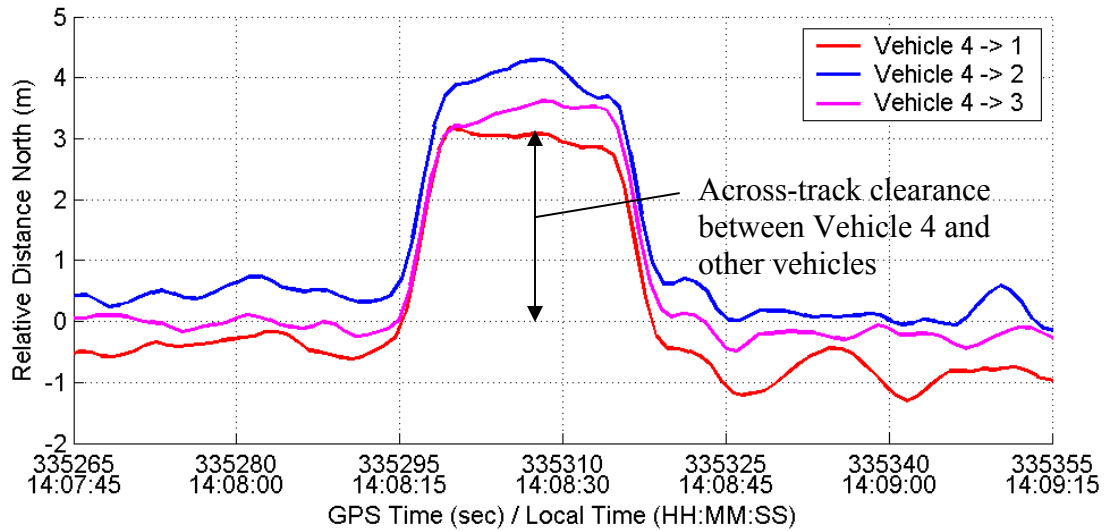
Figure 3.26:   Relative Distance North (Across-Track) during Passing Manoeuvre
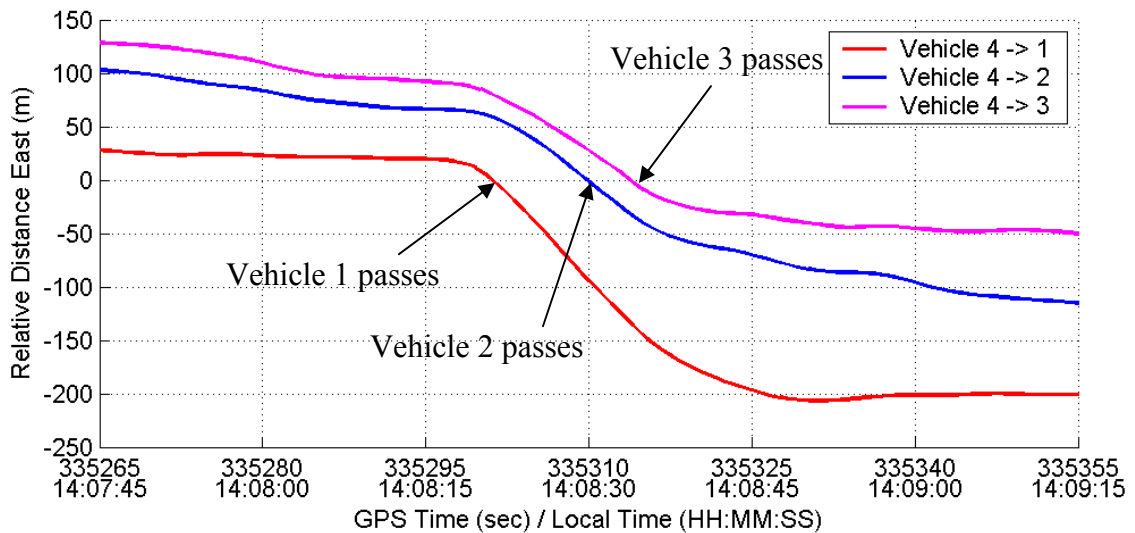
Figure 3.27:   Relative Distance East (Along-Track) during Passing Manoeuvre

The across-track and along-track measurements in Figures 3.26 and 3.27 combine to give Vehicle 4 a continuous update on the progress of the passing manoeuvre. For instance, the northward measurements show at least a 3 metre across-track clearance from all three

vehicles as the manoeuvre starts. This is followed by Vehicle 1 passing, which is indicated by the change in along-track relative distance of Vehicle 1 from positive to negative in the eastward direction (increase in along-track distance westward). Similarly, Vehicles 2 and 3 passed a few seconds later.

Sensing relative velocity to each vehicle is also necessary to successfully execute the passing manoeuvre. Relative velocity measured by Vehicle 4 during the manoeuvre, using the FLYKIN+^{TM} MBS output, is shown in Figures 3.28 and 3.29. Relative velocities of all three vehicles that passed Vehicle 4 show spikes of approximately 1 metre per second across-track velocity (measured as the northward component) at the start and the end of the manoeuvre perfectly overlapping with heading changes shown in Figure 3.25. The along-track relative velocity component also shows up to a 10 metre per second relative velocity during the passing manoeuvre. This measurement is critical in a CDS as the acceleration needed to clear the passed vehicles and rejoin in front will depend on it.
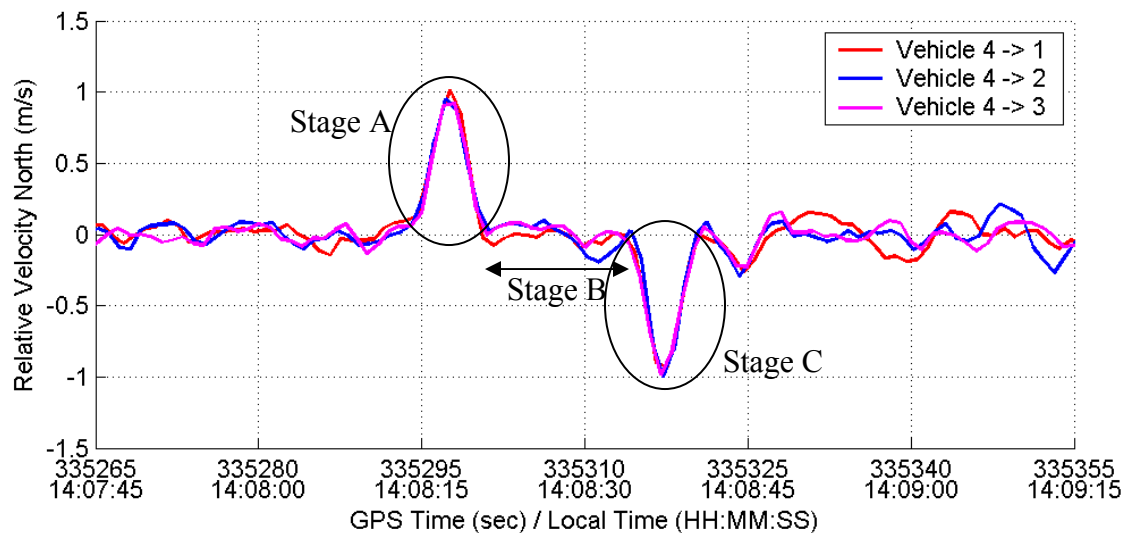
Figure 3.28: Relative Velocity North (Across-Track) during Passing Manoeuvre
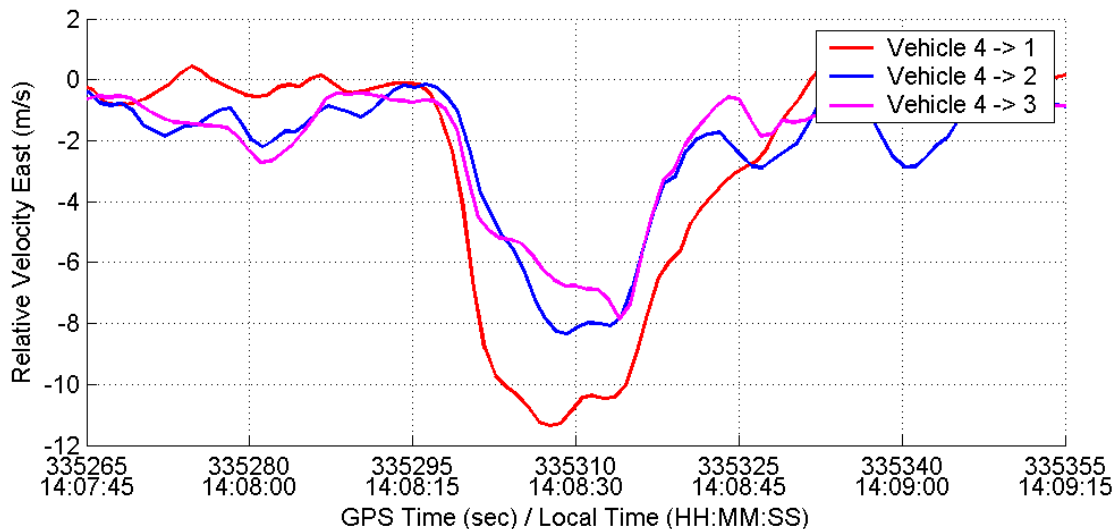
Figure 3.29: **Relative Velocity East (Along-Track) during Passing Manoeuvre**

3.4.3 Accuracy Over Long Distances

System accuracy is a critical issue in a CDS sensor subsystem. The system's accuracy in a platoon formation was illustrated previously; this section investigates the impact of vehicle-to-vehicle distance on the accuracy of measurements. The scenario is illustrated in Figure 3.30.
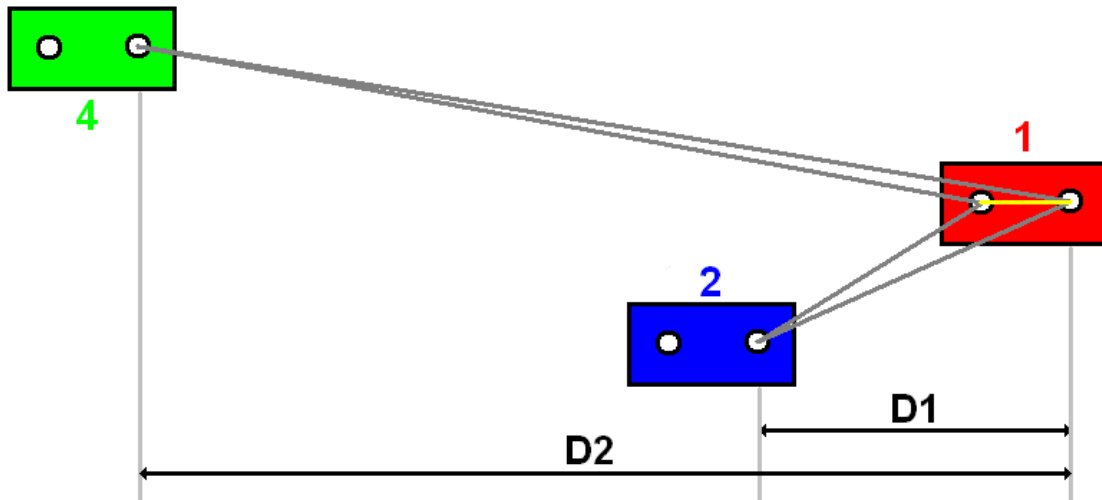
Figure 3.30: Computation of Inter-Antenna Vector on Vehicle 1 Using Other Vehicles as Base Stations at Varying Distances

In this scenario, the two antennas on the first vehicle are known to be a constant distance apart. The positions of each antenna relative to a reference station can be computed, and then differenced in order to give this inter-antenna measurement. This can be performed using a reference station on a nearby vehicle, as well as using a reference station on a farther away vehicle. Figure 3.31 illustrates the inter-antenna distance on Vehicle 1 as observed from Vehicles 2, 3, and 4 during the test. FLYKIN+^{TM} MBS output was used for this analysis. This shows centimetre-level accuracy for all three vehicles over the entire time.
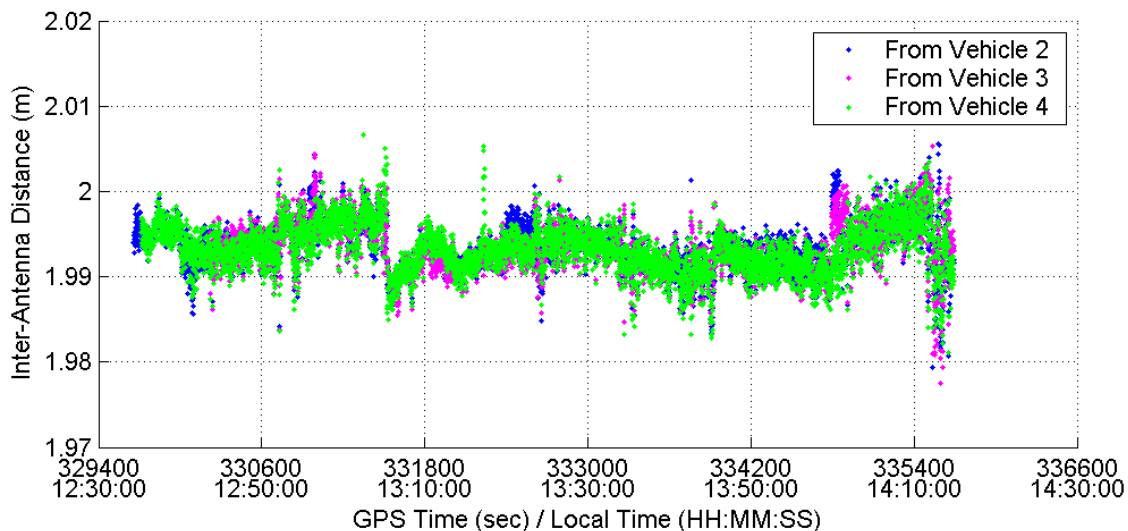
Figure 3.31: Inter-Antenna Baseline on Vehicle 1 Measured From Other Vehicles with respect to Time

The same inter-antenna baseline observation is plotted as a function of vehicle-to-vehicle distance in Figure 3.32. The accuracy of differential GPS is known to decrease as the distance between the reference and rover antenna becomes large. For this test, Vehicles 2 and 3 were close to Vehicle 1 the entire time, so all their measurements are near the beginning of the plot. The maximum distance observed between vehicles was around 7200 metres, which was between Vehicles 1 and 4. For this distance, the antenna baseline accuracy remained the same. This shows a very important advantage a GPS-based system would have over other systems that have a limited range. Figure 3.33 shows the inter-antenna distance for positions computed from the U of C base station, which was much farther away. Accuracy seems to decrease a bit at longer ranges, but not excessively, and this is longer range than would be expected to occur in a platoon.
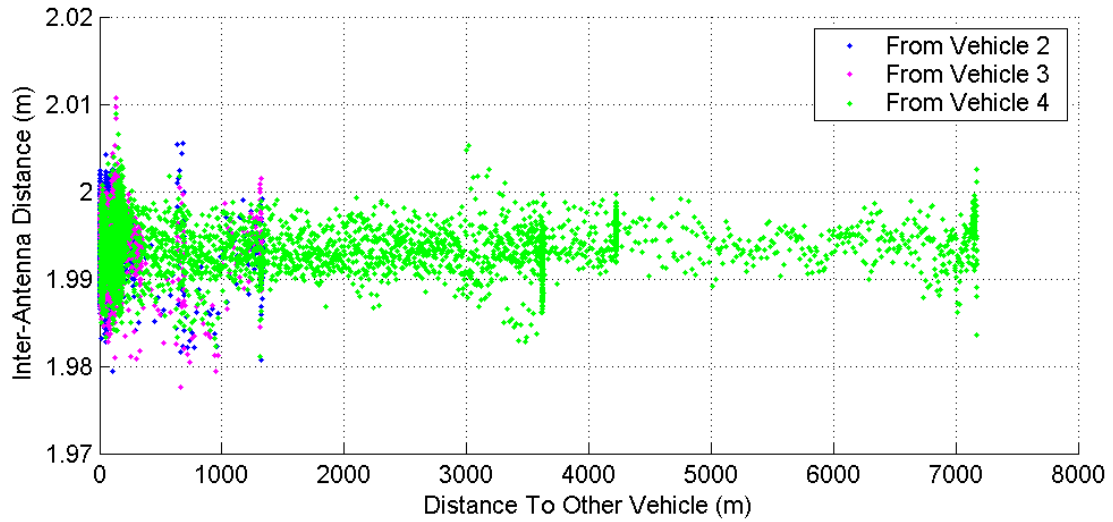
Figure 3.32: **Inter-Antenna Baseline on Vehicle 1 Measured From Other Vehicles with respect to Distance From Other Vehicle**
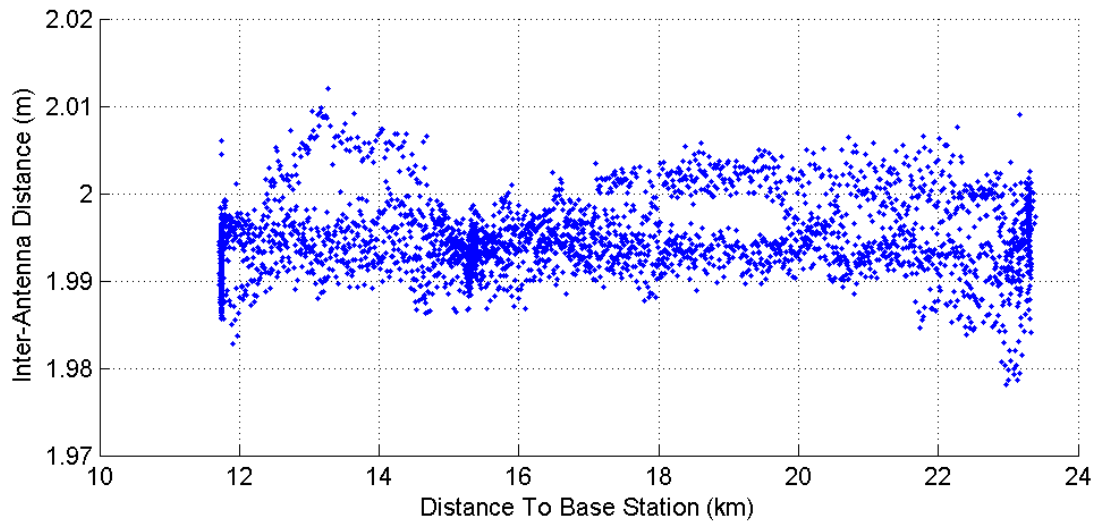
Figure 3.33: **Inter-Antenna Baseline on Vehicle 1 Measured from U of C Base Station with respect to Distance From Base Station**

In the relative velocity domain, comparable accuracies were obtained as illustrated in Figures 3.34 and 3.35. Apart from spikes in relative velocities resulting from turns, Figure 3.34 illustrates centimetre-per-second-level relative velocity accuracy between the two antennas in Vehicle 1 as observed from Vehicles 2, 3 and 4. Figure 3.35 shows that there is no accuracy degradation in observed velocities of antennas in Vehicle 1 as Vehicle 4 travels up to 7200 metres from Vehicle 1. Figure 3.36 shows that there is a slight reduction in accuracy when the baseline to the U of C station is 12 to 23 kilometres, though the error is still only a few centimetres per second.
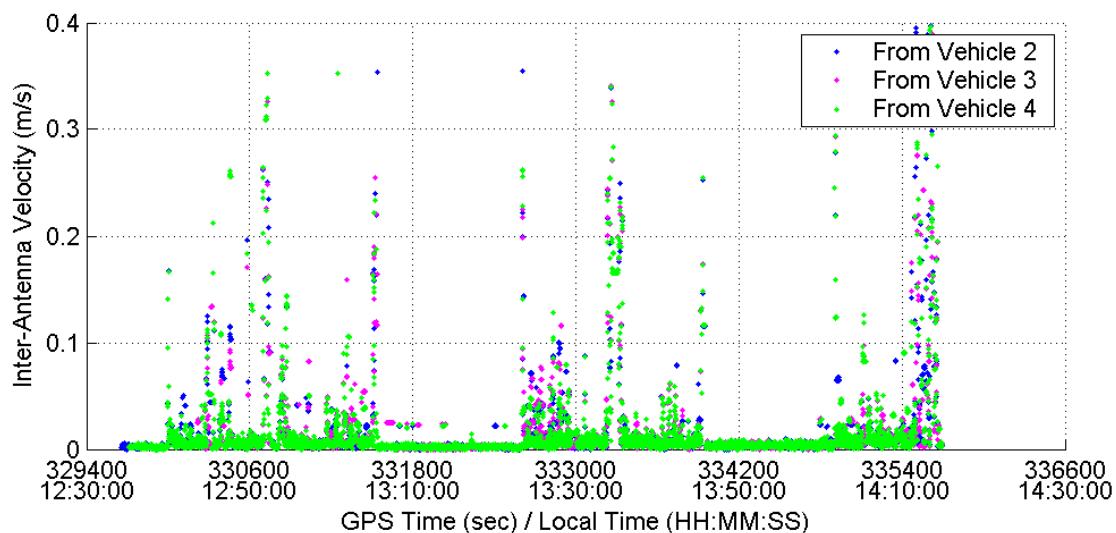
Figure 3.34: Inter-Antenna Velocity on Vehicle 1 Measured From Other Vehicles with respect to Time
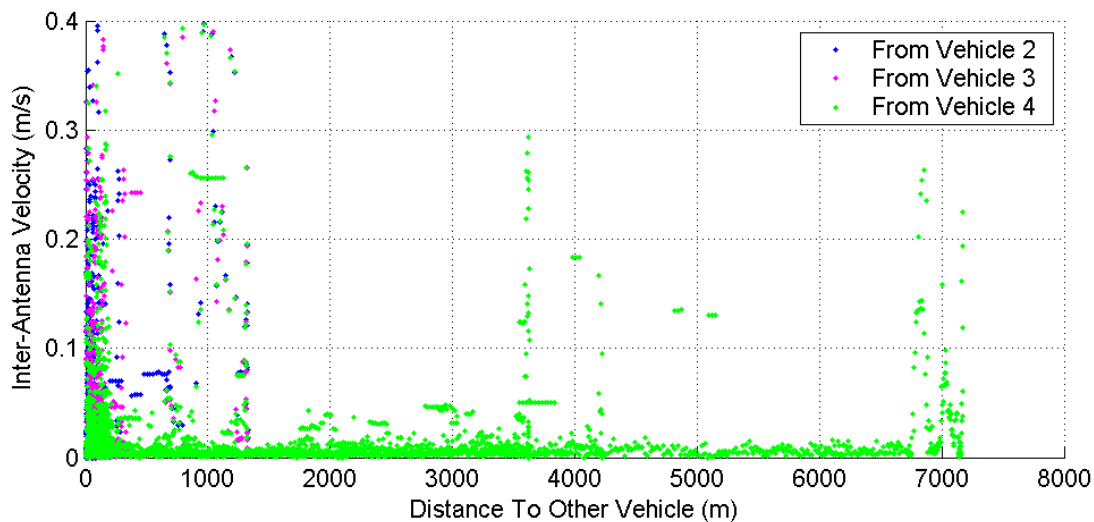
Figure 3.35: **Inter-Antenna Velocity on Vehicle 1 Measured From Other Vehicles with respect to Distance From Other Vehicle**
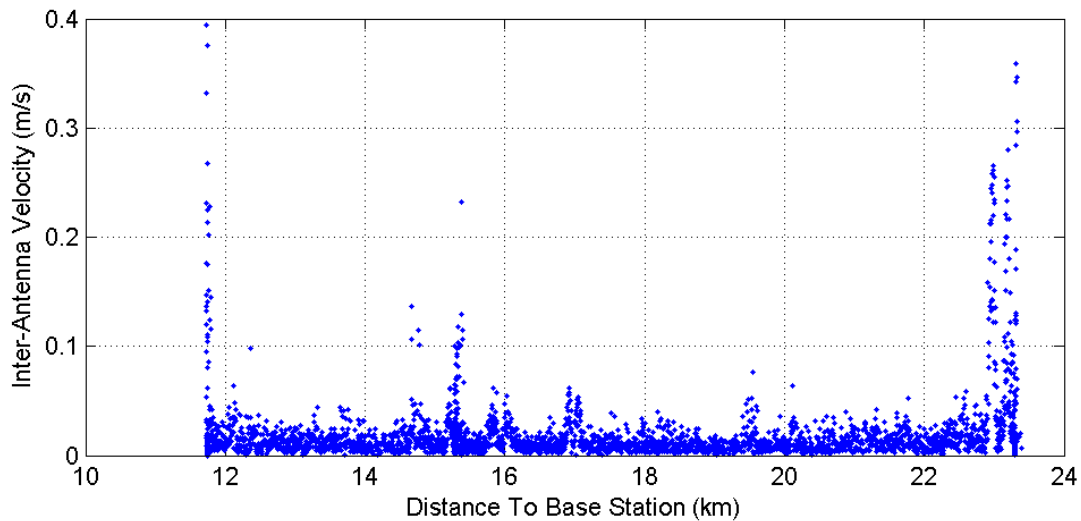
Figure 3.36: **Inter-Antenna Velocity on Vehicle 1 Measured From U of C Base Station with respect to Distance From Base Station**

3.5   Conclusions Regarding GPS as a CDS Sensor

A proof of concept field data analysis was presented for a precise GPS-based sensor subsystem for controlling platoons of vehicles as a part of a CDS.   Results of several innovative GPS-based precise positioning techniques such as the moving base station carrier phase processing technique are presented.   The results presented show the strengths of precise GPS in providing centimetre-level accuracy for positioning vehicles in a platoon formation.

The advantages provided by GPS with a moving base station positioning approach over alternative relative positioning techniques are illustrated.   GPS enables a vehicle in the platoon to position vehicles beyond the one immediately in front, which is critical in stability of vehicle platoons.   An analysis of relative positioning accuracy degradation with the distance between vehicles is also presented.

The results prove the fact that even though availability would become an issue in vehicle navigation in urban areas and other signal-blocking conditions, GPS can provide centimetre-level relative positioning capability and centimetre per second relative velocity determination under open sky conditions, which is the case for many highways where vehicle platoon control becomes a possibility.

4 Robot Test and Results

Since GPS has been shown to be a useful sensor for a CDS, the next step is to test it on a low cost test bed. For this purpose, mobile robots at the University of Sherbrooke were used. The Laboratoire de Recherche en Robotique Mobile et Systèmes Intelligents (LABORIUS) group in the department of Electrical and Informatics Engineering, University of Sherbrooke, is already involved in the Auto 21 Collaborative Driving project, and has been using these mobile robots in research. Control software has been developed for the robots, allowing them to be remote controlled, as well as having a robot autonomously follow a lead robot. Originally, the only sensor used in the autonomous following algorithm was a digital camera. This research sought to add GPS as well as other potentially useful sensors onto the robot platforms. These sensors were to be used individually and in combinations.

This research is solely devoted to evaluating the sensors, and will not become involved in researching the various forms of communication, or decision-making processes for the robots. The following sections discuss the equipment used and how it was used, how the data was processed, the tests performed and the results obtained.

4.1 Equipment

The equipment used was restricted by the availability of sensors within LABORIUS and the Position, Location, and Navigation (PLAN) group in the department of Geomatics Engineering, University of Calgary. Table 4.1 shows the equipment that was used on each of the robots. There was one lead robot and one follower robot, since there was not enough equipment available to reliably have a second follower robot.

Table 4.1:   Sensors on the Robots

Sensor	Leader	Follower
GPS	Yes	Yes
Laser	No	Yes
Camera	No	Yes
Sonar	Yes	Yes

The presence of each sensor on each robot is fairly straightforward. GPS must be present on both the leader and the follower in order to relatively position them. The laser is present solely on the follower, as it detects range to the leader. No laser is present on the leader, as it would not give any additional information in this setup. In a real situation, all vehicles could potentially be leaders at some point, and therefore all would be equipped with a laser. Also, the laser could be used as an additional sensor for obstacle avoidance. The laser could not be mounted facing backwards due to physical constraints. Similarly with the camera; the follower attempts to see the leader but there is nothing ahead of the leader to try to see, so the camera is only present on the follower.. As a corollary, a coloured cylinder is present on the rear of the lead robot, in order to facilitate the follower's vision functions. Sonar is present on both robots primarily because it was built in to the robots. The robots have forward facing as well as rearward facing sonars, so the leader might detect the follower at the same time as the follower detects the leader. A photo showing both robots is given in Figure 4.1. A diagram showing the equipment on the follower robot is given in Figure 4.2. The lead robot was similarly equipped, though without the laser and camera being active.

Figure 4.1: **Photo of Leader and Follower Robots**
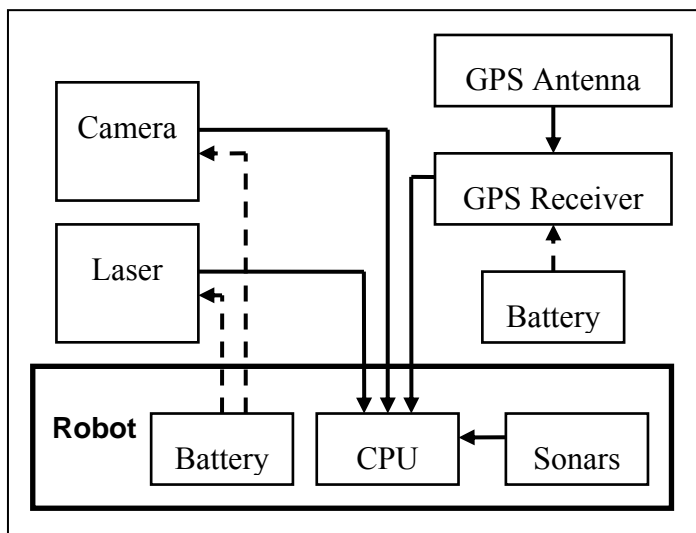
Figure 4.2: **Layout of Sensors on Follower Robot**

4.1.1 Robots

Most importantly, the robots used in this experiment must be described. They are Pioneer 2 – AT robots from ActiveMedia Robotics (ActiveMedia 2003). These robots have four wheels and a substantial platform on which sensors can be mounted. They have an array of eight front facing and eight rear facing sonars built in. Three serial ports allow for other sensors (GPS, camera, and laser in the follower's case) to be connected. A central processor as well as a hard drive and a wireless Ethernet for communication are also built in. The LABORIUS group has used these test platforms for several collaborative driving experiments (Michaud et al 2002, Lemay et al 2004).

4.1.2 GPS

The GPS units used on each robot are NovAtel DL-4 receivers, with NovAtel 702 antennas. This combination yields code measurements on L1 and carrier phase measurements on L1 and L2. Observations can be made at a maximum rate of 20 Hz. In addition to raw range measurements, ephemeris data was collected, as well as internally computed single point positions of each robot. More detailed specifications can be found at NovAtel (2003a) and NovAtel (2003b).

As mentioned previously, differential carrier phase observations with fixed ambiguities are required to provide sufficient accuracy. Differential processing is performed between robots, thereby eliminating the need for a static reference station. However, a static reference station was used to collect data to check results. A drawback of GPS is that line-of-sight to satellites is required from both robots. Another drawback is that although GPS provides high accuracy distance and azimuth observations between two antennas, we are interested in the local angle between robots, not the azimuth. In order to obtain this local angle from the azimuths, heading is required, as shown in Figure 4.3. Since only a single antenna GPS system is used, heading can not be determined as it was in the

vehicle test described in section 3 of this thesis. Instead, heading can be obtained using GPS when the robot is moving, by examining the velocity vector, which will have the same direction as heading. However, this is fairly poor accuracy when the robot is moving slowly, and is completely nonexistent when the robot is stationary.
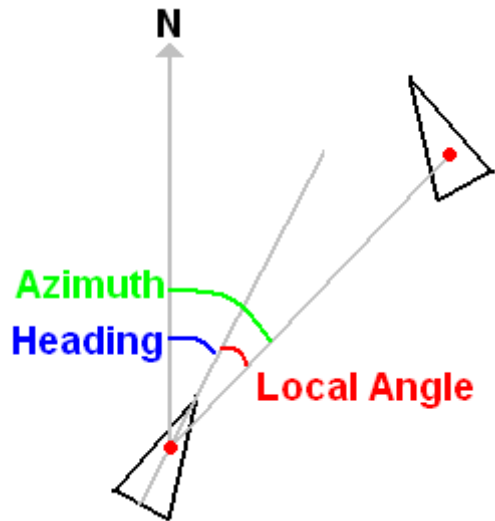
Figure 4.3:   Relationship Between Azimuth, Heading, and Local Angle

4.1.3   Camera

The camera is a Sony EVI-D30 PTZ camera. An Imagenation PXC200 frame grabber was used to capture images from the camera. Sony (2002) and CyberOptics (2002) give details on these devices. The camera has a pan of +/- 100 degrees, and a tilt of +/- 25 degrees. The frame grabber can obtain images with maximum resolution 640 x 480 in 24 bit colour.

Figure 4.4 shows what the camera sees, and Figure 4.5 shows the result of the camera algorithm detecting the specified colour. The researchers in LABORIUS have used a process similar to that described in Bruce et al (2000). The image is obtained in a YUV

format, which is a colour representation where one channel represents intensity while the other two represent the chromatics. This is more useful for identifying colours of varying intensity than the traditional red-green-blue formulation. A set of pixels in the image is identified by the user as being of the desired colour, and a set of possible values of the three channels is created. During navigation, pixels from the camera image are compared to the previously defined set, and classified as being a member of that colour or not. The process is very fast, as bitwise operators are used, as discussed in Bruce et al (2000). Identifying the x- and y-offsets as well as the dimensions of the coloured blob is simple once the coloured pixels have been identified.

As mentioned previously, observations from the camera are the x-offset, y-offset, width, and height of the coloured area of the image. Recalling Figures 2.1 and 2.2, and Equations 2.5 and 2.6, it is clear how the observations can be processed to compute a distance and angle to the lead robot. Since the focal length is unknown, but known to be constant for a test, and the relationship between pixels and real-world units is also unclear, all constant values were lumped into a single constant, as shown in Equation 4.1, and calibration was performed to determine the value. As described in section 2.2, a measurement using the height should give a more accurate measurement than using the width of the target, since the height is larger and therefore an error in the height measurement will be a smaller percent error than an error in width measurement. However, if the camera is too close to the target, the full height of the target is not seen, and therefore the width must be used. As mentioned previously, the main drawbacks of the camera is that line-of-sight from the follower to the leader is required, and the camera can occasionally be fooled by similarly coloured objects in the image.
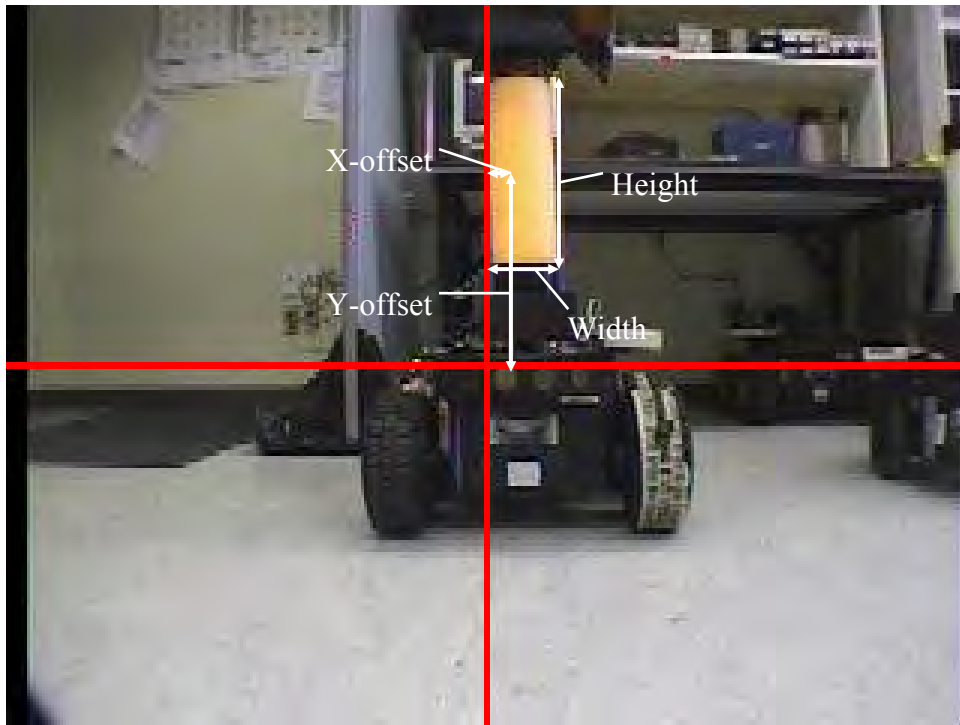
Figure 4.4:   **Image Seen by Camera**
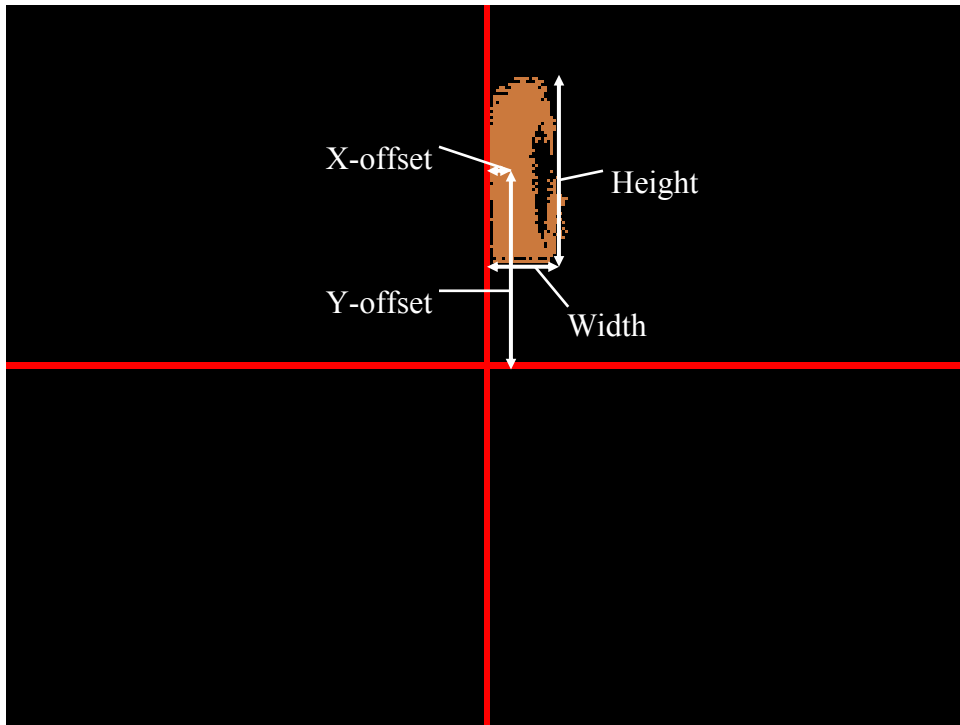
Figure 4.5: **Camera Algorithm's Analysis of Image**

$$D = a_H * \frac{1}{h} \quad \text{or} \quad D = a_W * \frac{1}{w}$$

$$f_W = \frac{a_W}{W}$$

$$a_{image} = \tan^{-1}(\frac{dx}{f_W})$$

$$a_{total} = a_{image} + a_{pan}$$

(4.1)

where

D   represents the distance from the camera lens to the object,

a_H represents the calibrated constant for use of height observations,

h   represents a height observation,

a_W represents the calibrated constant for use of width observations,

w   represents a width observation,

f_W represents the focal length (pixels) in the width domain,

W   represents the true width of the target, the diameter of the cylinder,

a_{image} represents the angle to the target in the image,

dx   represents the x-offset observation,

a_{total} represents the total angle from the follower to the leader, and

a_{pan} represents the camera pan angle.

4.1.4   Laser Scanner

The laser scanner on the robot is a SICK LMS-200. The important features of this unit are as follows. Range depends on the reflectivity of the target. The overall maximum is 80 metres. At 10% reflectivity, the maximum is 10 metres. This is sufficient for the research being performed. Accuracy also varies depending on local conditions, but may

be considered to be near 5 millimetres. This was investigated in this research. The laser scans from -90 to +90 degrees, in intervals of 0.25, 0.5, or 1.0 degrees. The 0.5 degree interval was chosen for our experiments. More details of the specifications can be found in SICK (2003).

Figure 4.6 shows a profile of the laser distance measurements over the range of angles, for the original test setup. An artist's conception of the test setup is shown in Figure 4.7. Figure 4.8 shows a profile using a new and improved setup that was used in the real-time tests, which will be described later. Figure 4.9 shows an artist's conception of this setup. To a human observer, it is clear in both images where the target is, but it can still be difficult to algorithmically determine. Line-of-sight from the follower to the leader is also required at all times.

The algorithm that was developed follows several steps. Firstly, narrow upward spikes were eliminated. Then, the data was slightly smoothed. Local minima were detected by searching for a change of slope of the profile from negative to positive. A check was made to ensure a large increase in range was present within a few degrees on either side of the local minimum. All choices were added to a list. This list was then searched for a result that was closest, and within a certain limited range of the previous epoch's result. This result directly gives a distance and angle measurement.
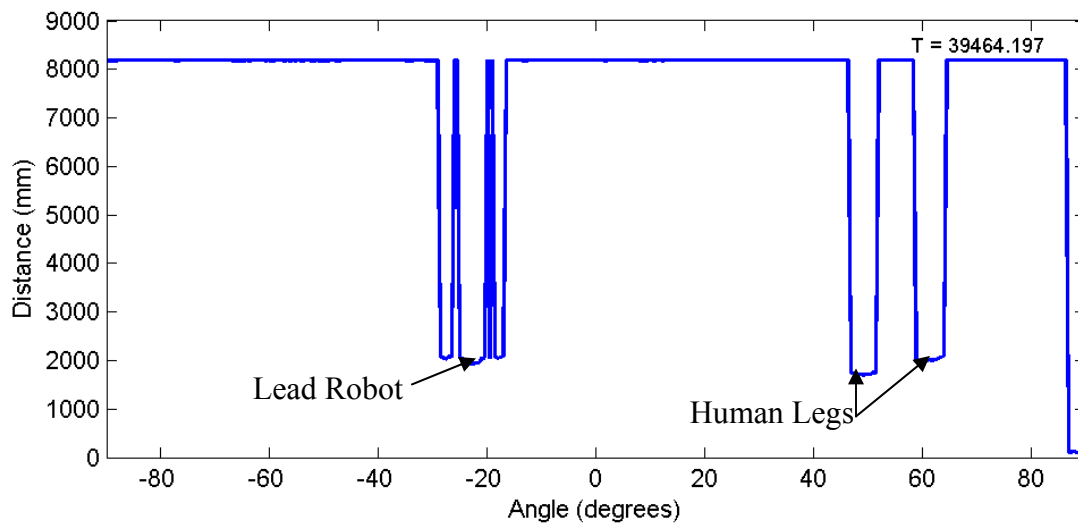
Figure 4.6: **Laser Profile using Original Setup**
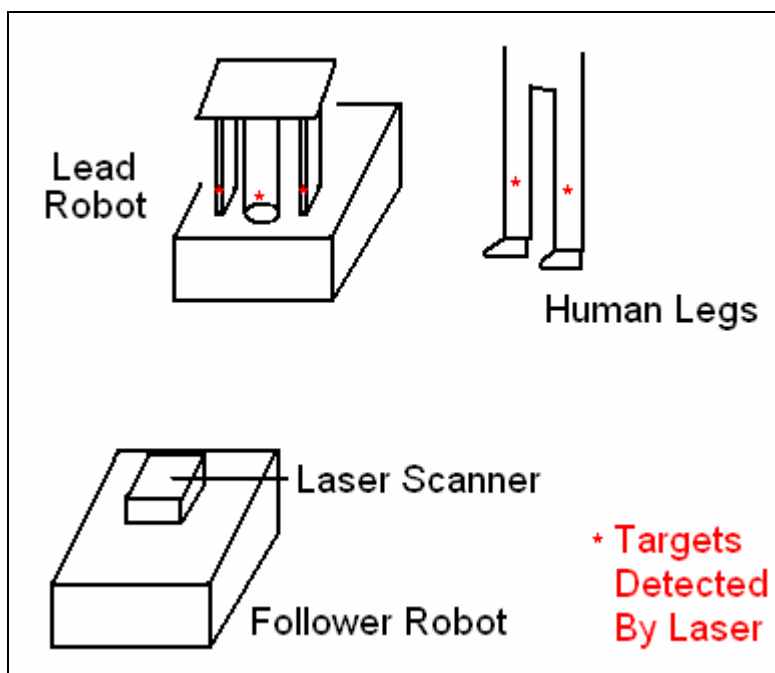
Figure 4.7: **Artist's Conception of Original Setup**
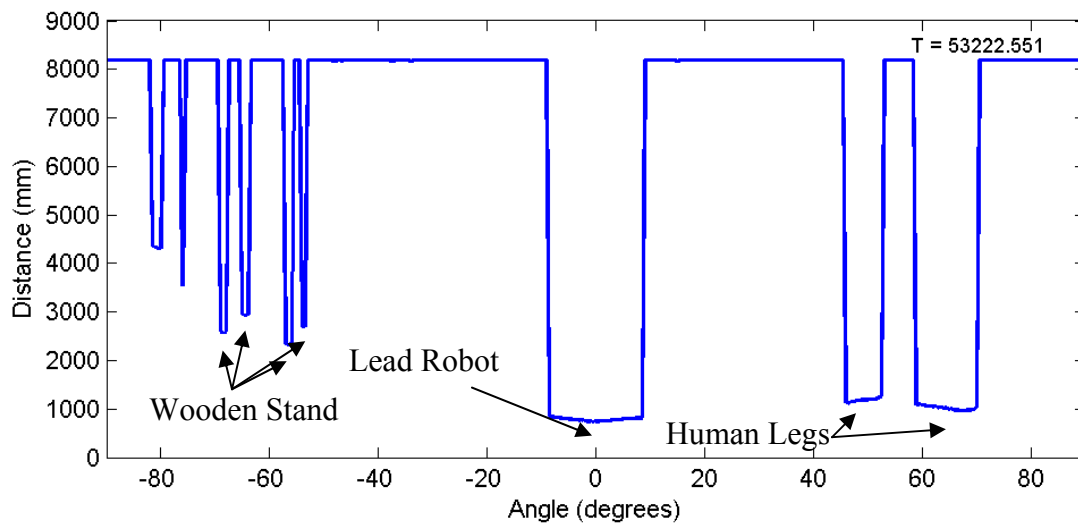
Figure 4.8:   Laser Profile using Improved Setup
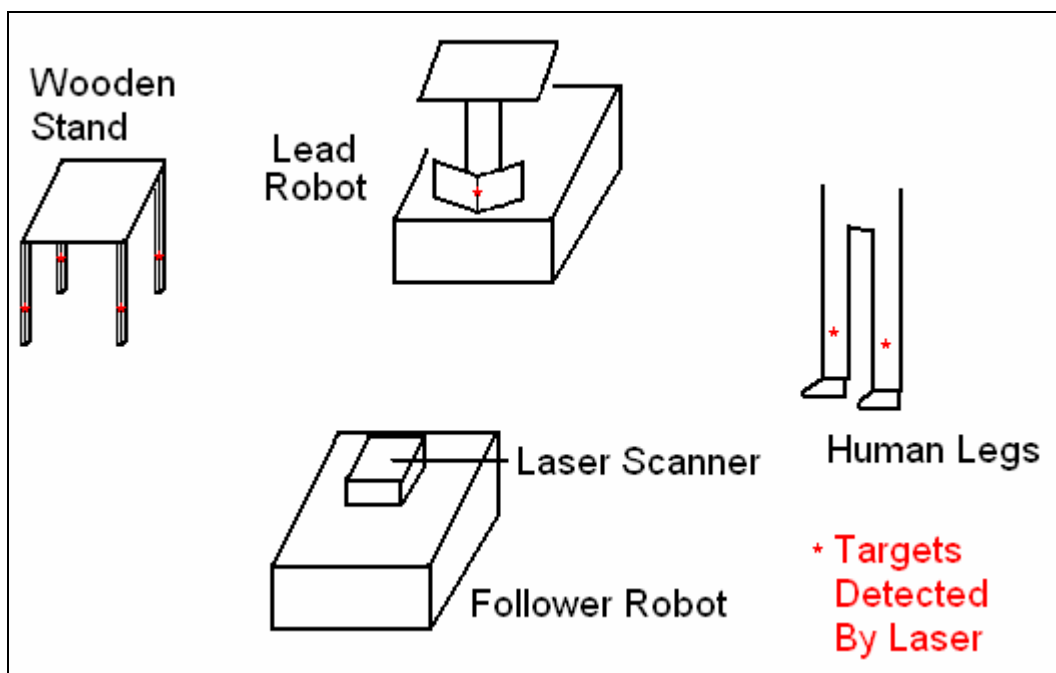
Figure 4.9:   Artist's Conception of Improved Setup

4.1.5   Sonar

The robots have eight front facing sonars, and eight rear facing sonars. These sonars are placed at angles of -90, -50, -30, -10, 10, 30, 50, and 90 degrees, relative to the robots frame of reference (where 0 degrees is forwards). The sonars have limited range, and emit signals in a 15 degree cone. As a result, they function well for tasks such as obstacle detection and maintaining an empty safety bubble around the robot, but are of limited use in reliably identifying targets.

Figure 4.10 shows a plot of the observations of the front sonars of the follower robot. It is clear that there is very poor spatial resolution. By examining an animation of the plots of sonar profiles as well as the laser profiles and camera measurements, it became clear that the sonars would not provide useful observations for relative positioning of the robots, and were therefore not used.
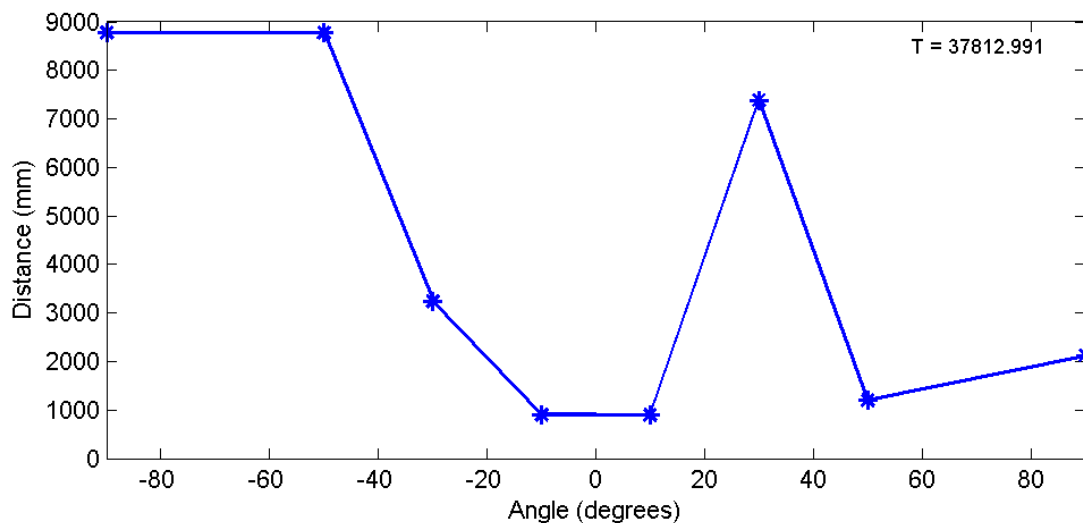
Figure 4.10:   Sonar Profile

4.2   Field Tests

Two sets of field tests were performed for this portion of the thesis. Firstly, a trip to Sherbrooke was made with GPS equipment for some initial data collection in late October, 2003. After this initial data collection was performed, the software for processing all data together was developed, and analysis of this data was performed. Once the software was complete and prepared to be used in real-time, a second trip to Sherbrooke was made in early November, 2004. During this trip, several data collection tests were done, using the newly developed software to process incoming data and output distance and angle values to be used by the follower robot for navigating. Qualitative observations were made, and the output of the real-time software was analysed. Also, all data was logged, so it could be analysed post-mission in the same manner as the data from the first trip.

For all tests, the data collection was performed outside and away from trees and buildings that would obstruct satellite signals in order to ensure GPS data was available. The mobile robots require dry conditions, therefore the tests had to be performed without rain or snow on the ground. The mobile robots also required a hard smooth continuous surface, such as pavement, and avoided inclines as the motor may not have been powerful enough to climb these.

In general, for all data collections, all systems were started up except the robots' motors, and then data logging started. Approximately 5 minutes of static initialization took place so that ambiguities could be fixed before motion. This static period of data would also be useful for post-mission analysis. The motors were then turned on and the robots were allowed to move. The robots drove around for a period of time, with the leader being remotely controlled from a laptop over the wireless Ethernet and the follower attempting to follow automatically, receiving manual assistance as required. At the end of the data

collection, the motors were first turned off, and another 5 minutes of static data were collected for possible post-mission analysis. All sensors and systems on the robots were then shut down.

A static reference station was present for all tests, consisting of a survey tripod with tribrach and antenna attached to it, with a GPS receiver and battery. Data was logged to the GPS receiver's internal compactflash card. The reference station was set up several metres from the test areas, with open sky conditions and away from conditions that may have created high multipath. Figure 4.11 shows an example reference station setup. No control points were present, and therefore the reference station was in a different location each time, with absolute position unknown. Therefore all analysis must be performed in a relative sense.

Figure 4.11:   Example of Reference Station Setup

Multiple data sets were collected for redundancy, though various situations can be created from a single good data set.   For example, signal loss can be simulated by removing some of the GPS data from the observation set.   While a true loss of data may be technically more valid, it is more difficult to test this situation.   Also, a true loss of data prevents the creation of reference values as described in section 4.4.   Each test was approximately 20 minutes.

Data was checked for quality before the data collection could be considered complete. This quality check included plotting of data from the robot sensors to ensure it looked

reasonable, as well as processing GPS data using existing fixed-ambiguity carrier phase software, such as FLYKIN+^{TM}.

Using the setup at the University of Sherbrooke, the main program that controls the robot functions as a loop. In each iteration of the loop, the sensors are polled, and then based on the resulting sensor data, action is taken. As a result, the data rate depends on the speed of the main loop of the program. There is some control of this, but it is based on the onboard computer's central processing unit (CPU) clock. The GPS will therefore not be synchronized with other sensors. The latest GPS data that is available at that run through the loop is used. This introduces some latency problems. Since the robots have relatively low dynamics, less than 1 metre per second, the maximum timing error of 0.05 seconds for 20 Hertz data would result in a maximum position error of 5 centimetres. It would be very rare for this maximum error to occur.

Several data output files were logged, and are described in Table 4.2. In addition to these, output files for the processed data were produced during the real-time test.

Table 4.2: Data Log Files Produced

Log File	Description
Follower Camera Data	CPU time and the camera observations (width, height, x-offset, y-offset)
Follower Laser Data	CPU time and the laser observations (distance measured at each of the angular increments)
Follower GPS Time	CPU time and the number of bytes read from the GPS at that time
Follower GPS Data	Raw GPS data from the entire experiment
Leader GPS Time	CPU time and the number of bytes read from the GPS at that time
Leader GPS Data	Raw GPS data from the entire experiment

As there were many tests performed, more details about the individual tests will be given in sections 4.5 and 4.6.

4.3 Processing Techniques

A Kalman filter is the standard choice for processing kinematic GPS data (Brown & Hwang 1992). In order to facilitate the use of sensors independently, as well as in combination, the software must be set up in a generic sense. This suggests the use of a Federated Kalman filter (Carlson & Beraducci 1993).

A Federated Kalman filter essentially processes each data source independently, and then combines the solutions. This makes it more useful for sensor integration systems. However, as will be seen, in this case there is actually little advantage over a centralized Kalman filter. Additionally, in Stephen (2000), it is shown that Federated Kalman

filtering can add unnecessary complications. Therefore, a centralized Extended Kalman filter will be used (Harvey 1998).

Since distance and angle are the observations that will be used from the camera and laser, and are the outputs of interest, it makes sense to have these as the parameters in the primary Kalman filter. The camera and laser are easily processed since the observations directly observe the parameters. This is why there would not be much advantage to using a decentralized filter. Additionally, object-oriented software modules for the Extended Kalman filter were already available. Processing of GPS is a bit more difficult. Normally, GPS processing results in a vector between the two GPS antennas in the form of three coordinate differences. This could then be converted into polar coordinates in a local level frame in order to observe distance, azimuth, and pitch. However, inspection of the equations showed that it would be simpler to directly process the GPS to observe distance, azimuth, and pitch. This is described in Harvey & Cannon (1997). Figure 4.12 shows the geometry between two GPS stations, in the Earth-centred Earth-fixed frame.
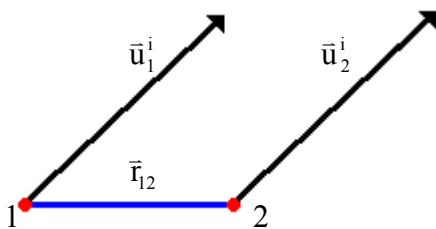
Figure 4.12:   Geometry Between Two GPS Stations and One Satellite

If the two GPS stations are relatively close together, the unit vector to a satellite $\vec{u}_j^i$ is virtually identical.

$$\vec{u}_1^i = \vec{u}_2^i = \vec{u}^i \tag{4.2}$$

Geometry can show that the difference in range to the satellite from each of the stations $\Delta\rho$ is equal to the dot product of the unit vector to the satellite $\bar{u}^i$ with the vector between the stations $\bar{r}_{12}$, in the Earth-centred Earth-fixed frame.

$$\Delta\rho = -\bar{u}^i \bullet \bar{r}_{12} \tag{4.3}$$

The vector between the stations in the Earth-centred Earth-fixed frame can be related to the vector between the stations in the local level frame using a transformation matrix.

$$\bar{r}_{12} = T\bar{b}_{12} \tag{4.4}$$

where T represents the rotational transform matrix and $\bar{b}_{12}$ represents the baseline vector from station 1 to station 2 in the local level frame. T can be expanded as follows:

$$T = \begin{bmatrix} -\sin(\phi)\cos(\lambda) & -\sin(\lambda) & \cos(\phi)\cos(\lambda) \\ -\sin(\phi)\sin(\lambda) & \cos(\lambda) & \cos(\phi)\sin(\lambda) \\ \cos(\phi) & 0 & \sin(\phi) \end{bmatrix} \tag{4.5}$$

where ϕ represents the geodetic latitude of the station and λ represents the geodetic longitude of the station. Similarly, $\bar{b}_{12}$ can be expanded as follows:

$$\vec{b}_{12} = \begin{bmatrix} \Delta N \\ \Delta E \\ \Delta U \end{bmatrix} = \begin{bmatrix} d\cos(a)\cos(p) \\ d\sin(a)\cos(p) \\ d\sin(p) \end{bmatrix} \tag{4.6}$$

where

    ΔN represents the change in northing from station 1 to station 2,

    ΔE represents the change in easting from station 1 to station 2,

    ΔU represents the change in height from station 1 to station 2,

    d   represents the distance from station 1 to station 2,

    a   represents the azimuth from station 1 to station 2, and

    p   represents the pitch from station 1 to station 2.

Now differential range can be expressed as a function of the distance, azimuth, and pitch.

$$\Delta\rho = -\bar{u}^i \bullet (T\vec{b}_{12}) \tag{4.7}$$

In the double difference domain, Equation 4.8 is produced.

$$\nabla\Delta\rho = -(\bar{u}^i - \bar{u}^j) \bullet (T\vec{b}_{12}) \tag{4.8}$$

The observation equations for code and phase, given in Equations 2.1 and 2.2, when expressed in the double difference domain, are now clearly functions of the distance, azimuth, and pitch.

$$\begin{aligned} \nabla\Delta P &= \nabla\Delta\rho + \nabla\Delta\varepsilon_P \\ &= -(\bar{u}^i - \bar{u}^j) \bullet (T\vec{b}_{12}) + \nabla\Delta\varepsilon_P \end{aligned} \tag{4.9}$$

$$\begin{aligned} \nabla\Delta\Phi &= \lambda\nabla\Delta\varphi + \lambda\nabla\Delta N + \nabla\Delta\varepsilon_\Phi \\ &= (-(\bar{u}^i - \bar{u}^j) \bullet (T\vec{b}_{12})) + \lambda\nabla\Delta N + \nabla\Delta\varepsilon_\Phi \end{aligned} \tag{4.10}$$

At this point, the parameters that have been identified are distance, azimuth, pitch, and local angle. It may appear that azimuth and local angle are redundant, since they may not be simultaneously observed by the same observation, and are related simply by an offset. The reason that both were included is because heading information relating the two is not always available. During the epochs that this data is not available, the filter should not have to reset, and therefore both parameters are kept in the filter.

In addition to the distance, azimuth, and pitch, double differenced ambiguities are estimated in float mode. As the values converge, ambiguity fixing is attempted using the LAMBDA method, after which point the ambiguities do not need to be estimated. If a new satellite is acquired, or if an ambiguity is found to be incorrect, a new double differenced ambiguity will be added to the filter, until it can be fixed and removed.

The physical properties of the observables dictate that they should be random walk processes. The distance, azimuth, pitch, and angle are not constant values, and so the random constant process does not apply. The time derivate of these parameters are not dependent upon the previous value of these parameters, so a Gauss-Markov process is not reasonable. A random walk process is the most appropriate. Double differenced ambiguities are by definition constants, and so the random constant process is used for these parameters.

Table 4.3 lists the observations identified so far, and the parameters that they observe.

Table 4.3: **Observations and Parameters Estimated in Main Kalman Filter**

Observation	Parameter Estimated
Camera Distance	Distance
Camera Angle	Angle
Laser Distance	Distance
Laser Angle	Angle
Differential GPS Code	Distance, Azimuth, Pitch
Differential GPS Phase	Distance, Azimuth, Pitch, Double Difference Ambiguities

In addition to this main Kalman filter, another Kalman filter must also operate. This second Kalman filter continuously estimates the position and velocity of the follower robot in single point mode. The position is important for the transformation matrix shown in Equation 4.5. The velocity is important if we wish to use the velocity vector as a source of heading information to combine with the azimuth so that GPS can contribute to local angle computation. The observations and parameters estimated in this second Kalman filter are described in Table 4.4.

Table 4.4: **Observations and Parameters Estimated in Secondary Kalman Filter**

Observation	Parameter Estimated
Single Point GPS Code	Latitude, Longitude, Height, Clock Offset
Single Point GPS Doppler	East Velocity, North Velocity, Up Velocity, Clock Drift

If a heading measurement is obtainable from the second Kalman filter's velocity output, it can then be used in combination with the azimuth computed in the main Kalman filter in order to estimate the angle in the main Kalman filter. Figure 4.13 gives an overview of

the processing algorithm that was used. Details of the state vectors, transition matrices, and design matrices for the main Kalman filter and the secondary Kalman filter are given in Appendix A and Appendix B, respectively.
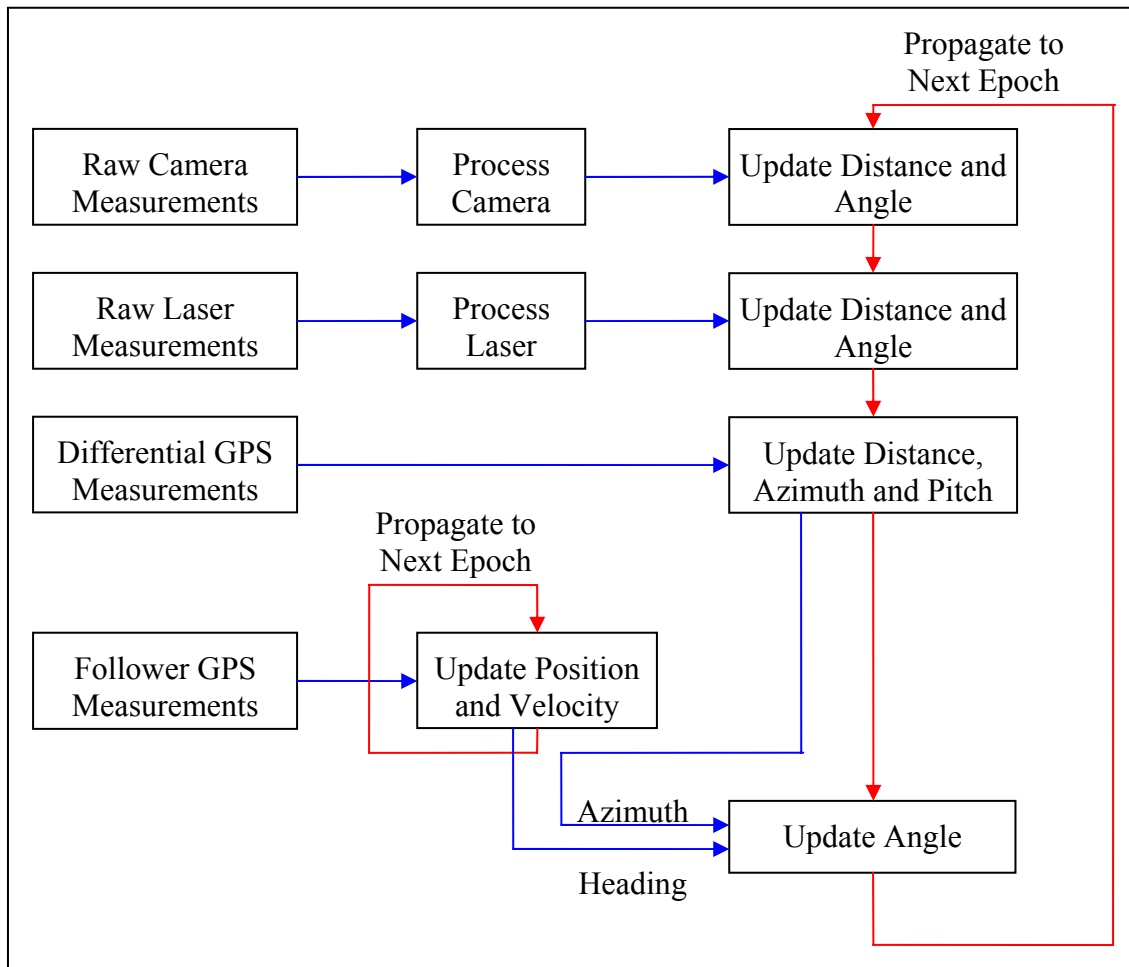

Figure 4.13: Processing Flowchart

A single program was created to process all data, using classes from the Navigation Development Library (NDL), department of Geomatics Engineering, University of Calgary (UTI Inc. 2002). The software had to be made to be platform independent, since development was being done on a Windows computer, but the final product would have

to be integrated with the environment used by the LABORIUS group who use the Linux operating system. An option file was used by the software, as this is the simplest way of adjusting input values such as which sensors to use, and keeping a record of the values used in each test.

At each epoch of processing, the first step is to prepare the data for processing. A record of camera data, a record of laser data, and a stream of GPS data are read into the program. The camera data and laser data are processed to obtain distance and angle measurements. The GPS data stream is decoded to obtain the latest epoch of GPS data available. Preprocessing, such as tropospheric corrections and elevation mask application, is performed on the GPS data. If data from any of these sources is not available, or a flag is set to not use that data source, that data is simply not processed in that epoch.

The second step is performed by the GPS single point processor. Data from the follower robot is processed to compute position and velocity of that robot. Of primary interest is the velocity, which is then converted into a heading measurement, if the velocity is deemed sufficiently high. A threshold of 0.1 metres per second was chosen based on examination of the velocity output. This heading measurement is used later by the differential processor.

The third step is taken by the differential processor. The camera and laser measurements are first used, and then the differential GPS measurements, as shown in Figure 4.13. Code is used, followed by phase measurements, after which ambiguity resolution is attempted using the LAMBDA method (de Jonge & Tiberius 1996). After the differential GPS has been processed, if a heading observation from the single point processor is available, it is combined with the azimuth output as a new observation to estimate the angle.

An option of using a pitch constraint was implemented into the program. A distance-azimuth-pitch formulation can be somewhat unstable for short distances between antennas. For example a metre of error in the relative position vector on a two metre baseline could translate into large azimuth or pitch errors, making it difficult for the filter to converge to the correct value. For the vector between the robots, it is known that there is a minimal change in height, and therefore a minimal pitch between the two robots. Therefore pitch can be constrained to zero. However, to allow the pitch to vary a bit to its true value, a pitch pseudo-observation can be used. This observation has a value of zero, and a standard deviation selected by the user. Unfortunately, this feature was not built into the program before the real-time tests occurred, and therefore can only be tested in post-processing. The pitch constraint only has effects on sensor combinations involving GPS, since pitch is not related to the observations of the camera and laser.

For the processing of multiple sensors, the noise values must reflect the relative accuracy of the various sensors. For the camera and laser, noise values were chosen heuristically based on examination of sensor measurements. For GPS, noise values were chosen based on past experience with this equipment.

Figure 4.14 shows the distribution of raw camera distance and angle measurements during the initial static time of the 31 Oct 2003 test. Figure 4.15 shows the distribution of raw laser distance and angle measurements during this same test. Table 4.5 shows the statistics on these raw data measurements.
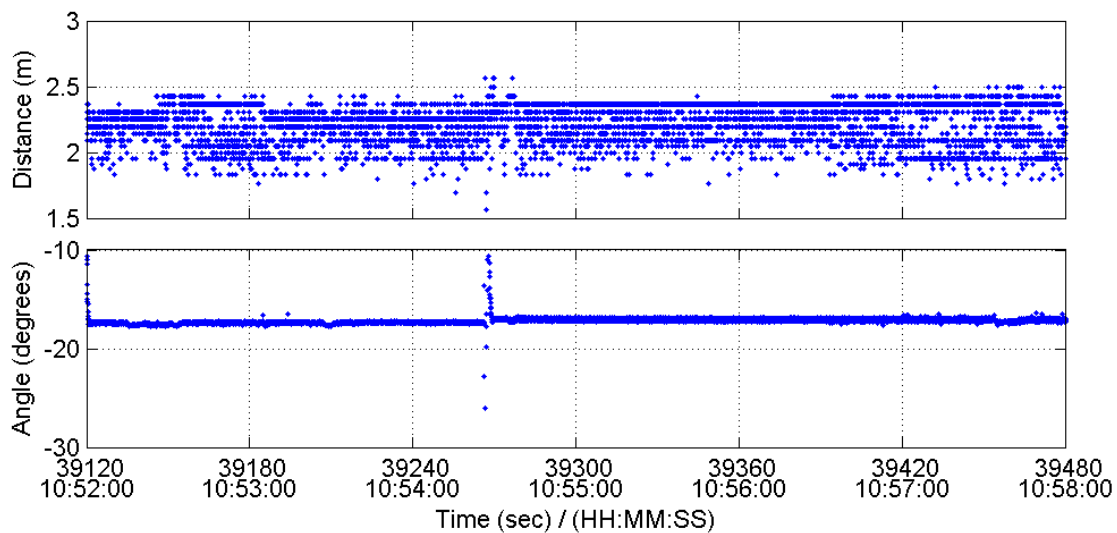
Figure 4.14:   Distribution of Raw Camera Measurements during Static Period
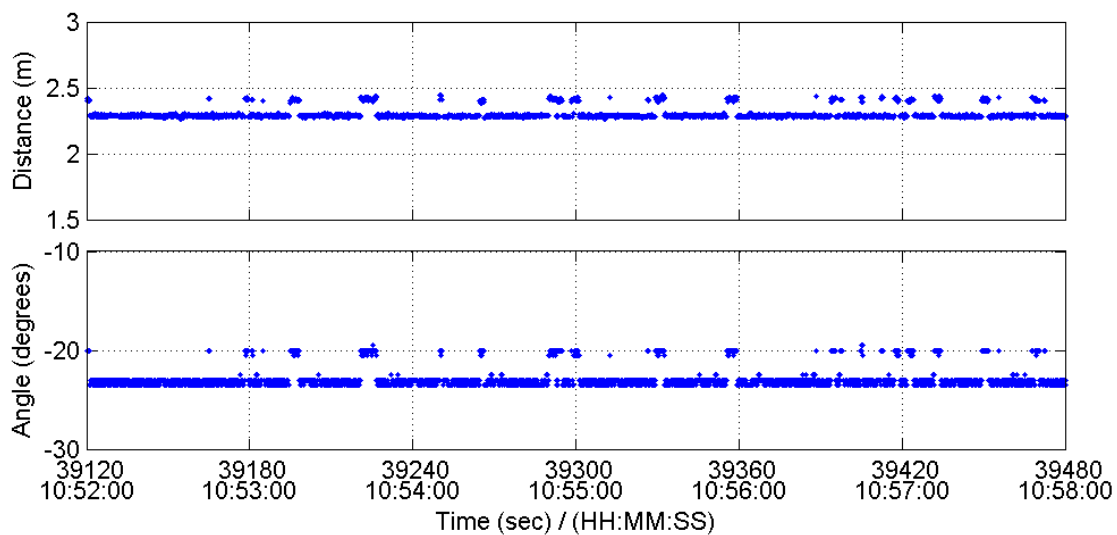
Figure 4.15:   Distribution of Raw Laser Measurements during Static Period

Table 4.5:   Standard Deviations of Raw Sensor Measurements

Observation	Standard Deviation
Camera Distance	17.2 cm
Camera Angle	0.75 degrees
Laser Distance	4.5 cm
Laser Angle	1.1 degrees

These values were not used directly however. Firstly, it makes sense that standard deviations of the measurements may be greater when the distance between the robots is larger. However, there was not time to investigate this apriori, and not enough data to investigate this aposteriori. Additionally, it was assumed that all sensors had been adequately and correctly calibrated apriori. However, it was seen that the observations occasionally had some biases that this standard deviation does not account for. Therefore, the standard deviations used were increased to envelope this potentially varying bias. Processing also showed this to improve the ability of the filter to resolve ambiguities to their integer values.   Having a higher standard deviation further emphasizes the role of the camera and laser as assisting sensors.

Standard deviations used are as shown in Table 4.6. Process noise was chosen as 10 centimetres per second for distance, and 0.1 degrees per second for angle, azimuth, and pitch.

Table 4.6: Noise Values Associated with Observations

Observation	Standard Deviation
Camera Distance	25 centimetres
Camera Angle	1 degree
Laser Distance	5 centimetres
Laser Angle	1 degree
GPS Code	50 centimetres
GPS Phase	0.02 cycles
GPS Doppler	0.1 Hertz

A problem apparent in the combination of sensors is that the sensors are clearly not collocated. The camera and laser are mounted near the front of the follower robot, while the coloured cylinder that they detect is located on the rear of the lead robot. Meanwhile, the GPS receivers are located near the centre of the robots. As a result, adjustments to observations had to be made in order to create a common reference frame. The laser and camera observations were adjusted to align with the GPS measurements. It is difficult to locate the focus point for the laser and camera, therefore constant offsets empirically derived from the data were used. The values are given in the sections 4.5 and 4.6 with the individual descriptions and evaluations of the tests. A constant offset is not the best choice, as the actual difference in distance measured by GPS versus the other sensors depends on the orientation of both robots. However, accurate headings of both robots would be required to make this more accurate correction, and this data is not available. In general, the robots stay oriented nearly in-line with each other. For the setup of the robots during the real-time tests, the maximum error would take place when the lead robot is rotated 90 degrees with respect to the follower robot, as shown in Figure 4.16.

This would result in an error of approximately 12 centimetres. However, this case is very unlikely to occur. If the lead robot had a different heading of about 45 degrees, the maximum error would be about 8 centimetres.
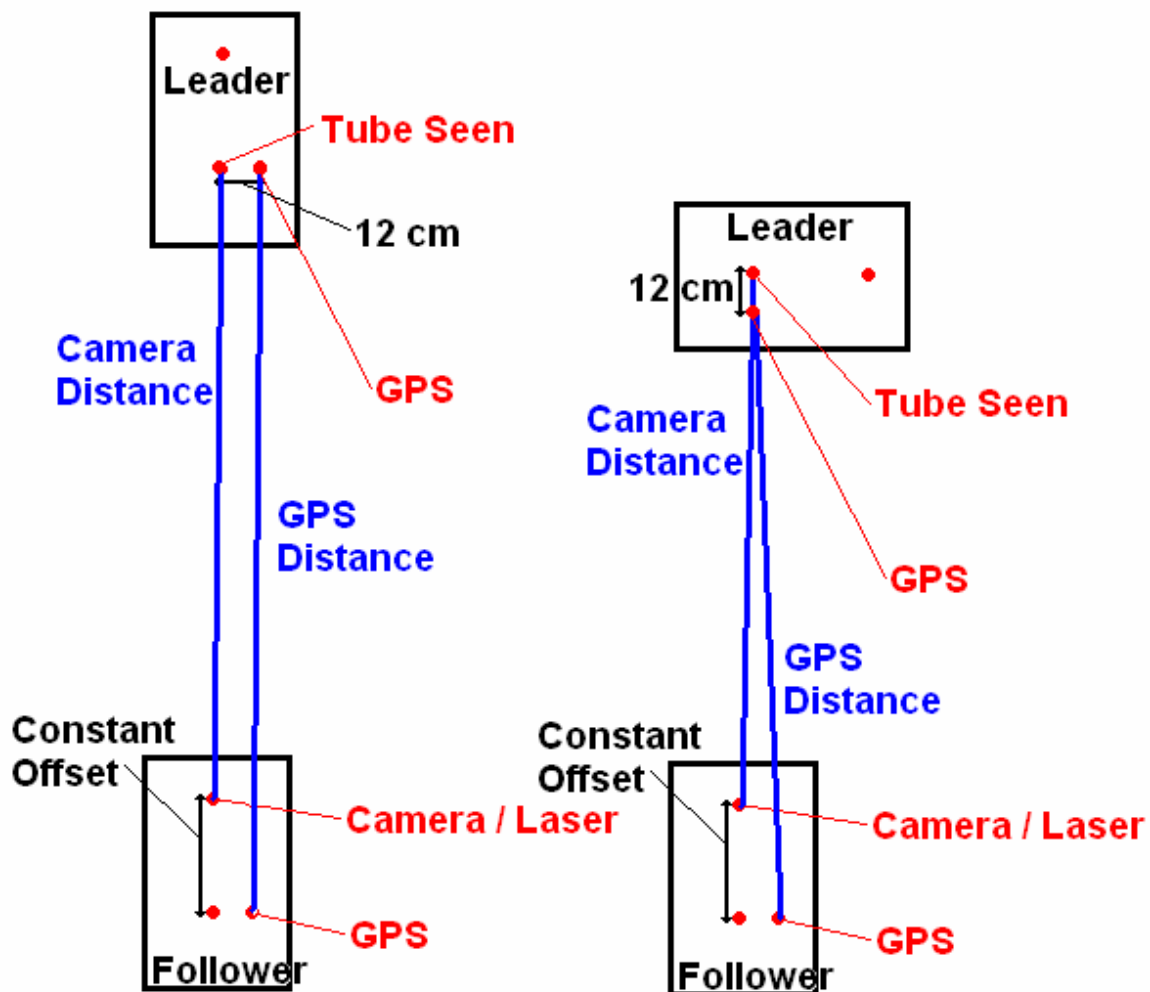

Figure 4.16: Maximum Error Incurred by Constant Offset Solution to Lack of Antenna Collocation

4.4 Evaluation Methods

There are a few approaches that can be taken to evaluate the results. The first is a qualitative observation of what appeared to happen during the test. This is fairly limited to observing whether the follower followed the leader or not, and the reasons why it may not have. Still, it can be quite useful.

The second is to look at the accuracy of the output of the processing. This can be analysed in two ways. The first is to compare to truth values. For these experiments however, no truth is available. Therefore, highly accurate reference values were created to approximately represent truth. Using dual frequency differential GPS from the static reference station to each of the robots with fixed ambiguities, accurate positions of both robots were produced and then differenced to produce accurate distance measurements. While this is not actually truth, it can be considered a pseudo-truth. In order to compare the test cases to the reference values, careful alignment of times must be performed. The reference values are tagged using GPS time, while the test cases are tagged using CPU time. This will create a slight additional loss of accuracy. As discussed previously, angle output is not produced from GPS processing, and so no pseudo-truth for angle can be created. Figure 4.17 shows the difference between regular processing with GPS and the creation of reference distance values.

Regular Processing

Reference Position Data Creation

Reference Station

Leader   Follower

Leader   Follower

Inter-antenna vector from Follower to Leader directly computed.

Position of Leader and Follower computed using static reference station. Inter-Antenna vector from Follower to Leader computed as

$$R_{F-L} = R_L - R_F$$
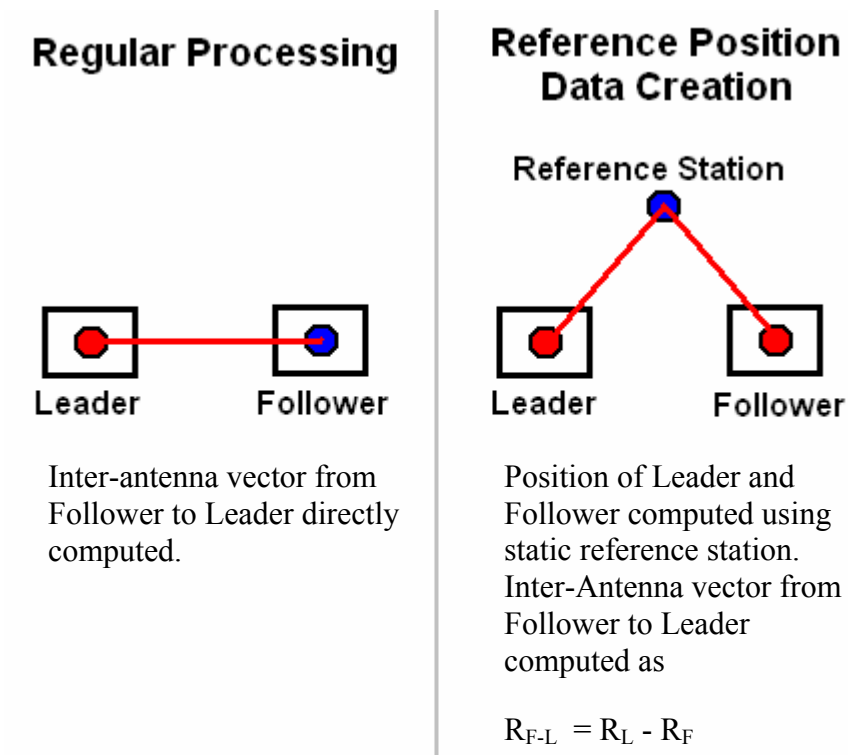
Figure 4.17: Comparison Between Regular Processing and Reference Distance Value Creation

The other method of evaluating accuracy is to examine periods of static data. During this time, while the truth value is not known, the value is known to be a constant. Therefore a standard deviation of the results can easily be produced as a measure of the error.

The next method of evaluation is to look at the time taken to resolve GPS ambiguities. We know that GPS gives highly accurate results once ambiguities are fixed, and therefore a shorter time to fix allows the use of the highly accurate measurements at a sooner time. Assisting GPS with other sensors such as the camera and laser should reduce this time to ambiguity fix. Petovello (2003) has shown this to be true for assisting GPS with inertial sensors.

Finally, the effects of additional sensors on system reliability can be examined. Intuitively, using another sensor, and thus additional observations, should improve the ability of the Kalman filter to detect faulty observations and remove them. Additionally, the effect of faulty observations that are not removed should also be reduced. The extent to which this actually takes place will be examined.

4.5   Initial Data Collection Test and Results

Results will be given here for the data set that was collected on October 31, 2003. Results for the real-time tests performed during the 2004 trip are discussed in section 4.6. This test took place under benign conditions, in a mostly empty parking lot at the University of Sherbrooke. The area, as well as the path of the robot, is shown in Figure 4.18. The north and east positions of the lead robot, with respect to the reference station, are shown in Figure 4.19.
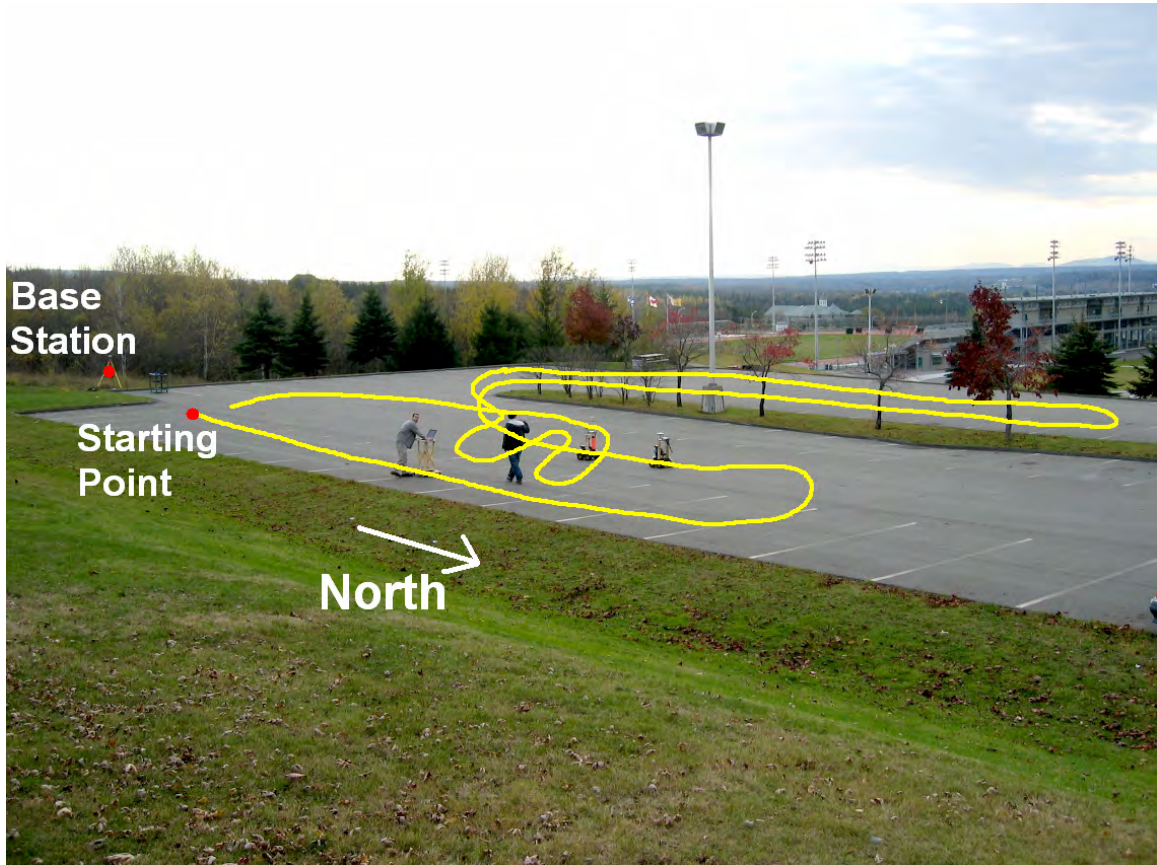
Figure 4.18:   Path of Robots on 31Oct2004 Test
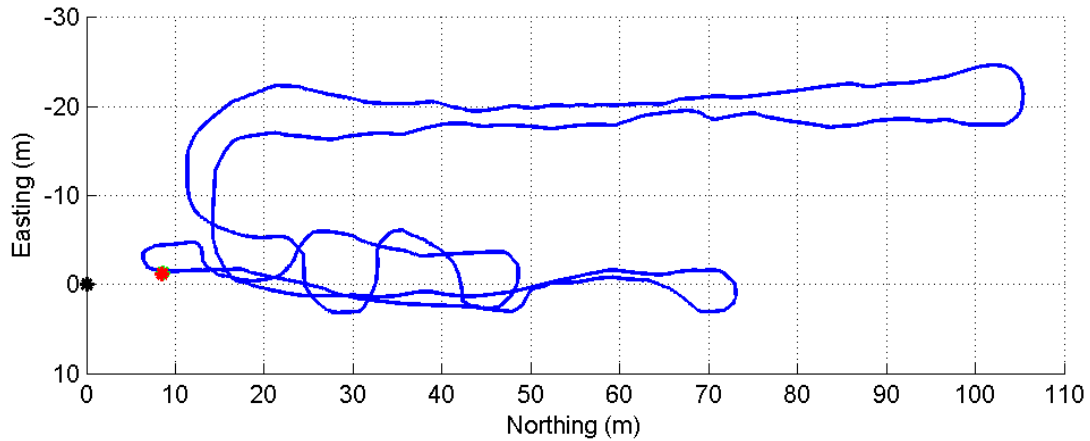
Figure 4.19:   North and East Positions of Lead Robot on 31Oct2004 Test

An average of eight satellites was tracked during the entire test, which lasted a total of 25 minutes. Distances between robots stayed in the 1 to 3 metre range. A static period of about five minutes took place at the beginning and end of the test for testing purposes. GPS data was logged at a rate of 20 Hz, while the camera and laser were logged on an as-polled basis. Polling took place at a rate of about 20 Hz, though the laser was only able to give new information at a rate of about 5 Hz.

4.5.1   Static Results

The first demonstration of results is to visually show the accuracy of the sensors' distance measurements. This is done by plotting the distance measurements over a few minute period of time during which the robots were not moving and therefore the distance should be constant. Figures 4.20 to 4.22 show the distance measured by GPS, the camera, and the laser. The camera and laser have had the collocation offset discussed earlier applied already to align with the GPS measurements.
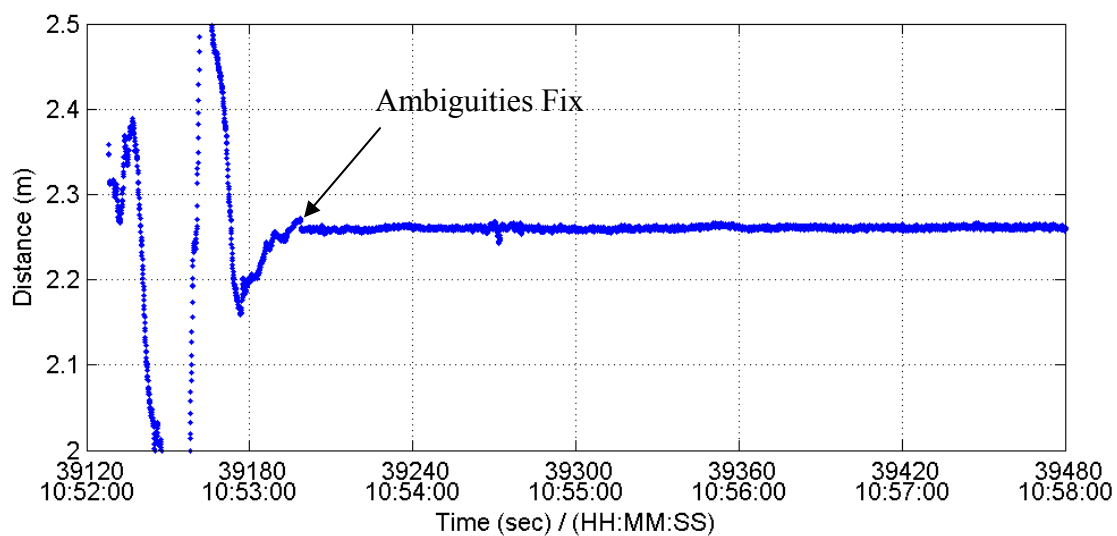
Figure 4.20:   GPS-Measured Distance during Static Time
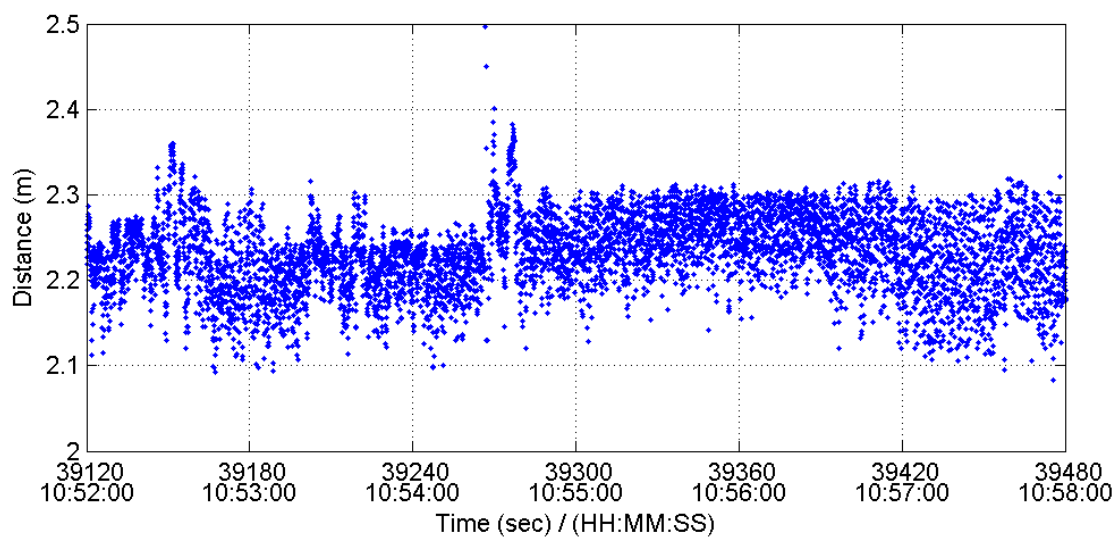
Figure 4.21:   Camera-Measured Distance during Static Time
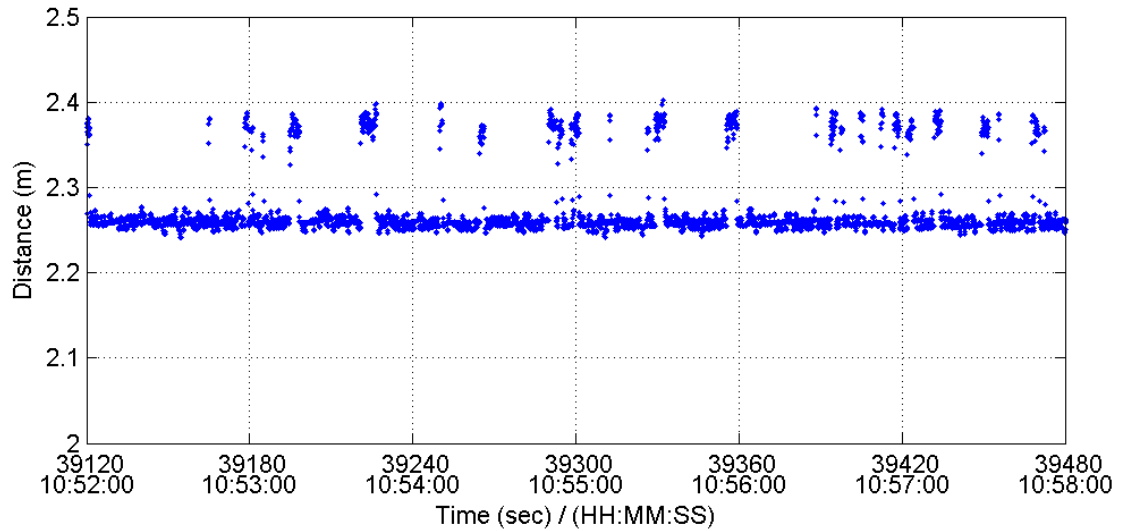
Figure 4.22:   Laser-Measured Distance during Static Time

The beginning of the GPS plot shows very poor results, as the measurement varies wildly. This is because the ambiguities have not yet had time to fix. Once the ambiguities have been fixed, the measurement stays very stable, within a centimetre.

The camera measurements show a much higher variance simply because this sensor is not as accurate. There is a scatter of values of around 10 centimetres.

The laser measurements generally remain within a centimetre of a mean value, but there are frequent jumps of around 12 centimetres. This occurs when the incorrect target is identified in the laser profile.

Figures 4.23 to 4.26 show the same static time period when the sensors are combined.
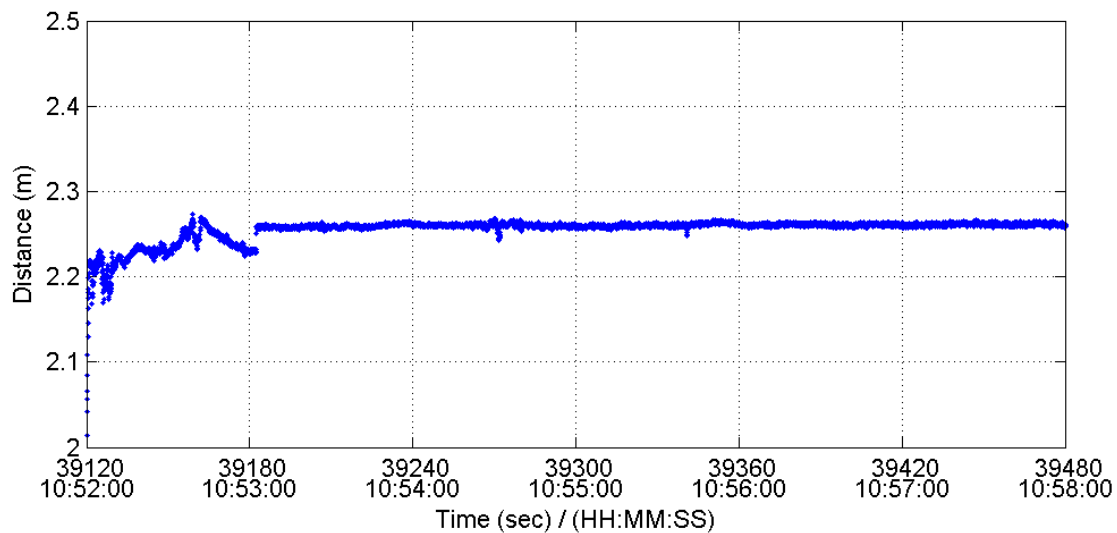
Figure 4.23:   GPS+Camera-Measured Distance during Static Time
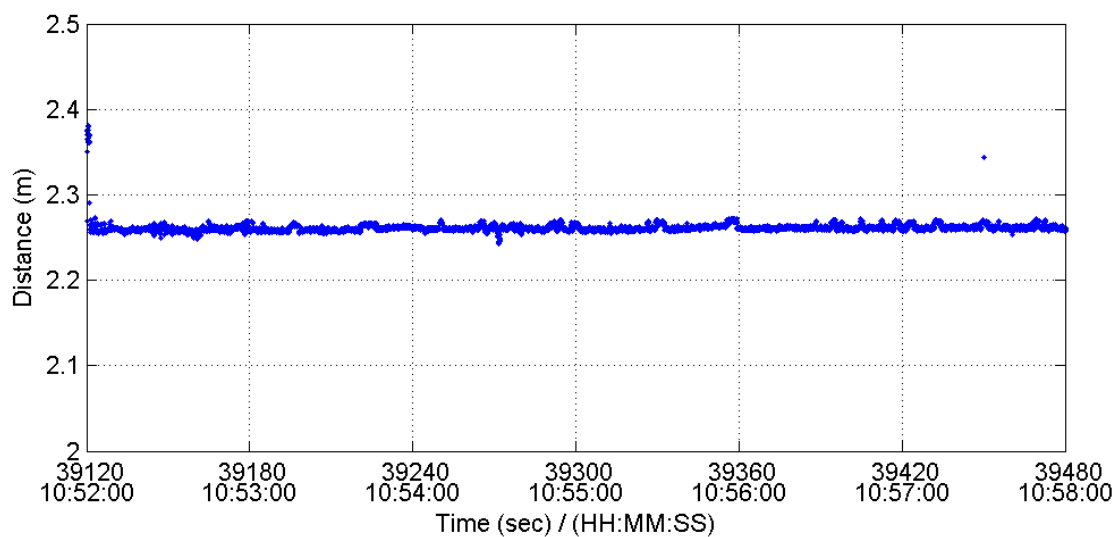
Figure 4.24:   GPS+Laser-Measured Distance during Static Time
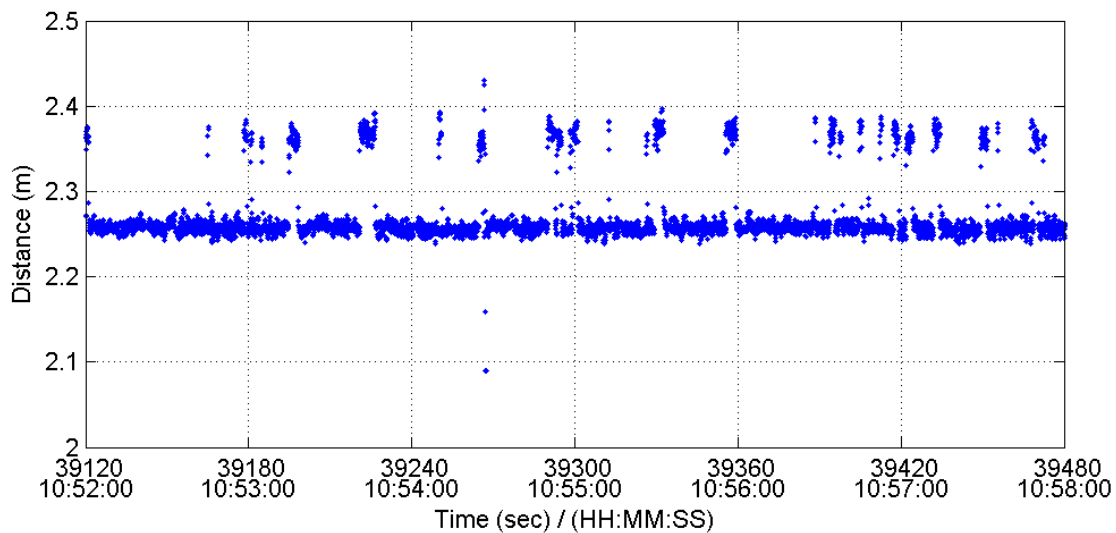
Figure 4.25:   Camera+Laser-Measured Distance during Static Time
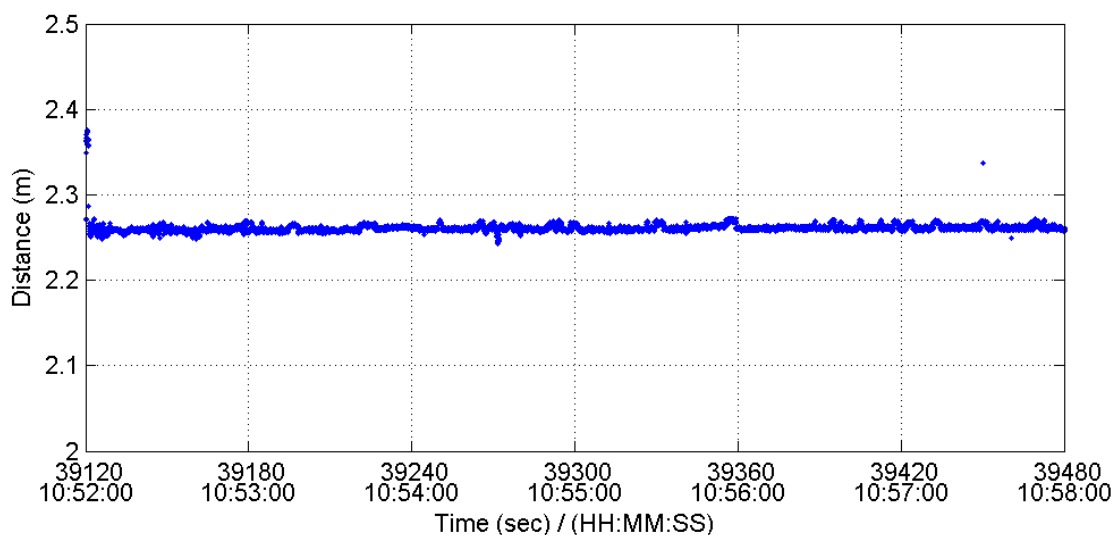
Figure 4.26:   GPS+Camera+Laser-Measured Distance during Static Time

When GPS is combined with the camera, results are improved. Firstly, during the GPS float-ambiguity time, the camera, with its lower standard deviation, keeps the output distance constrained close to its true value. Further, the ambiguities are then able to

resolve to their integer values sooner, as will be discussed later in the results. Once the ambiguities are fixed, the highly accurate GPS dominates.

When GPS is combined with the laser, results are further improved. The data at the beginning of the plot is closer to the true value since the laser is more accurate than the camera. After the ambiguities are fixed, the GPS solution is better than the laser, and so the outliers in the laser measurements have no effect, or are detected as blunders and removed.

When camera and laser measurements are combined, the higher accuracy laser dominates, and the output is virtually the same as the laser-only case. This is accurate except for the outliers created when the laser processing detects the wrong target.

Figure 4.26 shows what happens when all three sensors are combined. The result is virtually identical to the case in which GPS and laser are combined. This is because the laser measurement is available at almost all the same times as the camera measurement, and is much more accurate, and therefore the camera measurement is given so little weight it is not of value.

Plots showing the results when a pitch constraint is used are not given here. The plots appear approximately the same, except that ambiguities fix somewhat faster, as will be discussed later. When fixed ambiguities are used, statistics are the same as without the pitch constraint.

Table 4.7 shows the statistics of the output compared to the reference distance values. During the static period, no truth data is necessary to obtain the standard deviation of the output, since it should be constant, and this is shown in Table 4.8. All statistics are collected from a three minute time period, after ambiguities are fixed.

Table 4.7: Statistics for Distance during Static Period Compared to Reference Distance Values

Sensors	Mean (cm)	Standard Deviation (cm)	RMS (cm)	Number of Samples
GPS	0.0	0.0	0.0	2990
Camera	-1.5	4.6	4.8	2334
Laser	1.3	4.0	4.2	2649
GPS + Camera	0.0	0.0	0.0	2990
GPS + Laser	0.1	0.2	0.2	2990
Camera + Laser	1.3	4.1	4.3	2334
GPS + Camera + Laser	0.1	0.2	0.2	2990

Table 4.8: Statistics for Distance during Static Period Compared to Self

Sensors	Mean (m)	Standard Deviation (cm)	Number of Samples
GPS	2.260	0.2	3000
Camera	2.245	4.6	3000
Laser	2.274	4.0	3000
GPS + Camera	2.260	0.3	3000
GPS + Laser	2.261	0.3	3000
Camera + Laser	2.272	4.0	3000
GPS + Camera + Laser	2.261	0.3	3000
Reference Values	2.260	0.2	2990

It is interesting to note that the reference distance values had a 2 millimetre standard deviation in actual values, even though it should have been exactly zero if it were truth. Also, in the "error" statistics where the output is compared to the reference values, combinations involving GPS have zero standard deviation. This indicates the errors in the GPS output directly correlate with the errors in the reference values. No RMS is given in Table 4.8 as it would be meaningless. Mean in Table 4.8 is similarly not too useful, as it is an actual measurement value.

The angle should also be constant during the static period. Figures 4.27 to 4.29 show the angle measured by the camera and laser. The GPS gives no measurement for angle during the static period, because no heading information is available.
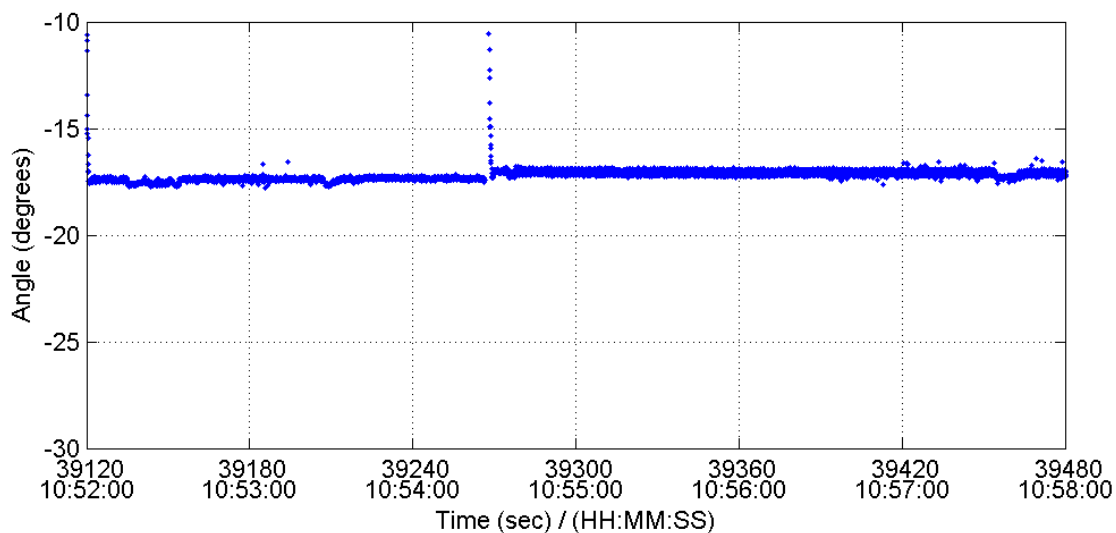
Figure 4.27:   Camera-Measured Angle during Static Period
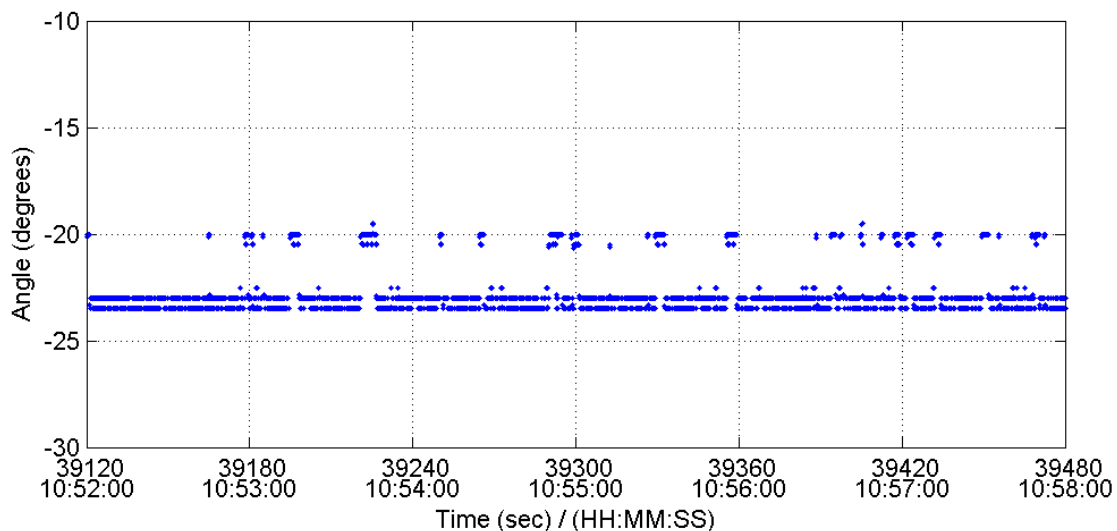
**Figure 4.28:   Laser-Measured Angle during Static Period**
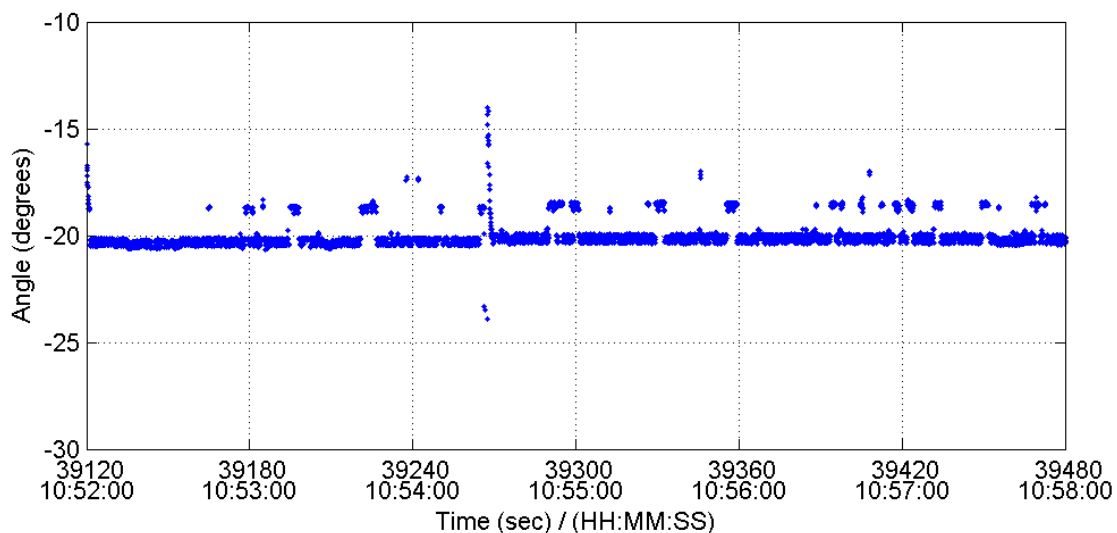
Figure 4.29:   Camera+Laser-Measured Angle during Static Period

During the static period of time, both the camera and the laser show nearly constant values of angle. At one point, some error occurs in the camera measurement. There is also a bit of an anomaly in the distance measured by the camera at this time. Most likely,

an error occurred in the image analysis stage of the processing, and the coloured tube was not properly identified. The laser shows a constant value, with occasional jumps. As mentioned before, these jumps are due to incorrect target identification. At the constant value, there appears to be two lines, due to the quantization (on 0.5 degree intervals) of the laser angle data.

When the camera and laser are combined, the result is a clear mix of the two, since both observations are given equal standard deviation. Errors existent in each sensor alone are still present, though with less magnitude. Table 4.9 shows the standard deviations of the angle values obtained from each sensor.

Table 4.9:   Statistics for Angle during Static Period Compared to Self

Sensors	Mean (degrees)	Standard Deviation (degrees)	Number of Samples
Camera	-17.3	3.2	3000
Laser	-22.8	1.1	3000
Camera + Laser	-20.1	2.5	3000

4.5.2   Kinematic Results

This section describes the distance and angle measurements obtained during a three minute long subset of the data during which the robots were moving. Figures 4.30 to 4.32 show the distance computed using each sensor during this period. The distance between the robots continuously varies during this period, from about 2.2 metres to 3.0 metres.
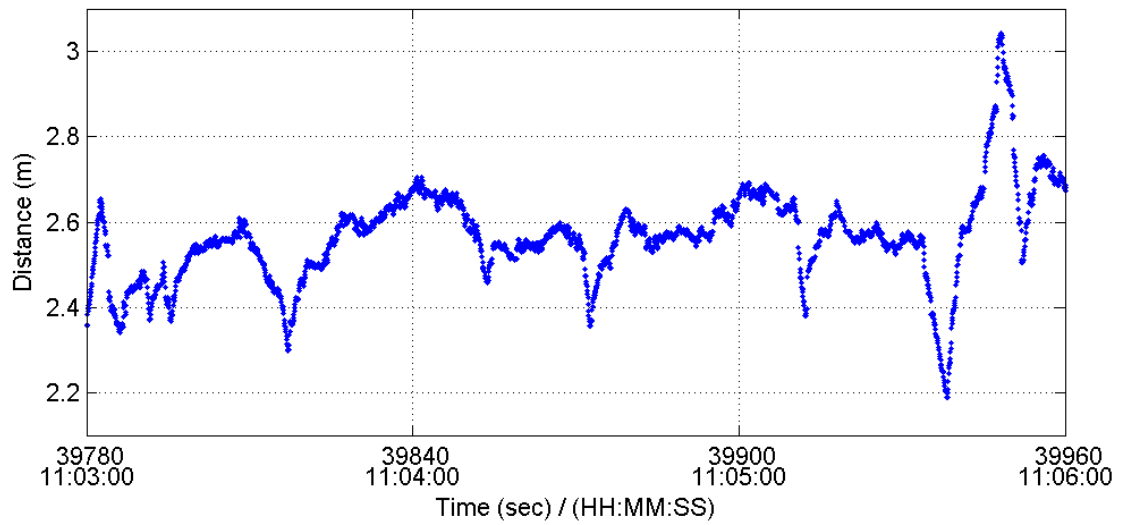
Figure 4.30:   GPS-Measured Distance during Kinematic Period
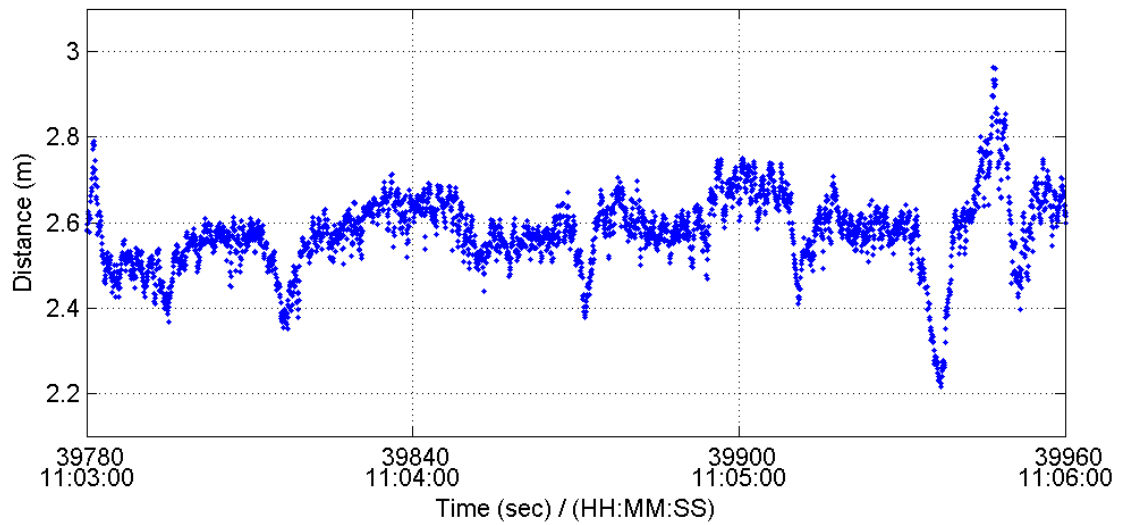
Figure 4.31:   Camera-Measured Distance during Kinematic Period
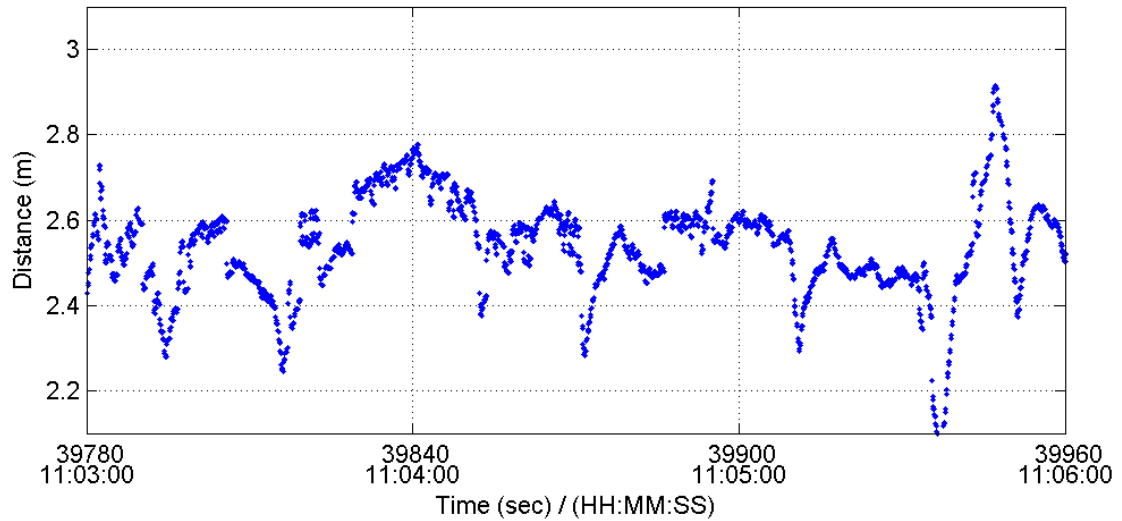
Figure 4.32: Laser-Measured Distance during Kinematic Period

From the plots, GPS appears to be the most precise. The camera data is not a lot worse, due to the filtering taking place in the Kalman filter. The laser appears precise, but has some occasional sharp jumps.

When combining the data sets, since data from all sensors was present during this time, the same phenomenon occurs as during the static period. The hierarchy of GPS, laser, and camera still applies. Any plot including GPS appears like GPS alone, any plot including laser without GPS appears like laser alone. Therefore, plots of combinations of sensors are omitted.

Table 4.10 shows the statistics of the distance measurements during the kinematic period described above.

Table 4.10: Statistics for Distance for Kinematic Period Compared to Reference Distance Values

Sensors	Mean (cm)	Standard Deviation (cm)	RMS (cm)	Number of Samples
GPS	0.1	0.5	0.5	2610
Camera	1.3	7.5	7.6	2029
Laser	-2.7	8.6	9.0	2325
GPS + Camera	0.1	0.5	0.5	2610
GPS + Laser	0.0	0.7	0.7	2610
Camera + Laser	-2.6	8.5	8.9	2029
GPS + Camera + Laser	0.0	0.8	0.8	2610

The GPS output is clearly the most accurate. Though as shown in the static period comparison between error with respect to reference values and error with respect to self, there may be some bias since GPS was used to create the reference distance values. The camera actually shows up as being more accurate than the laser, which is surprising. This may be due to errors in the laser identifying the correct target. When sensors are combined, since all sensor data is available, all combinations involving GPS give approximately the same accuracy as GPS alone.

Figures 4.33 to 4.35 show the angle measurements created during the same few minutes of kinematic data.
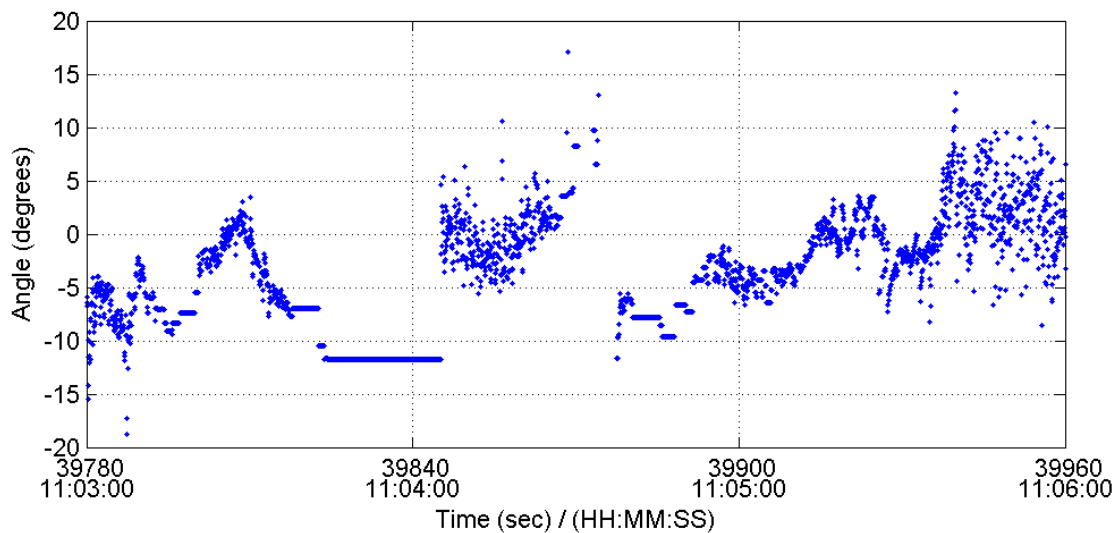
Figure 4.33:   GPS-Measured Angle during Dynamic Period
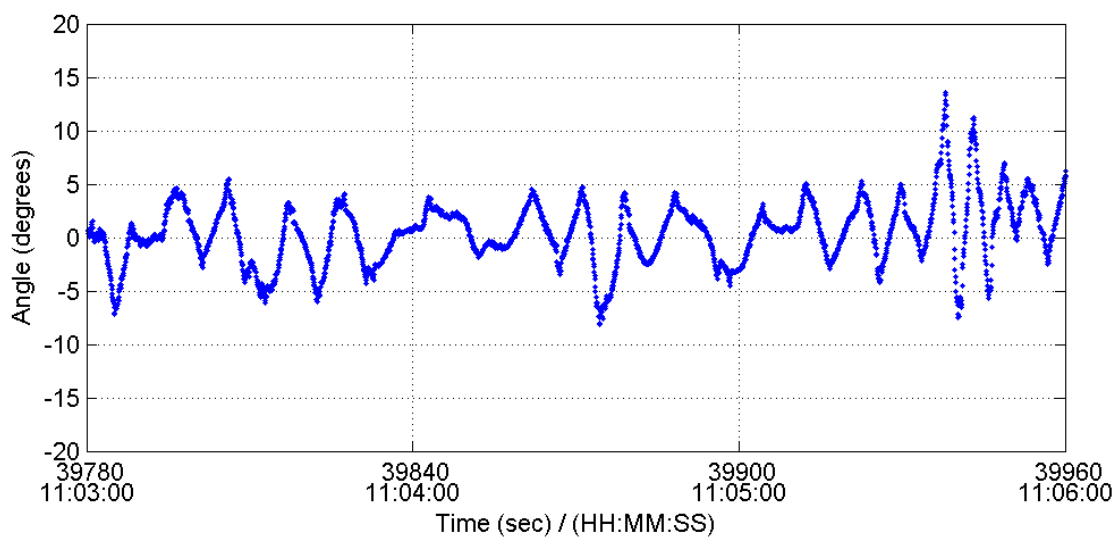
Figure 4.34:   Camera-Measured Angle during Dynamic Period
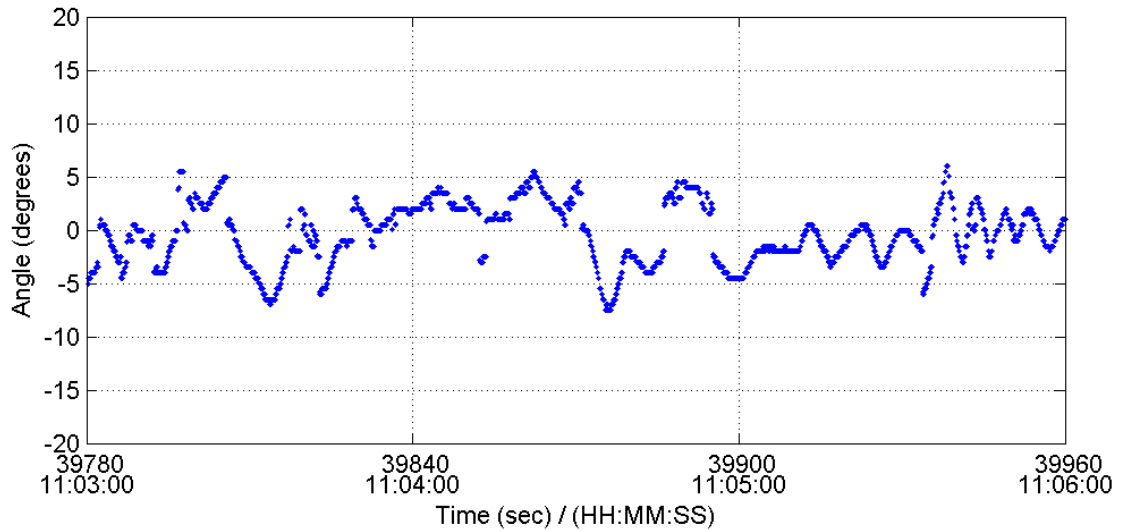
Figure 4.35: Laser-Measured Angle during Dynamic Period

All three plots follow approximately the same pattern. The camera and laser are clearly much closer together, and much more accurate, than the GPS. For some periods of time, the GPS does not even update values, since the follower robot's speed was too low to provide a reasonable heading measurement. For much of the time that GPS-derived angles are available, they are highly noisy. This shows for this application that a single antenna per vehicle system is not sufficient alone to provide useful angle measurements.

For angles, there is no truth data for comparison, and therefore no statistics.

4.5.3 Kinematic with GPS Data Outage Results

If the robots were to pass under a bridge, or near some tall buildings which block the line-of-sight to the GPS satellites, a GPS data outage would occur. If GPS was not assisted, there would be no measurements available during this time. Furthermore, once GPS is re-established, it takes some time for ambiguities to be resolved to their integer states. Therefore, combining GPS with other sensors should yield a significant improvement when data outages occur. GPS data was eliminated for a one minute period in the same

time frame as the previous dynamic plots to test the ability of assisting sensors to bridge an outage and aid in ambiguity resolution. Figures 4.36 to 4.38 show the results.
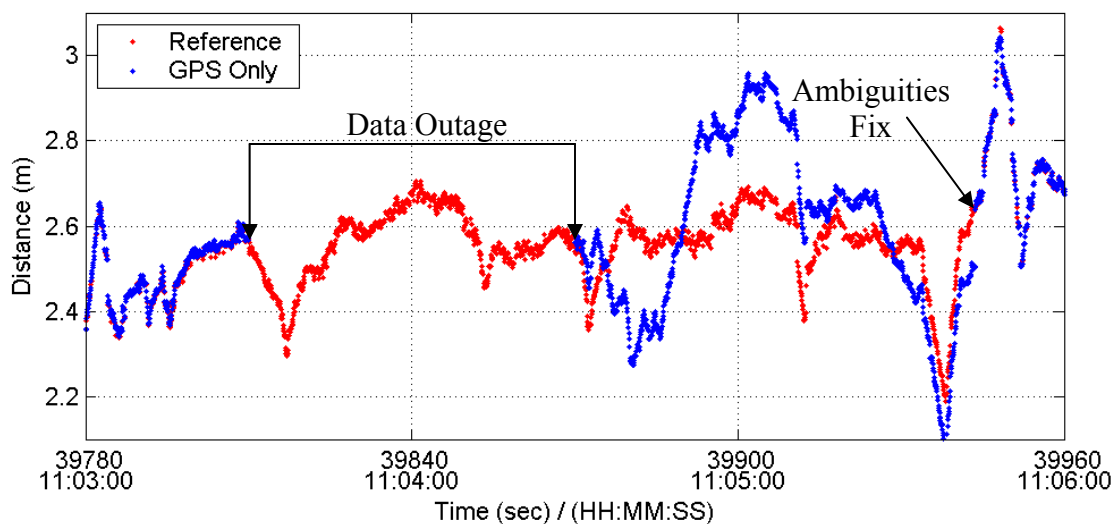
Figure 4.36:   GPS-Measured Distance during Dynamic Data Outage Period
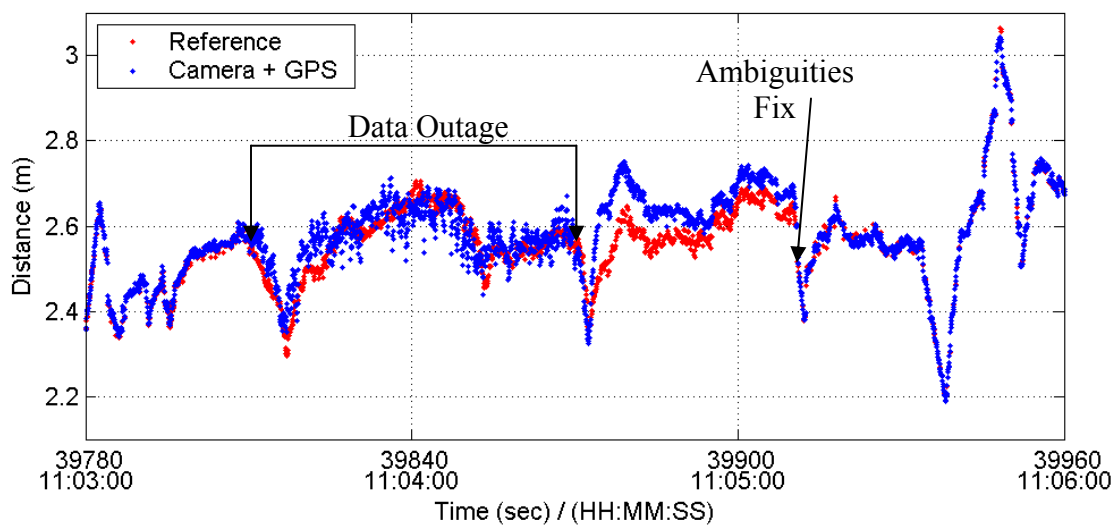
Figure 4.37:   GPS+Camera-Measured Distance during Dynamic Data Outage Period
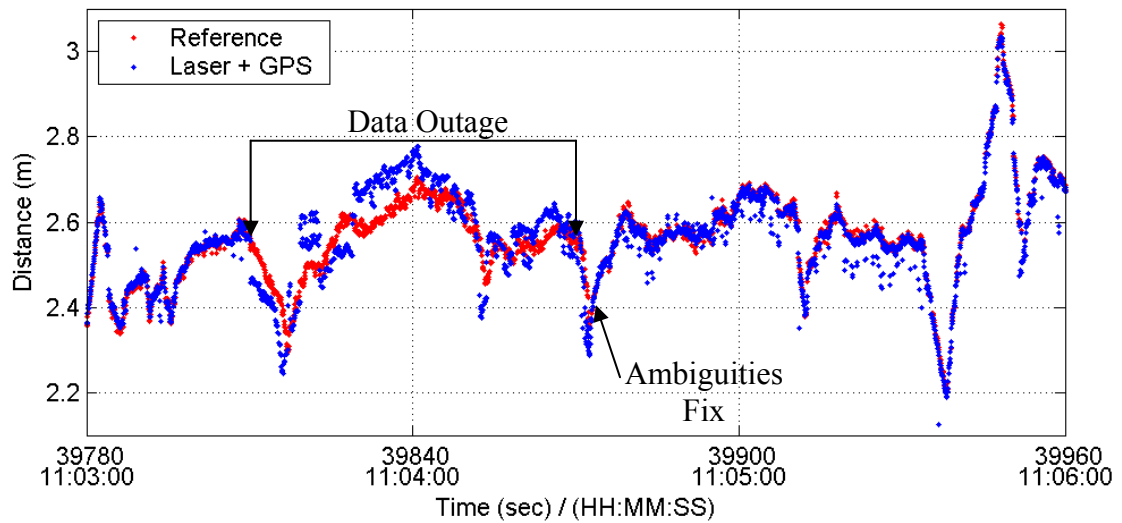
Figure 4.38:   GPS+Laser-Measured Distance during Dynamic Data Outage Period

In Figure 4.36, when GPS alone is used, there is no update to the distance measurement for a one minute period. Once GPS data returns, it is in float-ambiguity mode, and the accuracy is relatively poor. It takes more than another minute before ambiguities are resolved.

When camera data is present, the computed distance remains close to the reference distance throughout the data loss period, and after GPS data returns. The ambiguities are more quickly resolved than with the GPS-only case, after which point the accuracy is once again very high.

Adding laser data has much the same effect as adding camera data, though with higher accuracy.

Using the pitch constraint had more significant effects after this kinematic data outage compared to the initialisation at the beginning of the test. Figures 4.39 to 4.41 show the combinations when a pitch constraint was used.
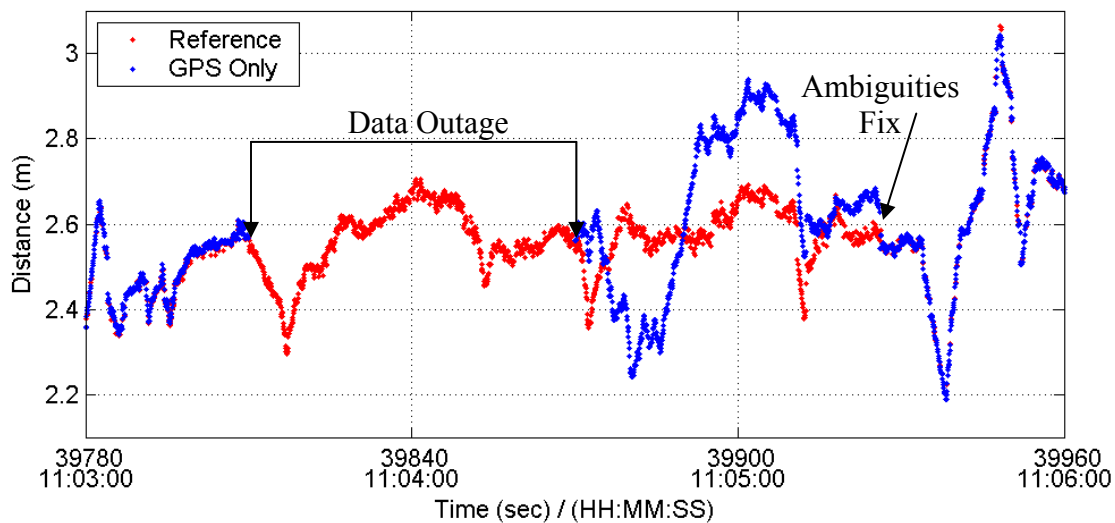
Figure 4.39: GPS-Measured Distance during Dynamic Data Outage Period using Pitch Constraint
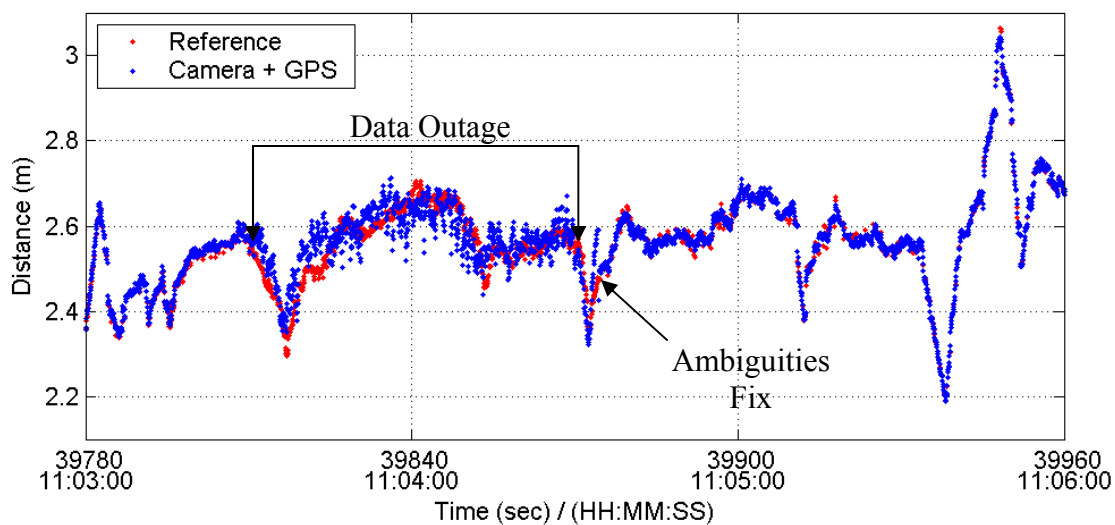
Figure 4.40: GPS+Camera-Measured Distance during Dynamic Data Outage Period using Pitch Constraint
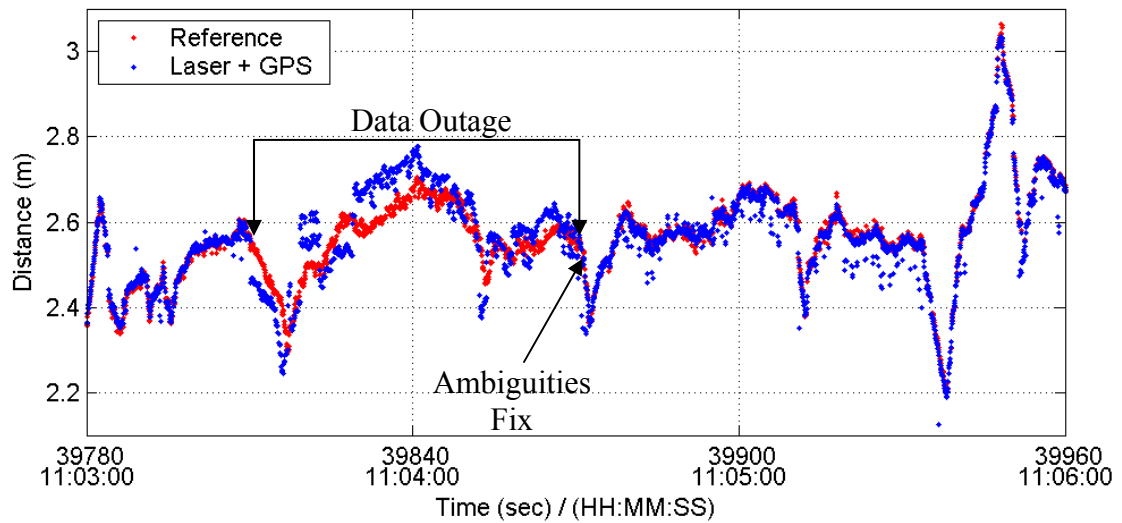
Figure 4.41: GPS+Laser-Measured Distance during Dynamic Data Outage Period using Pitch Constraint

When the pitch constraint was used, ambiguities resolved more quickly, especially in the case where camera and laser assisting was used. This is because now both distance and pitch are approximated, so the only parameter that GPS is solely responsible for is the azimuth. As a result, all components converge faster and ambiguities resolve more quickly.

Table 4.11 shows the accuracy during the data outage, and Table 4.12 shows the accuracy during the minute immediately following the data outage when GPS is once again present but with float ambiguities. In both cases, augmenting GPS with other sensors greatly improves the accuracy. GPS augmented by other sensors with the pitch constraint is more accurate than without the pitch constraint because ambiguities resolve faster, near the beginning of the minute following the data outage.

Table 4.11: Accuracies during Data Outage

Sensors	Mean (cm)	Standard Deviation (cm)	RMS (cm)	Number of Samples
GPS + Camera	1.2	4.7	4.9	880
GPS + Laser	1.7	6.4	6.6	880

Table 4.12: Accuracies during Minute After Data Outage

Sensors	Mean (cm)	Standard Deviation (cm)	RMS (cm)	Number of Samples
GPS	6.9	15.4	16.9	816
GPS + Camera	4.2	4.5	6.2	816
GPS + Laser	-0.5	1.5	1.6	816
GPS with Pitch Constraint	5.4	15.7	16.6	816
GPS + Camera with Pitch Constraint	0.1	1.9	1.9	816
GPS + Laser with Pitch Constraint	-0.3	0.9	1.3	816

4.5.4 Ambiguity Resolution Speeds

As mentioned previously, ambiguities should be resolved more quickly when other sensor data is present. This is because the other sensors constrain the value closer to its true value. Table 4.13 shows the time required to resolve ambiguities for GPS alone and in sensor combinations, with and without a pitch constraint, during the static time at the beginning of the test. Table 4.14 shows the same information for the resolution of ambiguities after the data loss described above.

Table 4.13: Time Required to Resolve Ambiguities during Initial Static Period

Sensors	Time to Resolve Ambiguities (seconds)	Percent Improvement
GPS	70.7	n/a
GPS + Camera	19.9	71.9
GPS + Laser	19.2	72.8
GPS with Pitch Constraint	66.4	6.1
GPS + Camera with Pitch Constraint	20.5	71.0
GPS + Laser with Pitch Constraint	10.4	85.3

Table 4.14: Time Required to Resolve Ambiguities After Kinematic Data Outage

Sensors	Time to Resolve Ambiguities (seconds)	Percent Improvement
GPS	73.6	n/a
GPS + Camera	40.6	44.8
GPS + Laser	2.8	96.2
GPS with Pitch Constraint	56.0	23.9
GPS + Camera with Pitch Constraint	4.4	94.0
GPS + Laser with Pitch Constraint	0.4	99.5

It is clear that in both cases, the time needed for ambiguity resolution is reduced by combining GPS with other sensors. The laser has a greater improvement than the camera, most likely because it is more accurate. Additional trials at different times throughout the test show the same trend of the camera augmentation showing some improvement and the laser augmentation showing greater improvement. The magnitude of the improvements was somewhat variable. This is primarily due to the camera not being perfectly calibrated, as well as the laser's inability to consistently identify the correct target.

Using the pitch constraint did not have a large effect on ambiguity resolution during the static period at the beginning of the test. However, it had a great effect on ambiguity resolution during the kinematic period. As mentioned, the distance-azimuth-pitch formulation is less stable than the easting-northing-up formulation. During a kinematic period when these variables are changing, it makes it even more difficult to converge. The pitch constraint makes sure that this parameter can not vary wildly, thereby allowing the other parameters to converge more quickly.

Additionally, when dealing with ambiguity resolution, noise values assigned to the sensors are particularly important. For example, if an overly low variance is given to the assisting sensor's data, then even if the measurement value is closer to the truth, the ambiguity search space is reduced so far as to exclude the true ambiguity set.

4.5.5 Reliability Improvement

The order of processing was camera, then laser, then GPS, as shown in Figure 4.13. As discussed in section 2.4, the first sensors used do not have their MDB improved from the use of later sensors. Therefore, most importantly, it is the MDB as well as the resulting PL of the GPS observations that should be examined to reflect the reliability improvements gained by the use of assisting sensors.

Figure 4.42 shows a plot of all MDBs for the entire test, using GPS alone, GPS with camera, and GPS with the camera and laser.
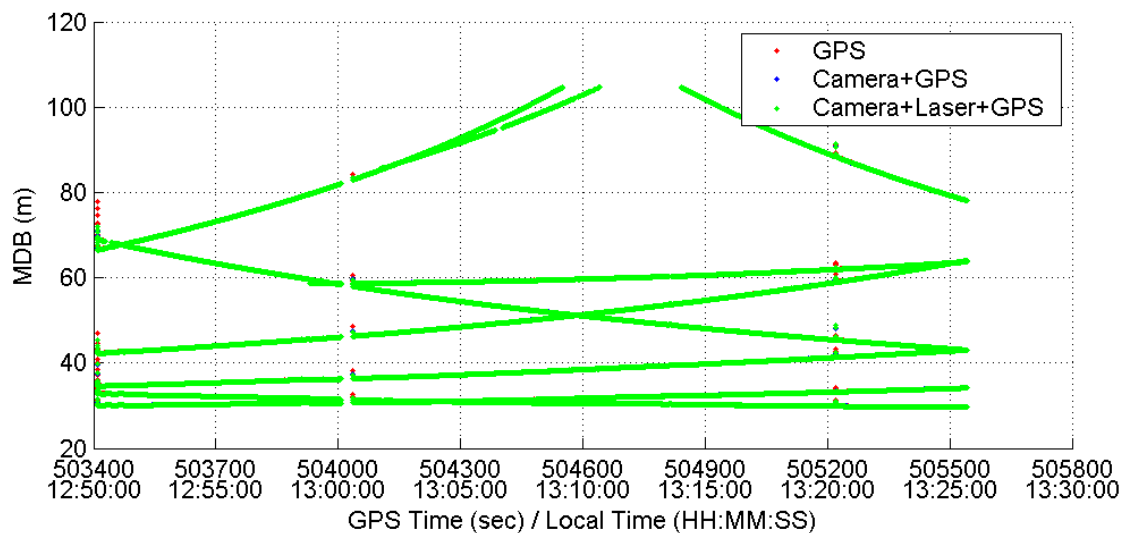
Figure 4.42:   MDB for Code Observations

Firstly, there appear to be several continuous lines. These correspond to different satellites. Variations over time occur due to changes in satellite geometry, affecting the accuracy of the measurements. Secondly, it appears that the result of GPS alone and in combinations is virtually the same. This is true, except at the beginning of the test, shown in Figure 4.43.
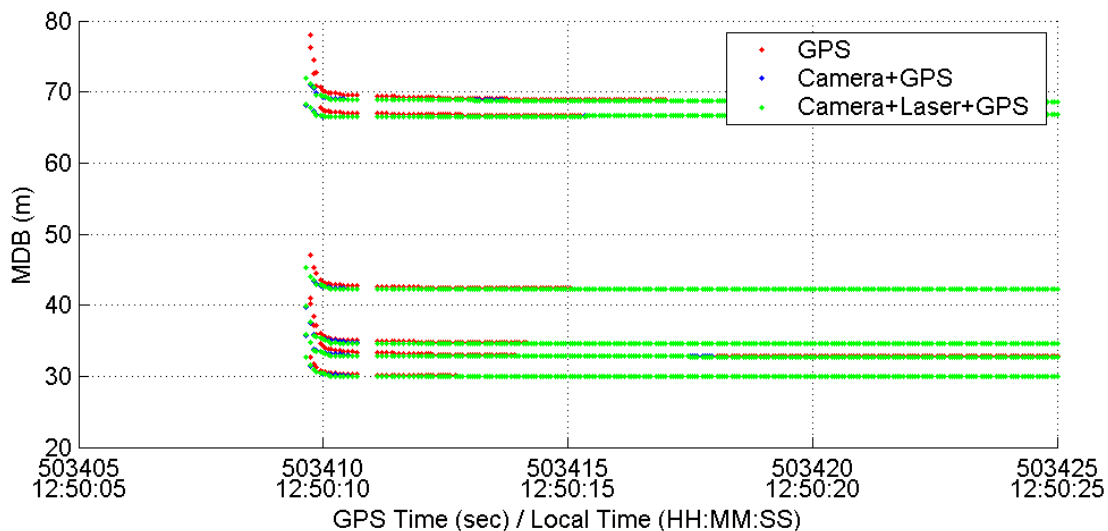
Figure 4.43:   MDB for Code Observations at the Beginning of the Test

Upon closer inspection, it is clear that at the very beginning, the combination of GPS with other sensors results in lower MDB values than GPS alone.   The MDB is proportional to the variance-covariance of the parameters. At the beginning of the test, initial estimates give relatively poor estimates of the parameters, which is reflected by their variance. The camera and laser are overall of higher accuracy, and are able to serve to quickly reduce the variance of the parameters. However, after a short time of filtering, the parameters have converged, and the variance of the parameters has become stable at a reasonably low level.   At this level, the camera and laser observations are no longer significantly reducing the variance of the parameters, and therefore the MDB is no longer improved by using these observations.

Often more noteworthy than the results of the MDBs are the PLs. Figure 4.44 shows the effects of the MDBs on the distance parameter throughout the test. After a short period of time the values are very close to zero, because the MDB has become small, and the observations are naturally weighted in the Kalman filter accordingly such that those with higher MDBs have less effect on the parameters. There are two other noteworthy points

in the figure, where the PL for GPS alone is high again. These occur after short periods of data loss. Figure 4.45 shows the effects at the very beginning of the test. When GPS is assisted by other sensors, the effect of the MDB is almost immediately very small, whereas for GPS alone an MDB could create significant errors for a short period of time. Figure 4.46 shows the effects at the beginning of the test, with the y-axis scaled to a more detailed level. It is clear that the effect of GPS blunders is virtually zero when an assisting sensor is present.
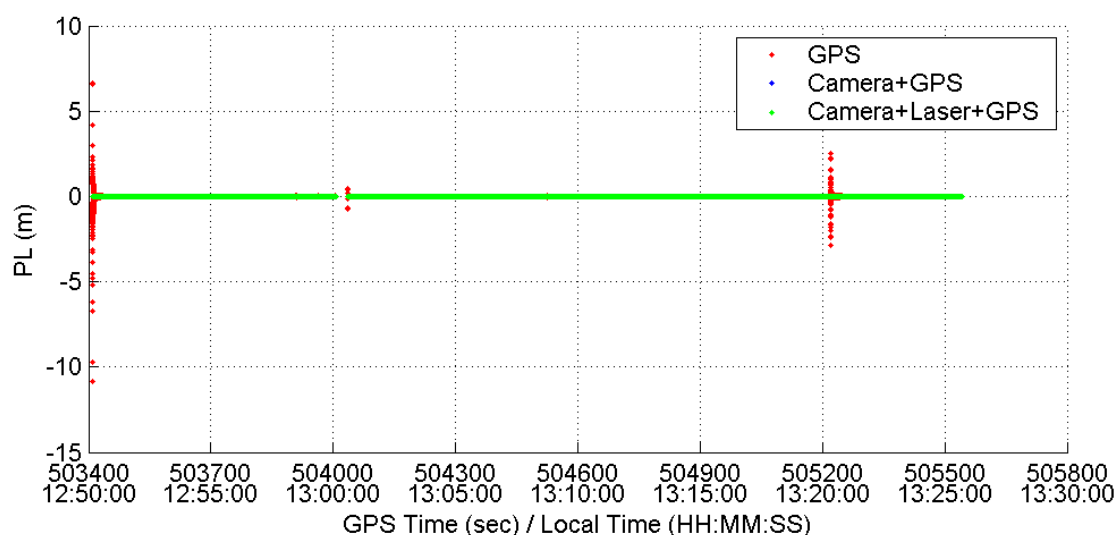

Figure 4.44:   Effect of Code MDB on Distance Parameter
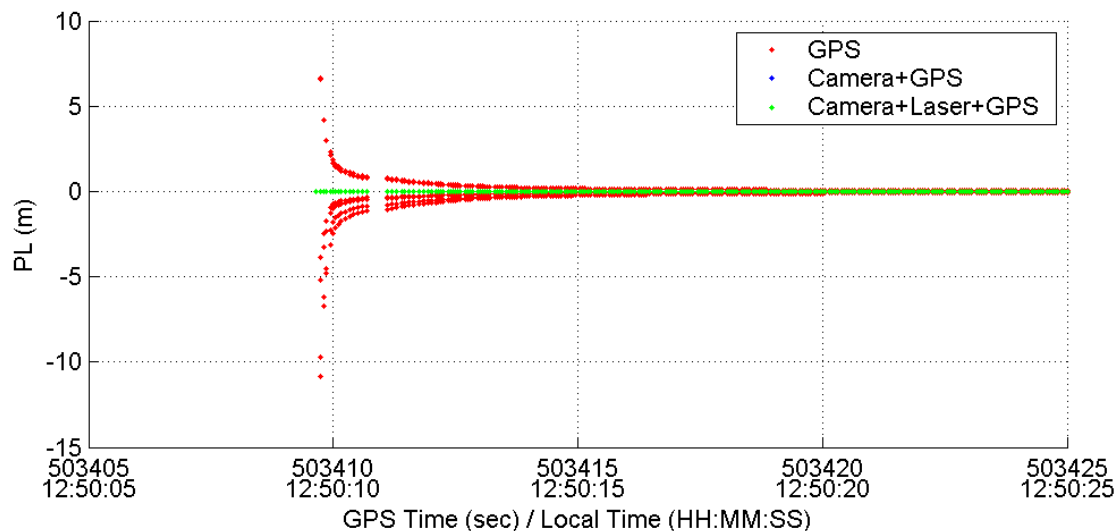
Figure 4.45:   Effect of Code MDB on Distance Parameter at Beginning of Test
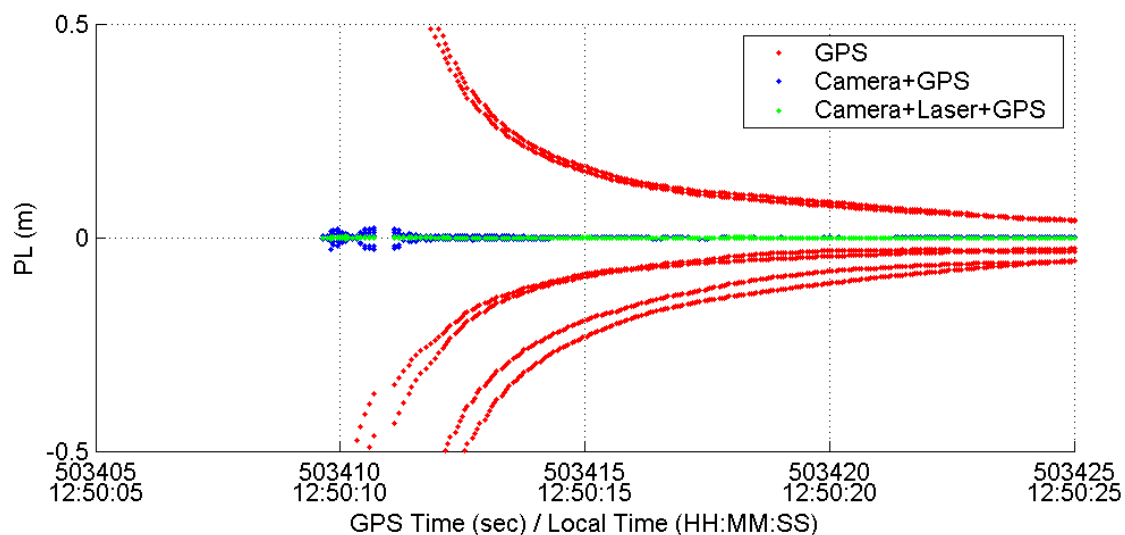
Figure 4.46:   Effect of Code MDB on Distance Parameter at Beginning of Test (zoomed)

The effects of code MDBs on distance have been shown. Much the same effect is seen in the effects of code MDBs on azimuth, pitch, and ambiguities.

All of the same trends as seen in code MDBs and PLs are seen when examining the carrier phase observations, except that the scale is much lower because the carrier phase observations are much more accurate.

4.6   Real-Time Tests

Here the results from the series of real-time tests that took place between November 8 and November 19, 2004, will be discussed. Several tests were performed in different locations and with different sensor combinations.

4.6.1   Laser-Only Real-Time Test

For the real-time tests, the robot was set up slightly different. A piece of cardboard was present at the base of the coloured cylinder, where the laser would be making measurements. This changed the laser profile to that shown in Figure 4.8. A photo showing the presence of the cardboard triangle on the lead robot is shown in Figure 4.47. This improved tracking significantly. However, occasionally tracking was still difficult. If the laser lost track of the target, the lead robot could occasionally be manoeuvred such that it entered the laser processor's search area, and the laser reacquired tracking. This was happening far too often in initial tests, and so the tracking threshold had to be relaxed. Still, the dynamics had to remain fairly low.

A photo of the test area and the path of the robots is shown in Figure 4.48.

Cardboard Triangle

Figure 4.47:   Follower and Leader Robots with Cardboard Triangle
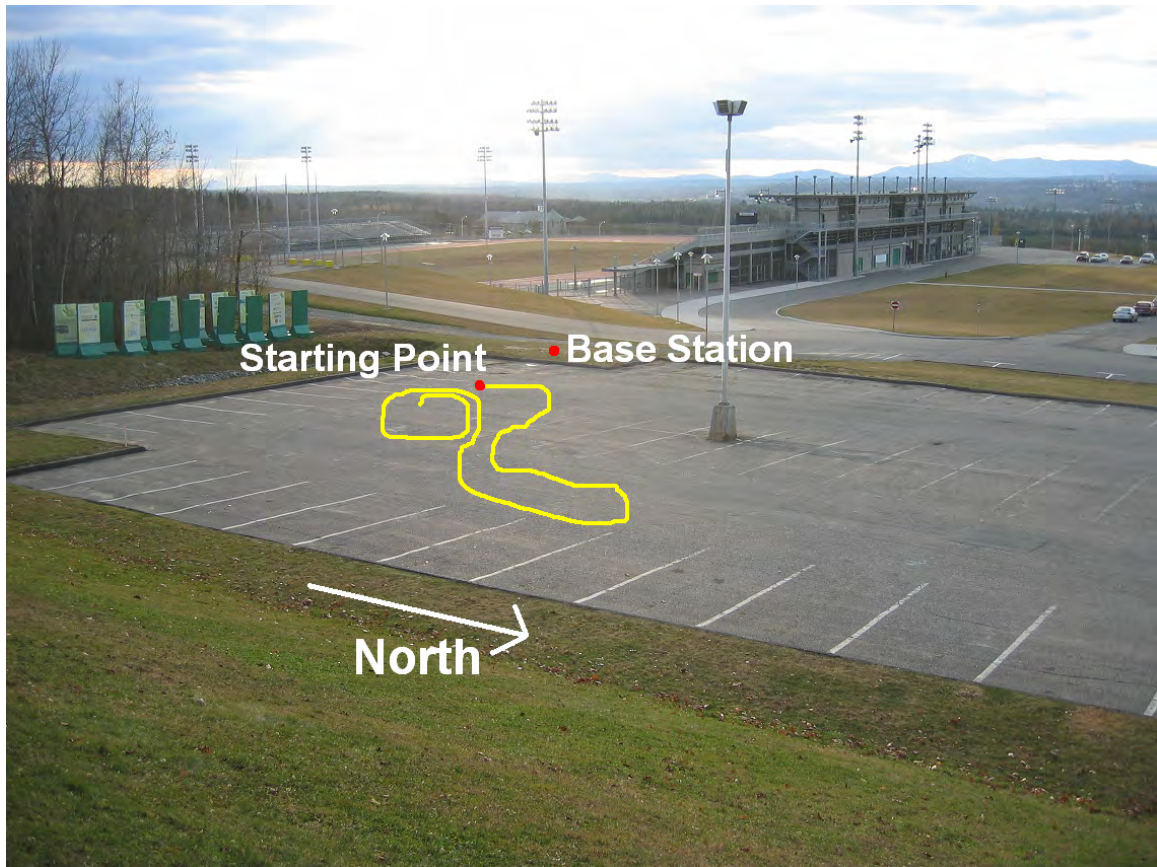
Figure 4.48:   Location of Laser-Only Real-Time Test

An interesting result discovered when analysing the data post-mission is that the GPS-derived positions had a significant time delay.   This time delay appeared to grow throughout the test. The postulated reason for this is lag in the network. Figure 4.49 shows the time lag during a kinematic period of the test. Although the follower robot still had its own GPS data up to date, there was a delay in the arrival of the leader's GPS data, and therefore the differential positions being computed were out of date.   Since it is mandatory to have up to date GPS data to relate the CPU time to GPS time for the use of the reference distance values, no comparisons to the reference values could be computed for this data set.
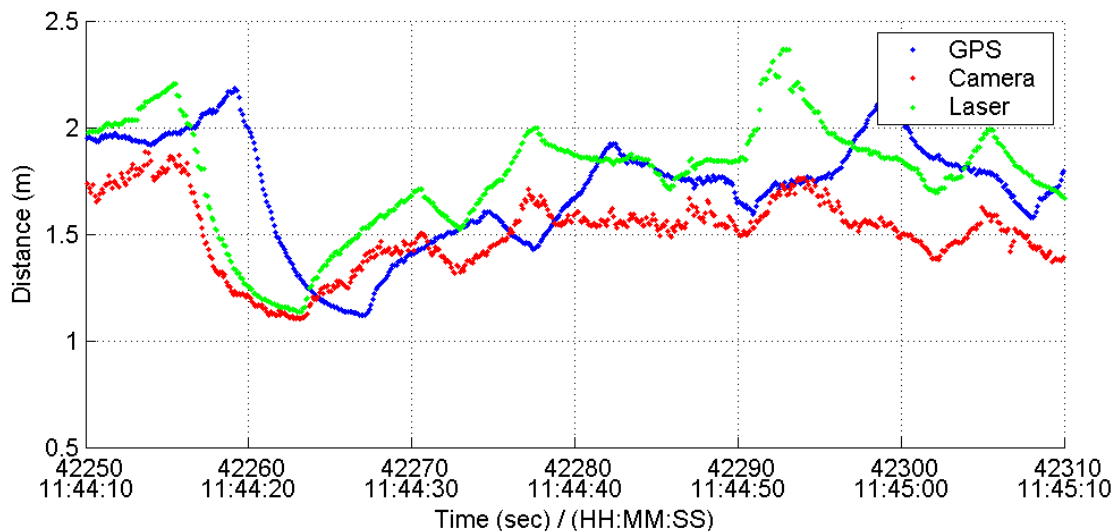
Figure 4.49: GPS, Camera, and Laser Output during Kinematic Period, Showing GPS Time Lag

A final result noted was that the offsets between the camera, laser, and GPS were not set perfectly. In post-processing, it is easy to change this, but not during a real-time test. As a result, when processing with the original incorrect offsets, addition of other sensors actually increased the time it took to resolve ambiguities. Tables 4.15 to 4.17 show the statistics during the initial static time. Note the differences in mean value in Table 4.15, indicating the incorrect offsets. Table 4.17 includes the times taken to resolve ambiguities with the original incorrect offsets, as well as with the corrected offsets. It is clear that applying the correct offsets is important for the sensor integration.

Table 4.15: Statistics for Distance during Static Period Compared to Self

Sensors	Mean (m)	Standard Deviation (cm)	Number of Samples
GPS	1.305	0.1	574
Camera	1.131	1.0	574
Laser	1.335	0.5	574
GPS + Camera	1.142	0.2	574
GPS + Laser	1.337	0.1	574
Camera + Laser	1.328	0.5	574
GPS + Camera + Laser	1.328	0.1	574
Reference Values	1.305	0.2	574

Table 4.16: Statistics for Angle during Static Period Compared to Self

Sensors	Mean (degrees)	Standard Deviation (degrees)	Number of Samples
Camera	0.97	0.12	574
Laser	-0.50	0.54	574
Camera + Laser	0.42	0.28	574

Table 4.17: Time Taken To Resolve Ambiguities during Initial Static Period

Sensors	Time to Resolve Ambiguities (seconds)	Percent Improvement
GPS	220.1	n/a
GPS + Camera	423.3	-92.3
GPS + Laser	391.0	-77.7
GPS + Camera (correct offset)	87.9	60.1
GPS + Laser (correct offset)	39.2	82.2

4.6.2   Camera + Laser Real-Time Test

The location of the camera + laser real-time test is shown in Figure 4.50. The incorrect offset discussed in the previous test had not been corrected yet when the laser was combined with the camera for a test. Figure 4.51 shows what happens as a result. While the laser is tracking, the output is quite stable. However, when the laser loses tracking, there is a sudden jump as the output switches to the camera values. If the laser reacquires tracking, the output jumps back to the laser values again.
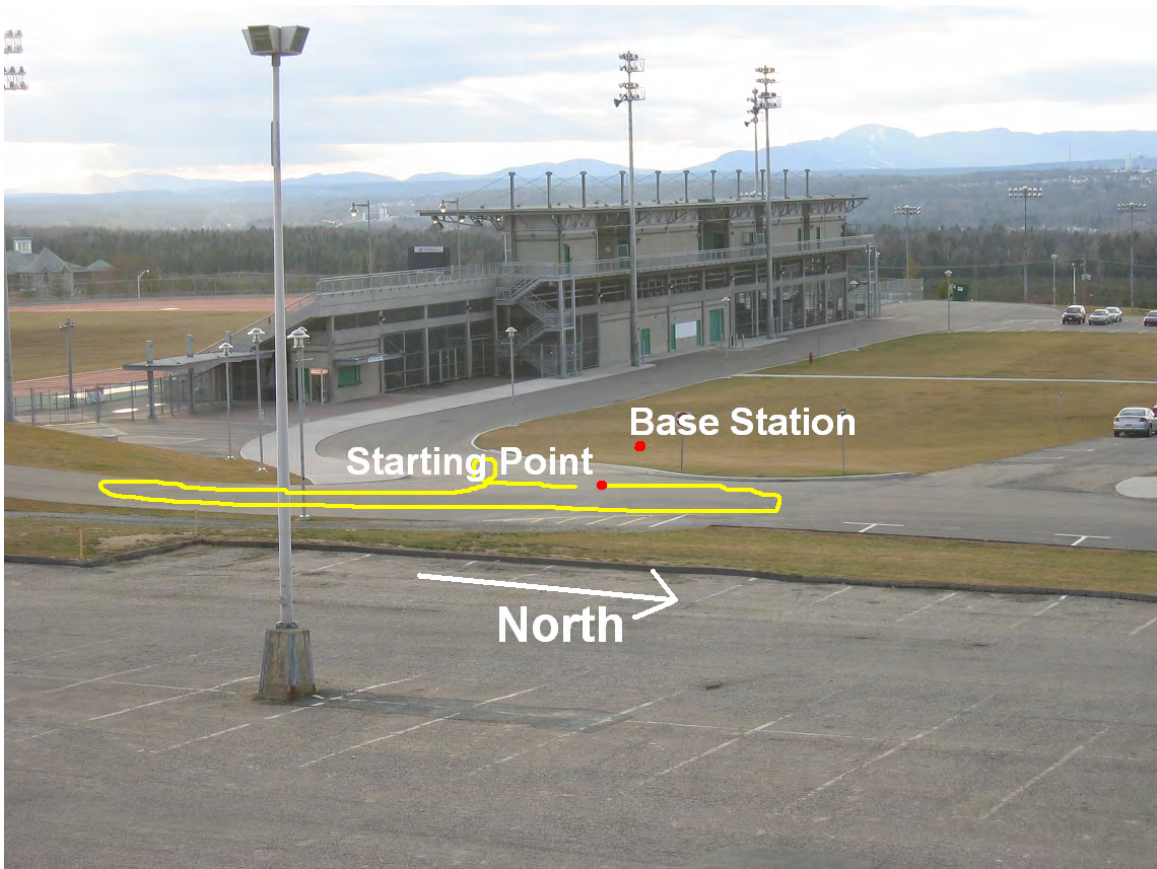
Figure 4.50:   Location of Camera + Laser Real-Time Test
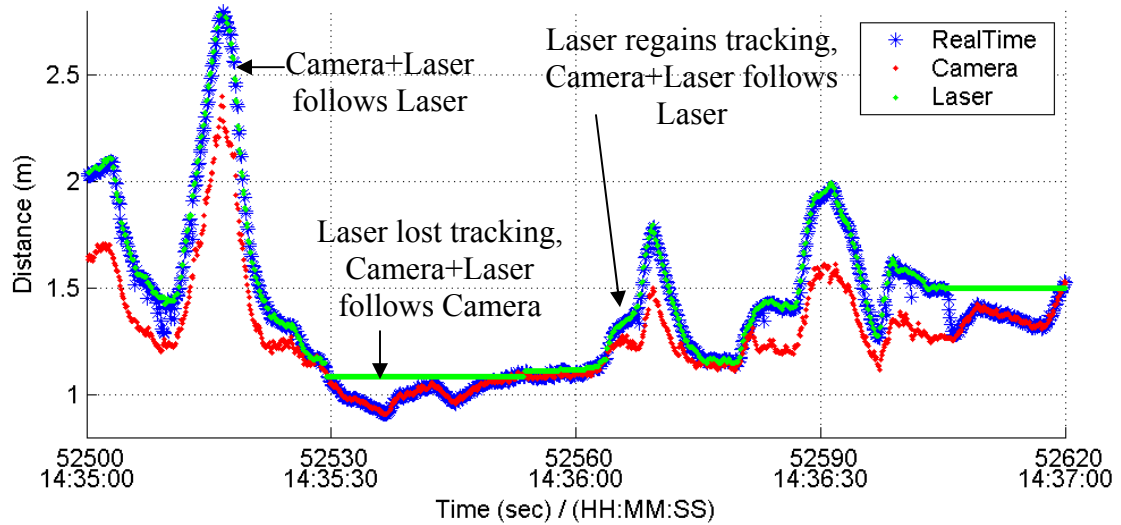
Figure 4.51:   Camera + Laser Test with Incorrect Offsets

By combining the laser with the camera, results were continuously available. Although the laser results are more accurate, laser tracking is still occasionally lost, and the presence of the camera ensures that distance and angle measurements are still available.

4.6.3   GPS + Camera Real-Time Test

The first major problem encountered when using GPS for navigation in real-time was the data lag that occasionally appeared in the previous tests. Once the ambiguities fixed, GPS had the lowest standard deviation, and therefore had the most influence over the output solution. When the robots were farther apart than they should be, the follower moved forward towards the leader. However, because of the GPS data lag, even though the follower had moved closer to the leader, the data showed that it was still far away. Therefore the follower continued to move forward, and actually rammed the lead robot. Eventually the GPS data caught up, and the follower robot learned it was too close. It then backed up. Once it was sufficiently far away, the data still showed that it was too close, so it continued to back up. It then became too far away, and when the data

eventually caught up and showed this, the robot rushed forwards again. This continued while GPS was used for navigation.

Steps were taken to try to eliminate the lag the network was creating. The entire test was set to run at 5 Hertz instead of 10 Hertz. Also, some GPS data that was unnecessary was no longer logged, reducing the amount of data transmitted and searched. These steps solved the problem of network lag.

Another problem experienced while using GPS combined with other sensors occurred when the assisting sensor lost sight of the lead robot. GPS continued to provide distance measurements, and based on that distance the follower robot decided whether to move forward, stay still, or move backwards. However, without the angle from other sensors, the follower would occasionally be moving in a completely incorrect direction.

In post-processing, similar results to those already seen in other tests were discovered. The presence of the additional sensor constrained the output values closer to the truth values while ambiguities were float, and allowed the ambiguities to fix to their integer values sooner. The test path for the GPS + camera test is shown in Figure 4.52.
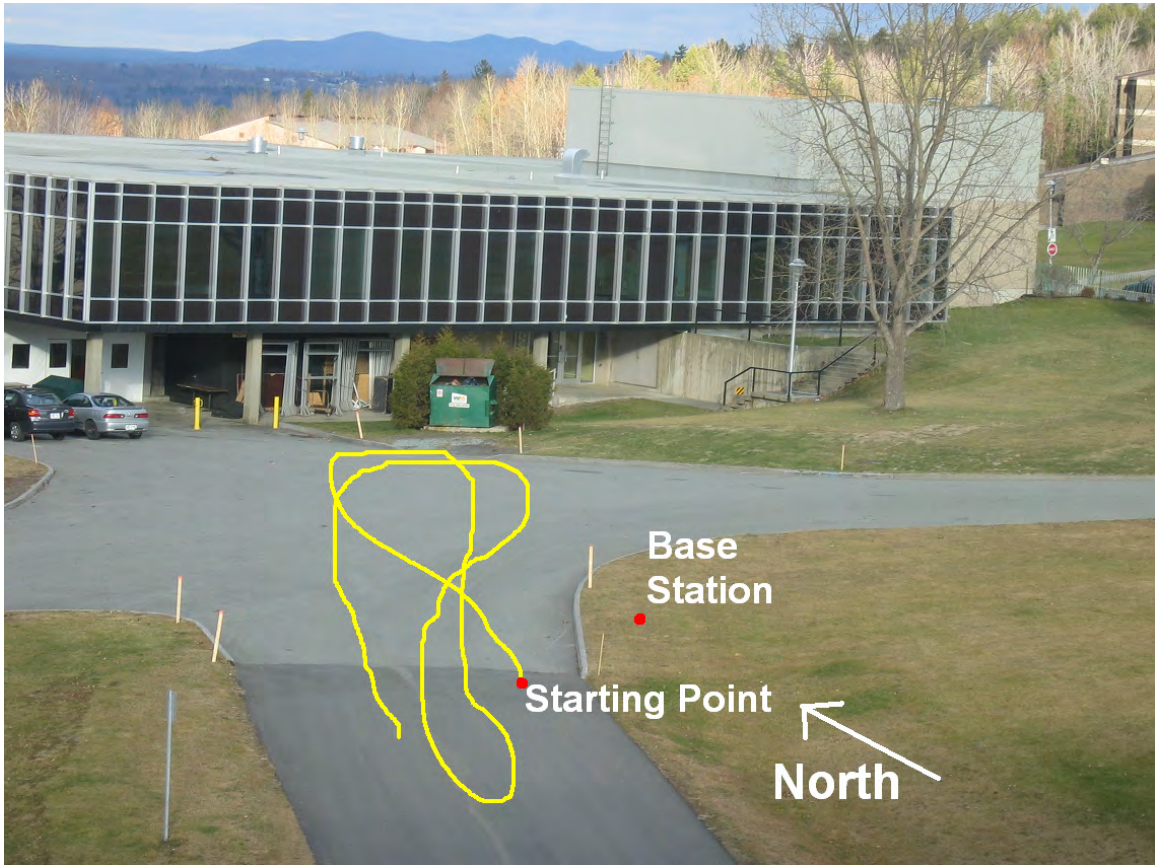
Figure 4.52:   Location of GPS + Camera Real-Time Test

4.6.4   All Sensors Real-Time Test

For the all sensors real-time test, there are several expected outcomes. Firstly, all sensors may be available at all times. As a result, whichever is most accurate at a given time will be dominating. If the laser is still tracking, it will be completely dominant over the camera. If the GPS has fixed ambiguities, it will be dominant over the other two. The path of the test using all sensors is shown in Figure 4.53.
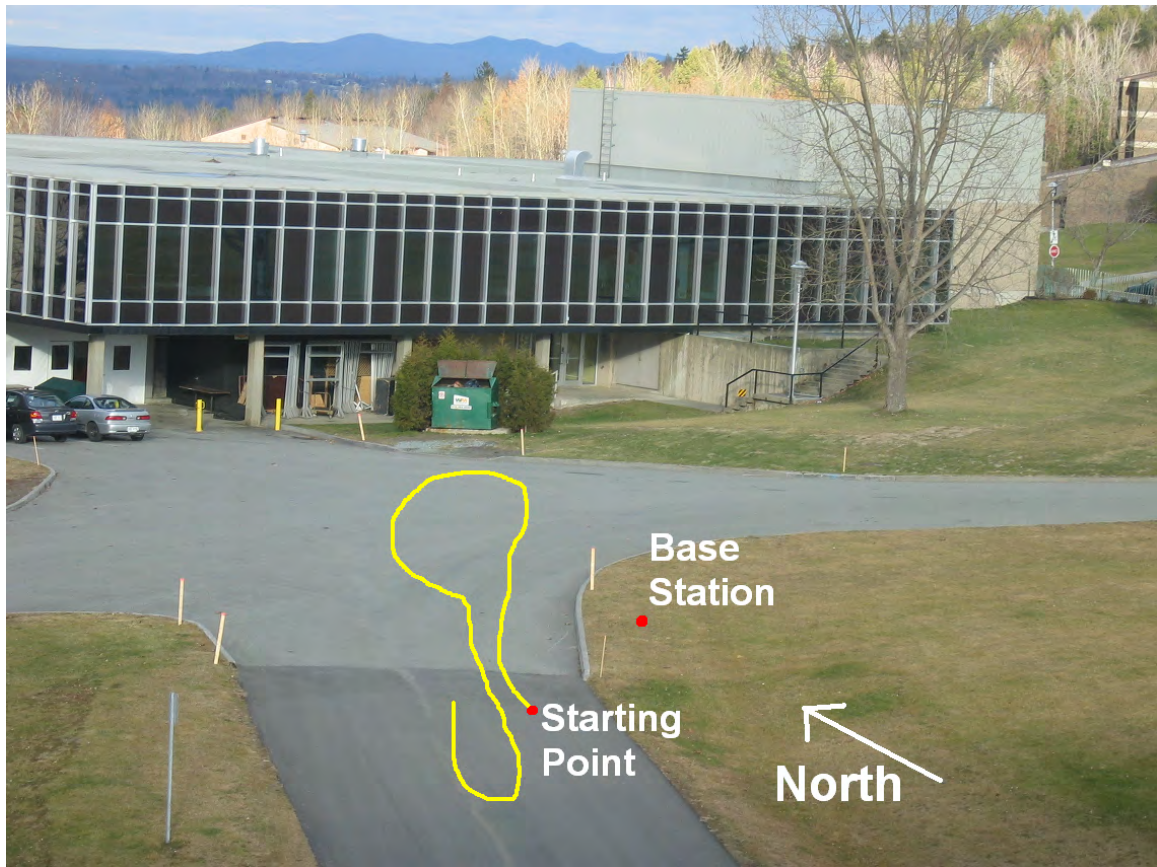
Figure 4.53:   Location of All Sensors Real-Time Test

The reference distance values, shown in Figure 4.54, shows that initially there was about 1.2 metres between the robots, then this distance suddenly increased to about 2.6 metres for some time. This was a manual move of the robots. Eventually the robots began moving. There is a period of time where no results appear. This occurs in all sensor plots, and must have been an error in the data collection, not the sensors or processing. Finally, the test ends with some static time.
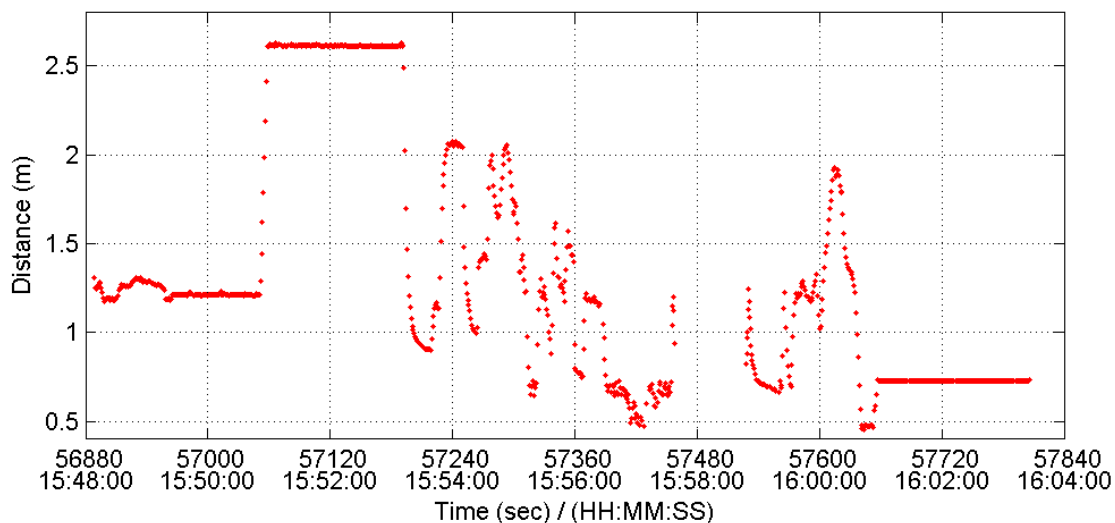
Figure 4.54:   Reference Distance Values during All Sensors Real-Time Test

GPS, shown in Figure 4.55, follows the same pattern as the reference data throughout. However, it takes a very long time to fix ambiguities. In fact, ambiguities do not fix at all throughout the static period at the beginning of the test.
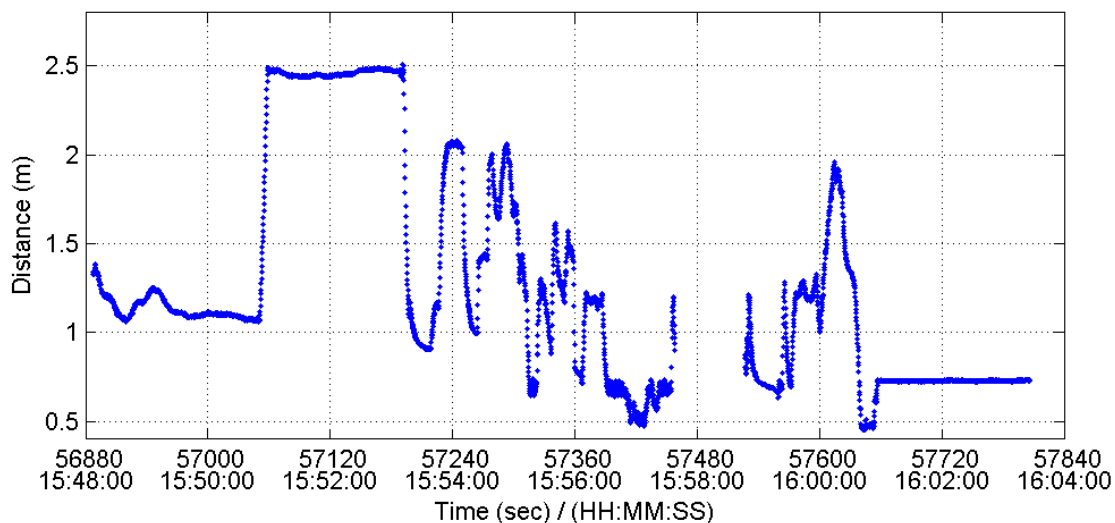
Figure 4.55:   GPS-Measured Distance during All Sensors Real-Time Test

The camera processing, shown in Figure 4.56, clearly follows the same pattern as the reference data. However, it is very noisy at higher distances. Also, although it is aligned with the reference data at the beginning of the test, and continues to be at moderate distances, the camera-measured distance appears to deviate from the reference distance at very short and very long distances. This suggests the camera calibration was not as accurate as it should have been.
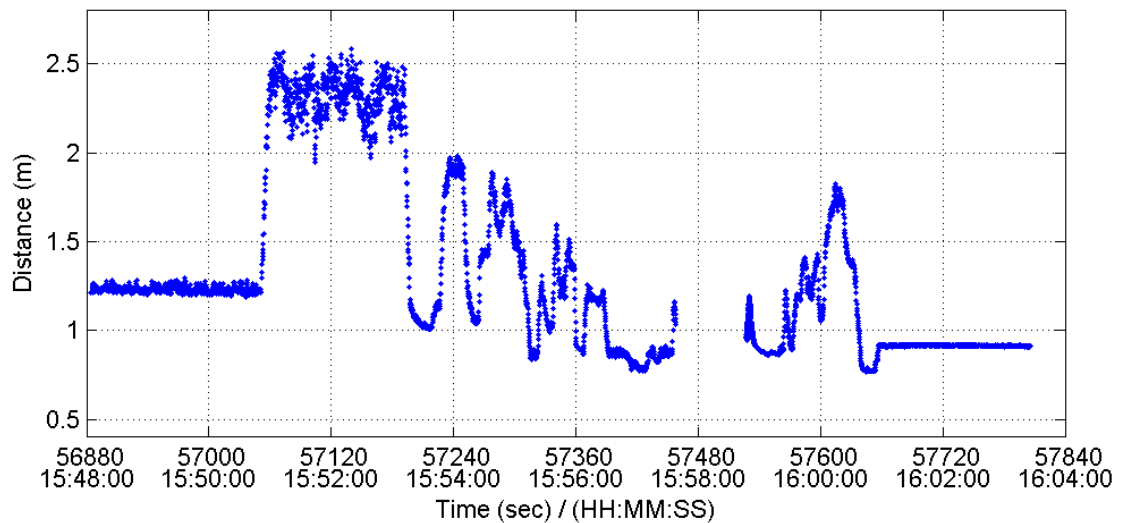
Figure 4.56:   Camera-Measured Distance during All Sensors Real -Time Test

The plot of the laser data in Figure 4.57 shows that it follows the same pattern as the reference data as long as it is tracking correctly. When there was a rapid increase in distance between the robots near time 15:51, the laser lost tracking, and thus provided no useful information for quite some time. Later on it appeared to reacquire, but continued to periodically lose tracking throughout the test. It is important to note that for this test and those to follow, a different lead robot was used since the original one broke. All the same equipment and software was set up on the new lead robot, however it is possible that some features such as the cardboard triangle were not positioned identically to the previous setup.
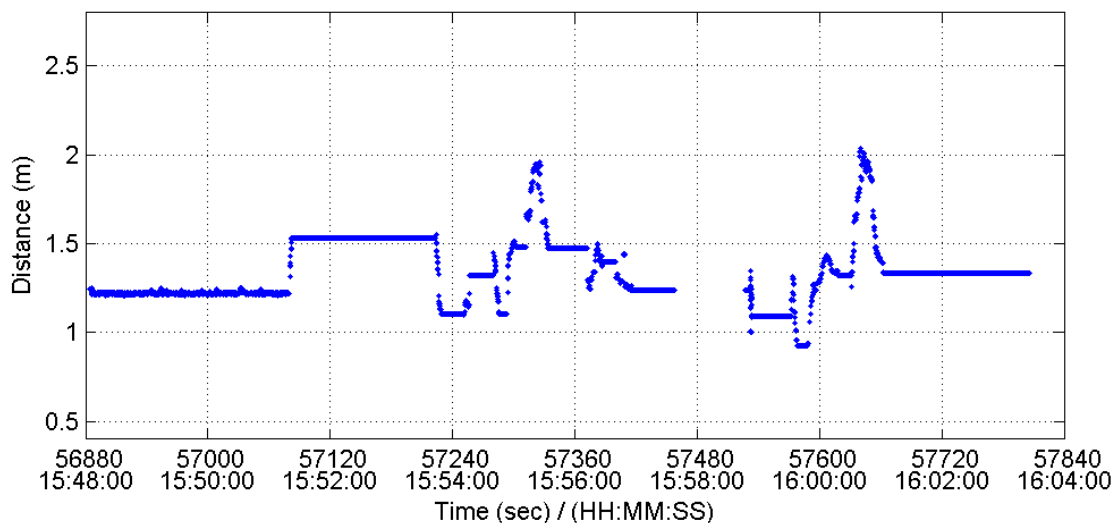
Figure 4.57:   Laser-Measured Distance during All Sensors Real-Time Test

When the camera is combined with the GPS, the output is approximately the same as the GPS alone, except at the beginning of the test where values are closer to the truth and GPS ambiguities are able to fix much faster. This is demonstrated in Figure 4.58.
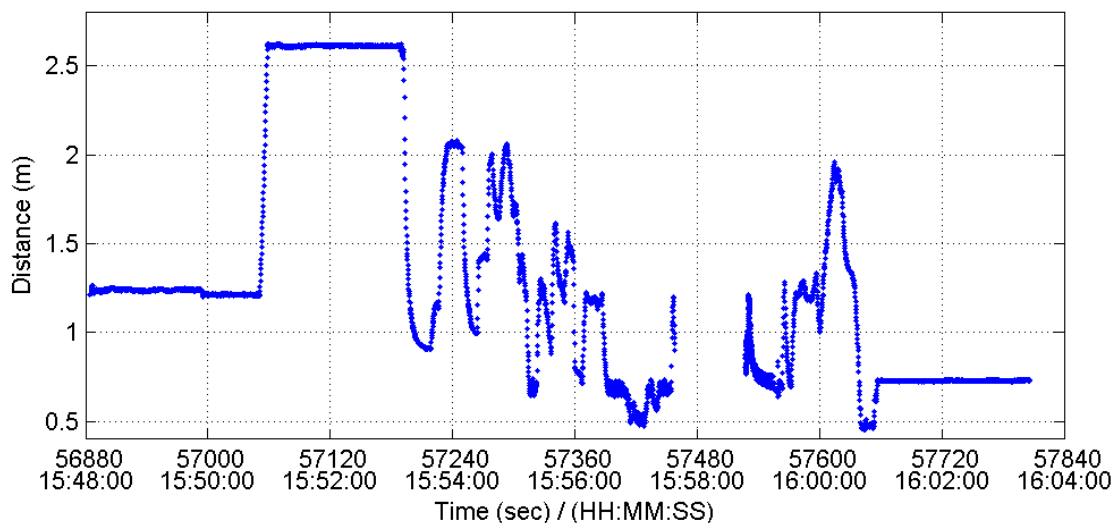
Figure 4.58:   GPS+Camera-Measured Distance during All Sensors Real-Time Test

When the laser was combined with the GPS, the results shown in Figure 4.59 were not at all as expected. The laser is quite accurate at the beginning of the test. However, ambiguities are unable to fix. The best explanation for this is that while it is true that the laser is quite accurate, it also has a low standard deviation value, which was perhaps lower than it should have been in this case. Therefore, although the laser values were close to the true values, the standard deviation of the solution was small enough that the ambiguity search space was too small to find the correct ambiguities. This data set was processed once again, using 10 centimetres for the laser standard deviation instead of 5 centimetres, and the ambiguities were able to fix successfully, and remain fixed throughout the data. The other notable thing about this plot is that the values near the end are much higher than expected. A closer inspection shows that laser data was only sporadically available during the middle of the test, leaving float-ambiguity GPS to provide the solution alone. However, processing float-ambiguity GPS without laser assistance resulted in values that were much closer to the reference data. Careful inspection of the data leads to the following conclusion. In the sporadic appearances of laser data during the middle of the test, the values were higher than they should have been, indicating an incorrect target identification. Since the laser observations still had low standard deviation, they pulled the float GPS away from the reference values. The GPS processing compensated by computing a pitch value of near 60 degrees, which obviously did not occur in reality. However, as mentioned in the background information, the distance-azimuth-pitch approach is somewhat less robust than the easting-northing-up formulation traditionally used.
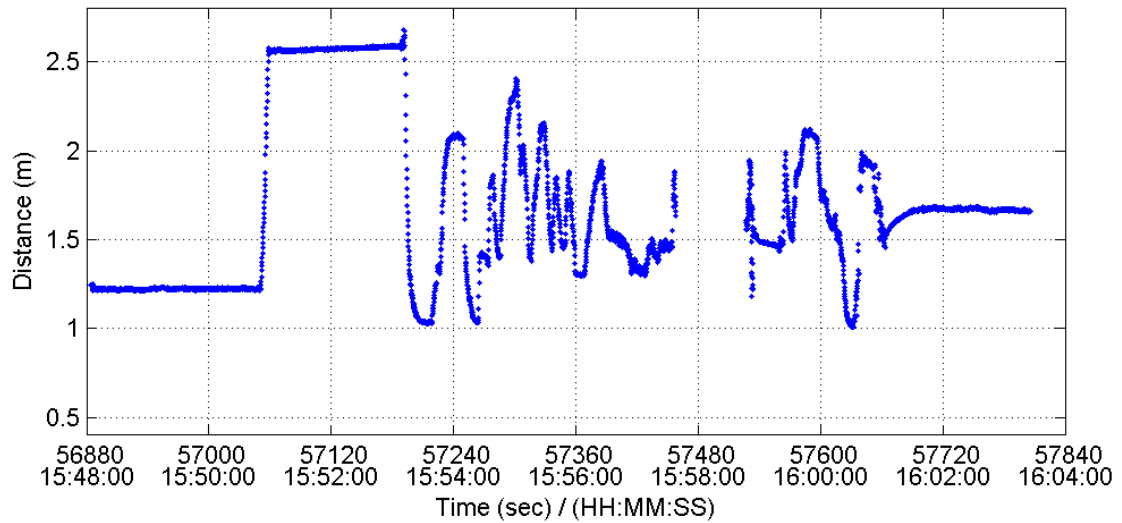
Figure 4.59:   GPS+Laser-Measured Distance during All Sensors Real-Time Test

In the processing where all sensors are used, shown in Figure 4.60, results look similar to those of the GPS + laser results. However, in the middle, the output is closer to the reference data, since the camera data remains present while the laser data does not. Again at the end, though to a lesser extent, the pitch value obtains a much higher value than is reasonable, and the distance output ends up much higher than it should.
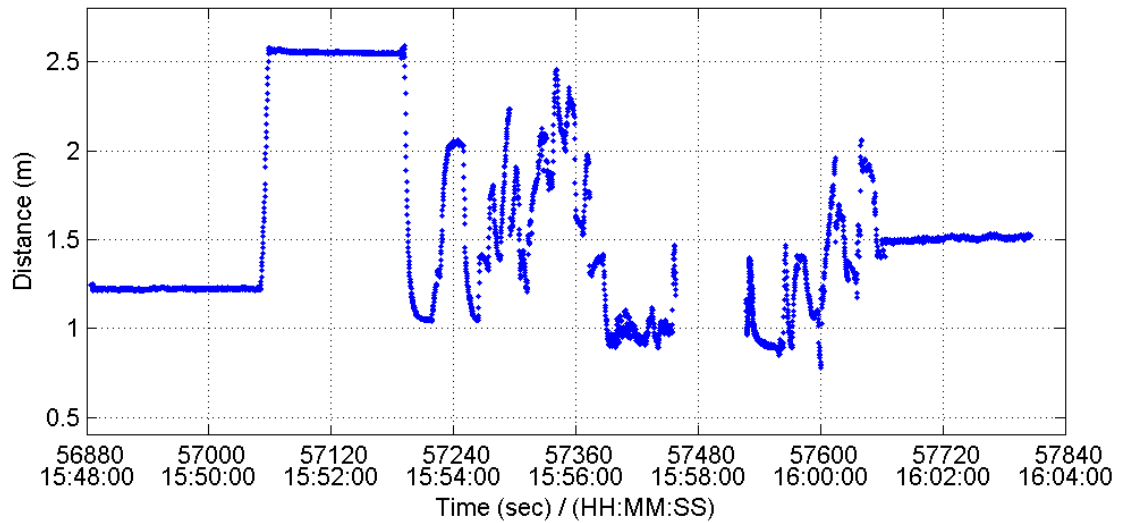
Figure 4.60: GPS+Camera+Laser-Measured Distance during All Sensors Real-Time Test

Improvements are seen when the pitch constraint is implemented. This is demonstrated in Figures 4.61 to 4.63. Firstly, when GPS alone is used, ambiguities resolve more quickly and are resolved during the initial static period. When GPS is combined with the camera, results with the pitch constraint are again very similar to those without the pitch constraint, except that ambiguities are resolved sooner at the beginning of the test. When GPS is combined with the laser, ambiguities fix when the pitch constraint is used but did not fix when the pitch constraint was not used. However, even though ambiguities are fixed and remain so throughout most of the test, near the end the laser starts tracking an incorrect target as discussed before, and this actually causes the ambiguities in the filter to be considered incorrect and reset, and then fix to incorrect values afterwards. That results in the output distance at the end of the test being incorrect.
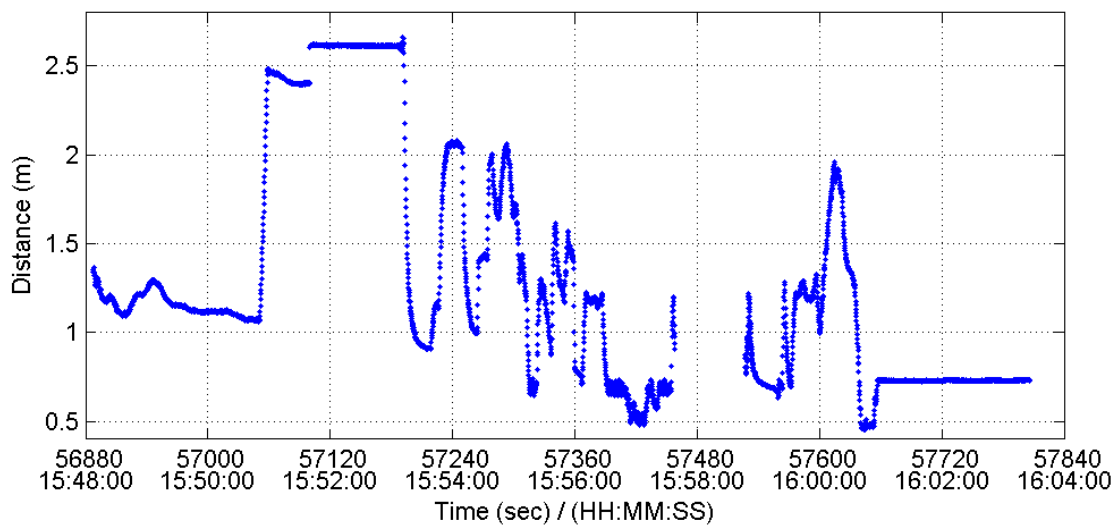
Figure 4.61: **GPS-Measured Distance during All Sensors Real-Time Test using Pitch Constraint**
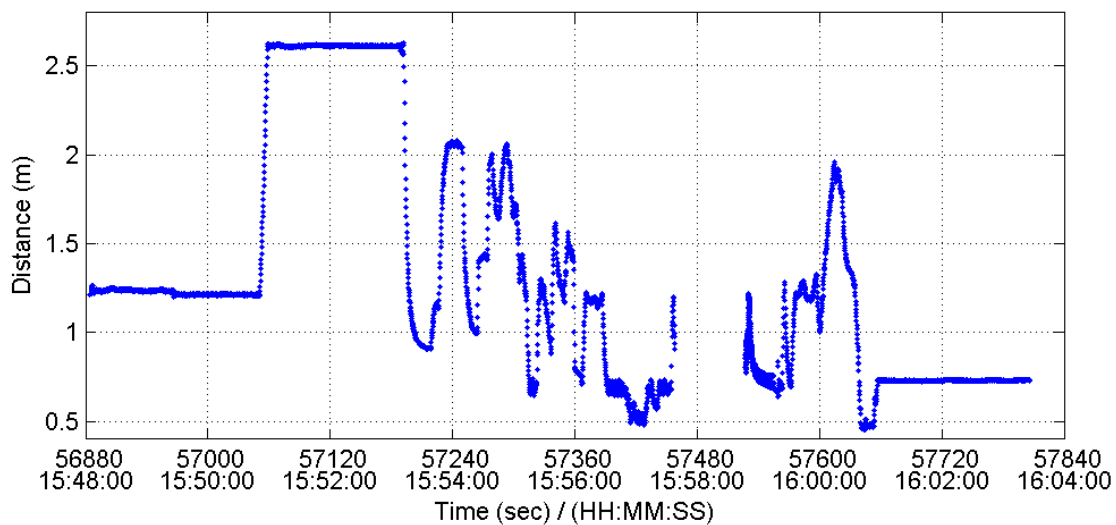
Figure 4.62: **GPS+Camera-Measured Distance during All Sensors Real-Time Test using Pitch Constraint**
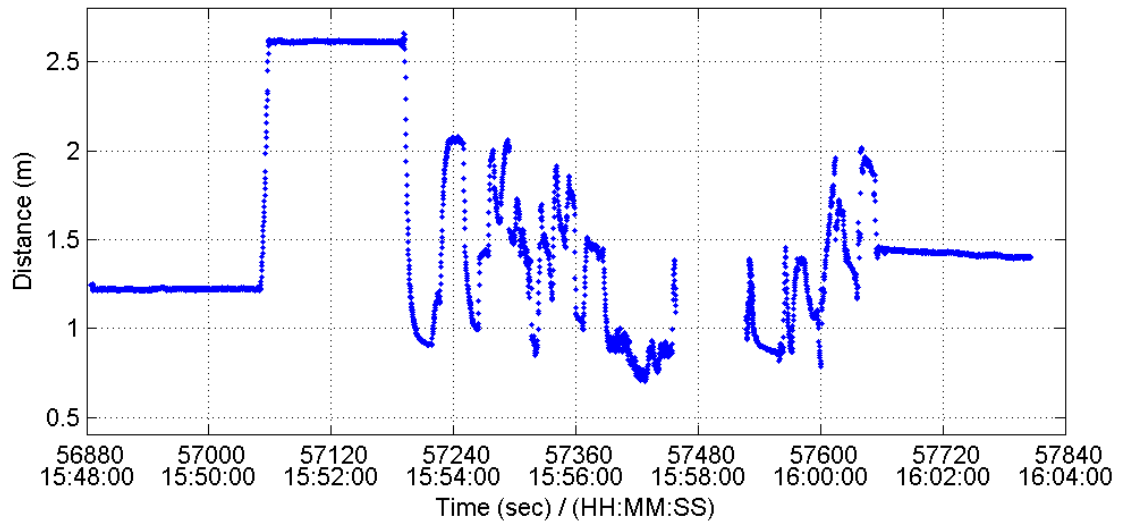
Figure 4.63: GPS+Laser-Measured Distance during All Sensors Real-Time Test using Pitch Constraint

4.6.5 GPS + Camera Real-Time Test with Physical GPS Blockage

During the final test, a GPS data blockage was created by creating a home made metal box to put over the GPS antenna for a portion of the test. This is shown in Figure 4.64. This device successfully blocked the GPS signal, although occasionally signals from one or two satellites were temporarily received.

Figure 4.64:   Follower Robot with Home Made GPS Blockage Box Mounted

During this test, the reference station ran out of batteries and therefore no reference distance values were created. However, no truth would have been created during the GPS blockage anyways. The approximate path of the robots is shown in Figure 4.65.
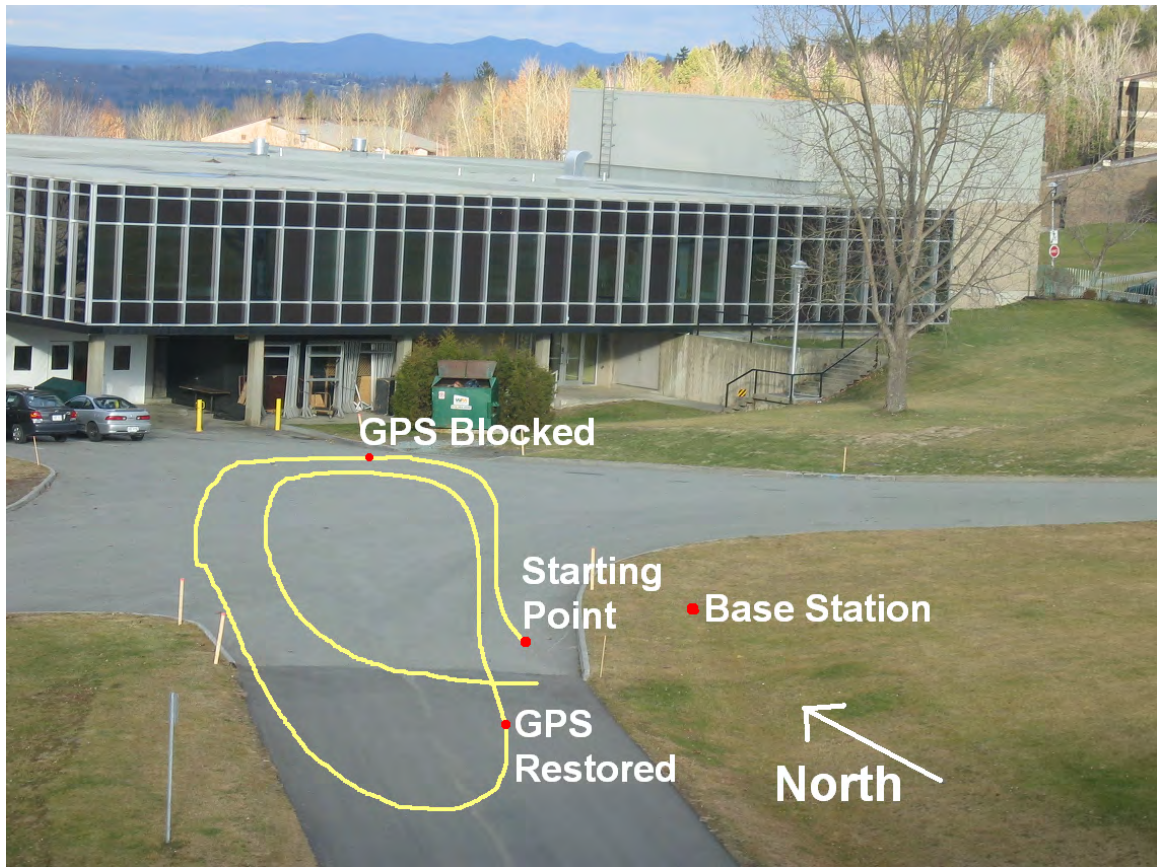
Figure 4.65: **Location of GPS Blockage Real-Time Test**

The computed distance throughout the entire test is shown in Figure 4.66. During the initial part of the test, most of the output was similar, therefore the focus of the analysis will take place during and after the GPS blockage. In these figures, the GPS blockage period is marked by a red rectangle.
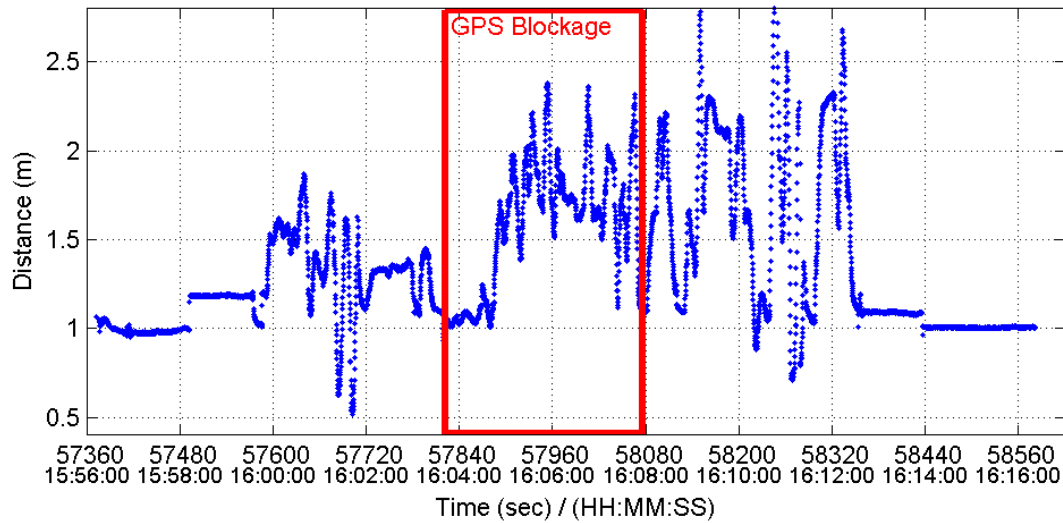
Figure 4.66: Real-Time (GPS+Camera) Measured Distance during GPS Blockage Real-Time Test

When GPS was used alone, there was no valid output during the data outage. Occasionally the GPS received some satellite signals and used these to try to update the parameters, but this had very poor accuracy. In fact, the poor results ended up creating a 180 degree change in azimuth combined with switching the output distances to be negative. This plot simply took the absolute value of distance and changed all azimuths corresponding to negative distances by 180 degrees. GPS ambiguities were able to fix some time after GPS data was restored, and the results for the rest of the test are good.
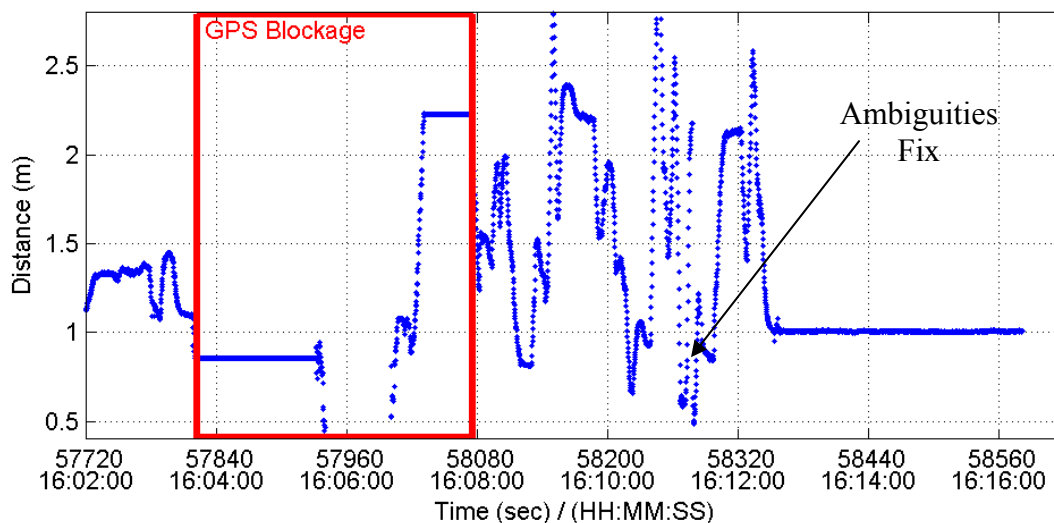
Figure 4.67:   GPS-Measured Distance during GPS Blockage Real-Time Test

The camera-only processing was not affected whatsoever by the GPS data blockage. The quality of the output is the same during the blockage as before and after the blockage.
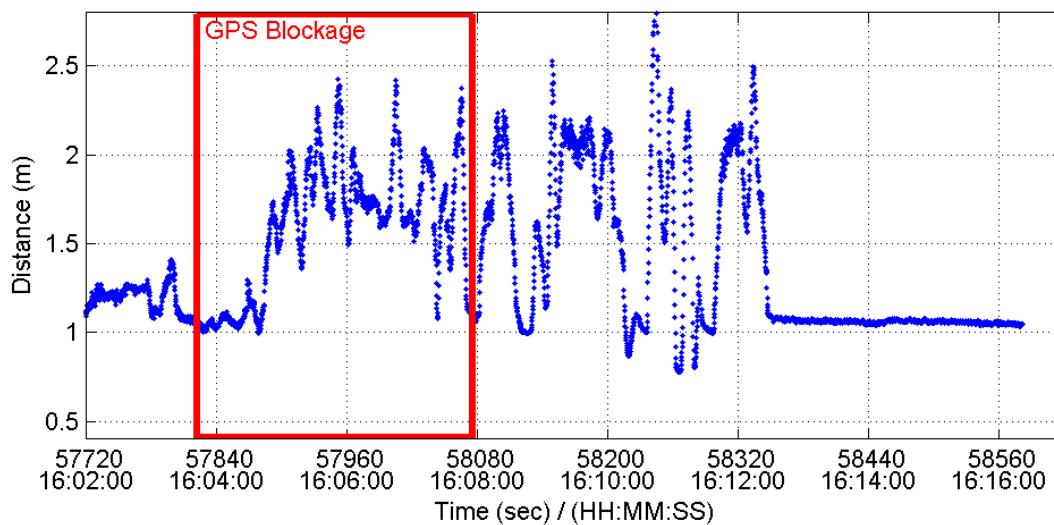
Figure 4.68:   Camera-Measured Distance during GPS Blockage Real-Time Test

Laser alone was also unaffected by the GPS blockage. Output in the blockage time remained high quality. However, laser tracking was lost for some time near the beginning of the GPS outage, and at the end of the GPS outage. Near the end of the test, the laser became on track again, though the output distance value is far from the truth. This is because another target appearing similar to the lead robot was detected in the laser processor's search space, and this was tracked.
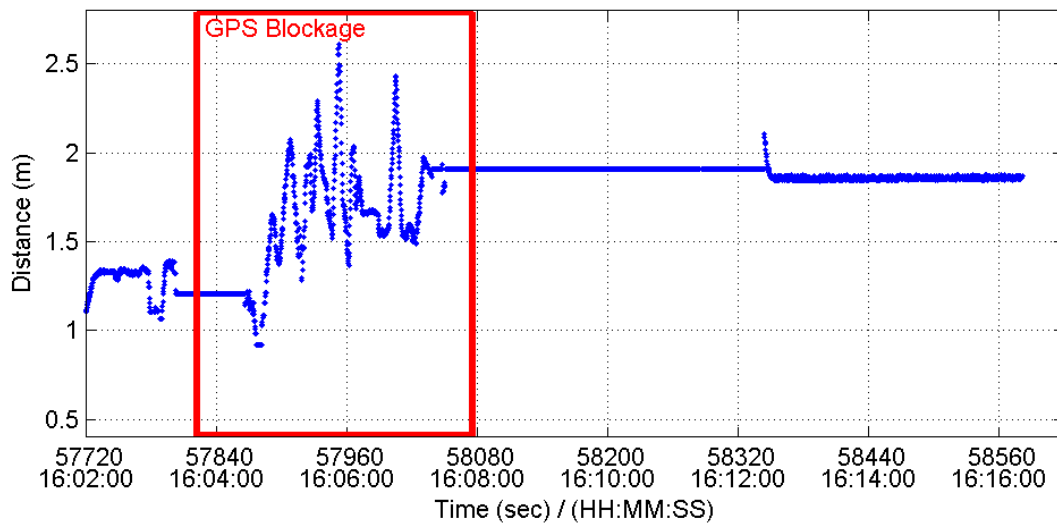
Figure 4.69: Laser-Measured Distance during GPS Blockage Real-Time Test

When GPS was combined with the camera, a combination of the best of both worlds resulted. Before the GPS blockage, the high quality GPS was used. During the GPS blockage, the camera was used. After the GPS blockage, the camera was used for quite some time, until the GPS was able to fix ambiguities once more. Unfortunately, the GPS took longer to fix ambiguities when combined with the camera compared to when it was used alone. As mentioned in the previous test, the camera's calibration may not have been optimal, and therefore it may not have helped the GPS in this case.
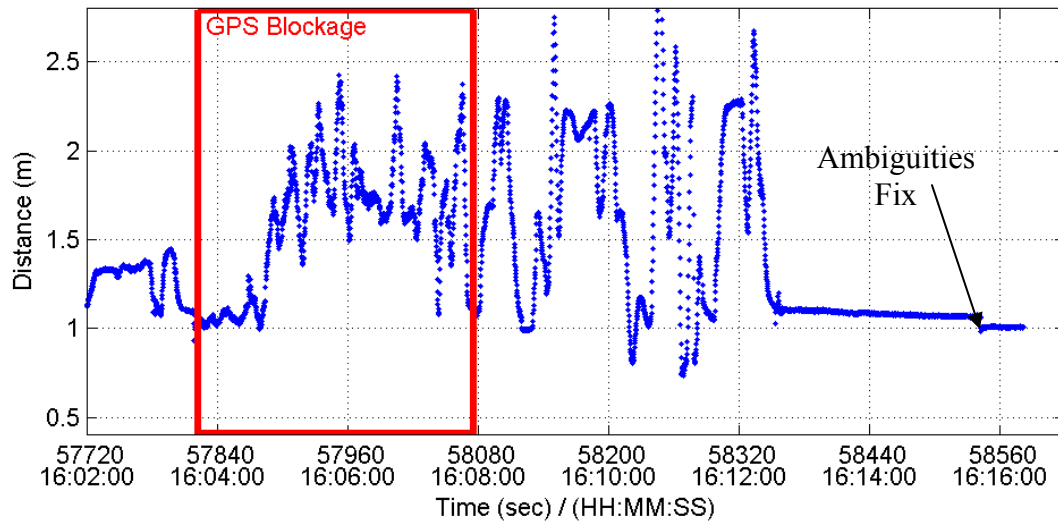
Figure 4.70: GPS+Camera-Measured Distance during GPS Blockage Real-Time Test

When GPS is combined with the laser, the GPS is used prior to the blockage. At the beginning of the blockage, the laser was not tracking the leader, and therefore no output was available. However, tracking was reacquired and the robot could navigate during the data outage. Tracking was once again lost near the end of the GPS blockage, and therefore once GPS was reacquired, it was used in float mode alone to navigate. No angle would have been available during this time. Ambiguities were able to fix, but the laser started tracking an incorrect target and as a result the ambiguities actually fixed to the wrong values. This incorrect ambiguity set was not identified prior to the end of the test.
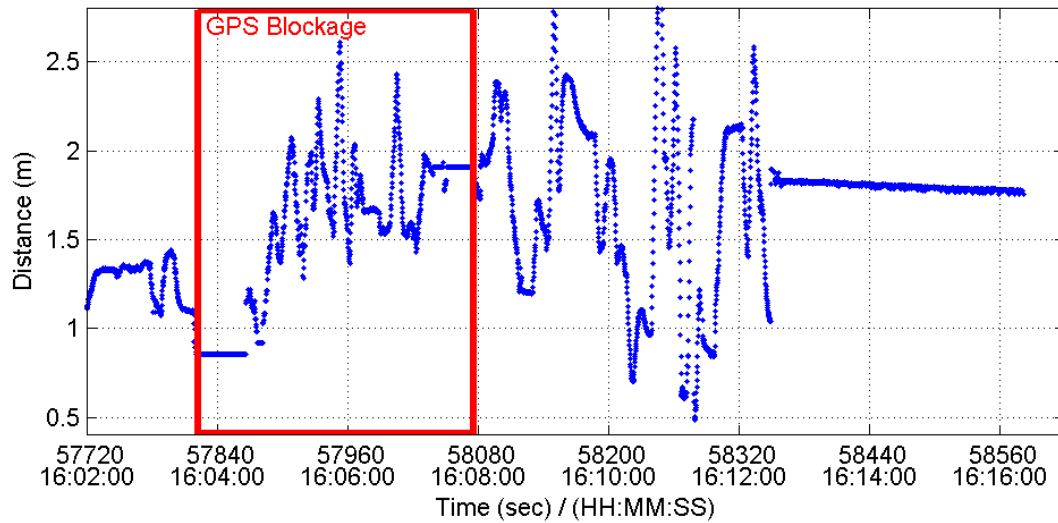
Figure 4.71: GPS+Laser-Measured Distance during GPS Blockage Real-Time Test

When all sensors were combined, whatever sensors were available contributed to the output. At the beginning, GPS was used. When GPS became blocked and the laser lost tracking, the camera still gave useful output. Once the laser reacquired its target, its accurate measurements were used. When the laser lost tracking again, the output returned to the camera values. GPS became available once more, and the camera combined with float-ambiguity GPS produced the output, until the ambiguities fixed. Ambiguities did not fix to the incorrect values in this case when the laser started tracking the wrong target, because of the continued influence of the camera.
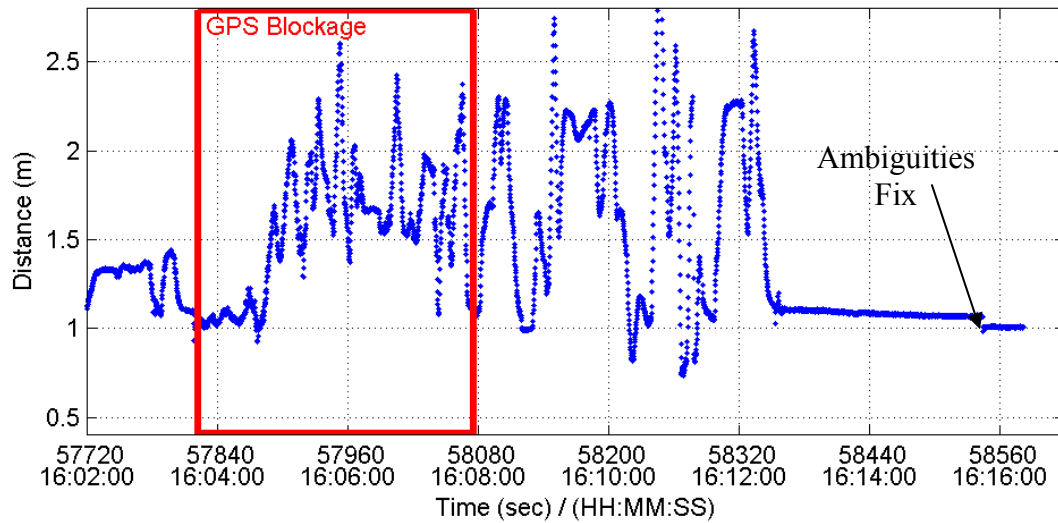
Figure 4.72:   GPS+Camera+Laser-Measured Distance during GPS Blockage Real-Time Test

When pitch constraints were used, the same effects as previously seen took place. In the GPS-only case, ambiguities resolved somewhat sooner, both at the beginning of the test, and after the GPS data outage. When GPS and camera were combined, again the ambiguities were able to resolve faster. In this case, the camera augmentation was better than the GPS alone, which was not the case in this experiment without the pitch constraint. When the GPS and laser were combined, again the ambiguities resolved faster. And as with the case where no pitch constraint was used, the laser tracked an incorrect target and caused the ambiguities to be fixed to incorrect values.

5 Conclusions

The first goal of this research was to demonstrate the ability of GPS to serve as a CDS sensor. GPS was mounted on several vehicles which then performed manoeuvres on a highway. Post-processing demonstrated that indeed GPS is a useful sensor for collaborative driving systems. A moving base station technique with carrier phase processing was developed and demonstrated to be functional.

The second goal was to test the use of GPS with other sensors on a low cost platform. GPS and a laser scanner were added to mobile robots which already used a digital camera to navigate. Each sensor has some advantages and disadvantages. A program was developed to process the sensor data alone and in combinations, leading to the successful use of GPS, a laser scanner, and a camera for autonomous navigation on a low cost test bed.

5.1 GPS as a CDS Sensor

The evaluation of GPS as a sensor for a CDS yielded the following results.

1. A moving base station technique, that is, differential GPS processing between two moving antennas, was clearly possible. This eliminates the need for static GPS reference stations nearby, thus reducing infrastructure costs. The moving base station technique appeared to provide slightly, but not significantly, lower accuracy than the static base station approach.

2. GPS can provide centimetre-level positioning and centimetre-per-second-level velocity accuracy. This was demonstrated by examining the inter-antenna position and velocity differences between two antennas on the same vehicle. The inter-antenna distance was nearly constant throughout the tests, while the inter-antenna

velocity was near zero during times that the vehicle was not changing orientation. A two antenna system can accurately give headings of vehicles. This can be quite useful for a CDS, as it relates information on upcoming features of the road, and can explicitly demonstrate manoeuvres such as changing lanes.

3. Processing can be performed from one vehicle to any other vehicle in the platoon, providing that the GPS data from that vehicle is available. This allows vehicles to position themselves with respect to other vehicles in the platoon. Vehicles may also observe the relative velocity along-track and across-track. Combined, these give the vehicles a great deal of useful information about the other vehicles in the platoon. GPS continues to provide high accuracy over all distances that would reasonably be expected to occur in a platoon.

4. GPS may not be used for navigation in some areas where frequent signal blockage occurs. However, most highways where a CDS would primarily be used have a sufficiently open sky. Exceptions to this include mountainous areas and tunnels, in which GPS would require assistance from the driver or from another sensor. A technology known as High Sensitivity GPS allows GPS acquisition in signal blockage conditions, however the accuracy is sufficiently poor that it would not be directly useful for relative positioning of vehicles for navigation.

5.2   Combination of GPS with other Sensors on a Low Cost Test Bed

The second part of this thesis showed the successful use of GPS, a camera, and a laser scanner for autonomous navigation on a low cost test bed. These sensors were used alone and in combination. Each sensor has some advantages and disadvantages. The conclusions reached are as follows.

1. GPS provides accurate distance measurements, but some initialisation time is required to reach fixed-ambiguity mode. Also, fixed ambiguities can be lost when the satellite signal is blocked. GPS as used in this set up was not able to continuously or accurately provide local angle from the follower to the lead robot. This is because a single antenna GPS system can not provide the heading of the robot while the robot is stationary, and can only provide heading with low accuracy when the robot is moving.

2. The camera was able to give immediate and continuous angle and distance results with little processing. However, the distance measurements have a much lower accuracy compared to GPS. It is difficult to evaluate the accuracy of the angular measurements.

3. The laser was also able to give immediate results, with much higher accuracy than the camera. Laser observations are not always present due to the difficulty present in identifying the lead robot in the laser profile. It is difficult to evaluate the accuracy of the angular measurements.

4. The camera and the laser both require a well defined object on the lead robot that must be in view at all times. The laser is especially sensitive to the shape of this object. This is not very practical for real applications.

5. By combining the GPS with the camera or laser, continuous distance and angle measurements are available. The GPS ambiguity resolution time is decreased, allowing the use of the high accuracy GPS distance measurements. When the GPS signal is blocked, the vehicle may continue to navigate, though with slightly lower accuracy, using the other sensors alone. When camera or laser observations are blocked, GPS continues to provide accurate distance measurements, but angular measurements are unavailable.

6. A pitch constraint helps to stabilize the distance-azimuth-pitch formulation, allowing parameters to converge faster, leading to quicker ambiguity fixes. The pitch constraint is more useful in kinematic data than static data, as the motion can cause the parameters to vary more wildly. The pitch constraint helps the cases where GPS is augmented by another sensor more than when there is no augmentation.

7. Robots must be able to continuously transmit important data to each other in a timely manner. Otherwise, a sensor may begin to lag behind the others and create errors.

8. Reliability is improved by the use of additional sensors. Most notable, the minimum detectible blunder and the protection level are greatly improved at the beginning of the test or after any GPS data outage.

5.3 Recommendations

A few recommendations can be made for various reasons. Some modifications could be done to improve performance of sensors. Others could simply extend the testing scope of the system.

1. The change in the shape of the rear of the lead robot for the real-time tests provided a significant improvement in the ability of the laser to track the leader. It may be possible to further alter the shape of the rear of the leader to make the process even better. This would most likely take the form of an even pointier shape to be identified. This would create a more precise point on the leader to be located.

2. Using two antennas on each vehicle, as shown in the first part of this thesis, provides continuous heading observations. These are very useful for a CDS. They

can be used to allow GPS to provide relative angle measurements from the follower to lead robot without having to rely upon the assisting sensors. Also, having heading information available allows for the use of a superior transform in order to align the observations from sensors that are not collocated. Thirdly, having multiple GPS antennas creates the possibility of adding constraints (Harvey 1998) in order to resolve the differenced ambiguities faster and with higher reliability.

3. In these tests, only one leader and one follower were used. It would be useful to attempt to use more robots. In this case, middle robots would act both as follower and leader. There would be a higher computational load, as well as more data being sent over the network, but improvements may be seen in ambiguity resolution by using multiple antennas (Luo 2001).

4. A common timing system should be created for all sensors. As it was, GPS data was being precisely obtained on specific intervals of GPS time. However, other sensors were being polled by the main loop of the program on a less precise time basis. Since the GPS data came as a stream, the most recent data in the stream had to be identified. If the other sensors could be polled at certain GPS times, this would make sure all data was processed appropriately, rather than having some variable lags.

6 References

ActiveMedia Robotics LLC. (2003) "Pioneer 2 All-Terrain Robot" http://www.activrobots.com/ROBOTS/p2at.html, Accessed Nov 27, 2003

Auto21 (2003) "Collaborative Driving: Take Both Hands off the Wheel" *Auto Innovation Winter 2003*, Vol 1:1, http://www.auto21.ca/news/Auto_Innovation_winter_02E.pdf

Bajikar, S., A. Gorjestani, P. Simpkins, and M. Donath (1997) "Evaluation of In-Vehicle GPS-Based Lane Position Sensing for Preventing Road Departure" *IEEE conference on Intelligent Transportation Systems*, 9-12 November, pp. 397-402

Bétaille, D. and P. Bonnifait (2002) "Vehicles Modeling and Multi-Sensor Smoothing Techniques for Post-Processed Vehicles Localisation" *Proceedings of the ION GPS-2002*, Portland, OR, 24-27 September, pp. 2412-2422

Boggs, M. (2001) "Global Positioning System Advanced Targeting System" *Proceedings of the ION NTM-2001*, Long Beach, CA, 22-24 January, pp. 426-431

Brown, R. G. and P. Y. C. Hwang (1992) *Introduction to Random Signals and Applied Kalman Filtering*, John Wiley and Sons, Inc., New York

Bruce, J., T. Balch, and M. Veloso (2000) "Fast and Inexpensive Color Image Segmentation for Interactive Robots" *Proceedings of the 2000 IEEE/RSJ International Conference on Intelligent Robots and Systems*, Tagamatsu, Japan, 31 October – 5 November, pp. 2061-2066

Buchberger, M., K.-W. Jörg, and E. Puttkamer (1993) "Laserradar and Sonar Based World Modeling and Motion Control for Fast Obstacle Avoidance of the Autonomous Mobile Robot MOBOT-IV" *IEEE International Conference on Robotics and Automation 1993*, Atlanta, GA, 2-6 May, pp. 534-540

Cannon, M. E. (2001) "Engo 561 Satellite Positioning Winter 2002 Vu-Graphs" ENGO 561 Course Lecture Notes, Department of Geomatics Engineering, University of Calgary

Cannon, M. E., S. Skone, Y. Gao, Y. Moon, K. Chen, S. Crawford, and G. Lachapelle (2002) "Performance Evaluation of Several Wide-Area GPS Services" *Proceedings of the ION GPS-2002*, Portland, OR, 24-27 September, pp. 1716-1726

Cannon, M. E., C. Basnayake, S. Crawford, S. Syed, and G. Lachapelle (2003) "Precise GPS Sensor Subsystem for Vehicle Platoon Control" *Proceedings of ION GPS/GNSS-2003*, 9-12 September, Portland, OR, pp. 213-224

Carlson, N. A. and M. P. Beraducci (1993) "Federated Kalman Filter Simulation Results" *Proceedings of the ION AM-1993*, Cambridge, MA, 21-23 June, pp. 421-435

CyberOptics Corp. (2002) "Imagenation PXC analog, color and monochrome frame grabbers" http://www.imagenation.com/pdf/pxc200.pdf, Accessed Nov 27, 2003

Da, R. (1997) "Investigation of a Low-Cost and High-Accuracy GPS/IMU System" *Proceedings of the ION NTM-1997*, 14-16 January, Alexandria, VA, pp. 955-963

de Jonge, P. J., and C. C. J. M. Tiberius (1996) "The LAMBDA method for integer ambiguity estimation: implementation aspects" *Delft Geodetic Computing Centre LGR series*, No. 12.

El-Sheimy, N. (1996) "The Development of VISAT – A Mobile Survey System for GIS Applicaitons" PhD Thesis, UCGE Reports Number 20101, Department of Geomatics Engineering, University of Calgary

El-Sheimy, N., C. Ellum, and A. Tabsh (2001) "A Low-Cost Portable Mobile Mapping (PMM) System Integrating GPS, Attitude Sensors, and a Digital Camera" *Proceedings of the ION GPS-2001*, Salt Lake City, UT, 11-14 September, pp. 464-472

Farrel, J. and M. Barth (2001) "Integration of GPS/INS and Magnetic Markers for Advanced Vehicle Control" *California PATH Research Report UCB-ITS-PRR-2001-38*, University of California, Riverside, CA

Frankel, J., L. Alvarez., R. Horowitz, and P. Li (1994) "Robust Platoon Maneuvers for AVHS" *Technical Report 94-9*, California Partners for Advance Transit and Highways (PATH), Institute of Transportation Studies, University of California, Berkeley, CA, November

Gao, Y. and X. Shen (2001) "Improving Ambiguity Convergence in Carrier Phase-Based Precise Point Positioning" *Proceedings of the ION GPS-2001*, Salt Lake City, UT, 11-14 September, pp. 1532-1539

Gelb, A. (1974) *Applied Optimal Estimation*, The Massachusetts Institute of Technology Press, Cambridge, MA

Goad, C. C. and L. Goodman (1974) "A Modified Hopfield Tropospheric Refraction Correction Model" *American Geophysical Union Fall Annual Meeting*, San Francisco, CA

Grejner-Brzezinska, D., C. Toth, and Q. Xiao (2000) "Real-time Tracking of Highway Linear Features" *Proceedings of the ION GPS-2000*, 18-22 September, Salt Lake City, UT, pp. 1721-1728

Hallé, S., B. Chaib-draa, and J. Laumonier (2003) "Car Platoons Simulated as a Multiagent System" *Agent Based Simulation 4*, Montpellier, France, March, pp. 57-63.

Hanks, P. ed (1985) *Collins Dictionary of the English Language*, William Collins Sons & Co. Ltd., Glasgow, United Kingdom. p. 438

Harvey, R. (1998) "Development of a Precision Pointing System Using an Integrated Multi-Sensor Approach" MSc Thesis, UCGE Reports Number 20117, Department of Geomatics Engineering, University of Calgary

Harvey, R. and M. E. Cannon (1997) "Operational Results of a Closely Coupled Integrated Vehicle Heading System" *Proceedings of the ION GPS-97*, Kansas City, MO, 16-19 September, pp. 279-288

Hofmann-Wellenhof, B., H. Lichtennegger, and J. Collins (2001) *GPS Theory and Practice*, Springer-Verlag/Wein, New York

Honma, S. and N. Uehara (2001) "Millimeter-Wave Radar Technology for Automotive Application" Technical Reports, Mitsubishi Electric, June 2001 http://global.mitsubishielectric.com/pdf/advance/vol94/vol94_tr5.pdf

Hoyle, V. A., S. H. Skone, and N. A. Nicholson (2004) "4-D Tropospheric Tomography using a Ground-Based Regional GPS Network and Vertical Profile Constraints" *Proceedings of the ION GNSS-2004*, Long Beach, CA, 21-24 September, pp. 892-901

International GPS Service (IGS) (2004) "IGS Product Table" http://igscb.jpl.nasa.gov/components/prods.html, accessed Dec. 5, 2004

Kaplan, E. ed (1996) *Understanding GPS: Principles and Applications*, Artech House Inc., Norwood MA

Kato, S., S. Tsugawa, K. Tokuda, T. Matsui, and H. Fujii (2002) "Vehicle Control Algorithms for Cooperative Driving With Automated Vehicles and Inter-vehicle Communication" *IEEE Transactions on Intelligent Transportation Systems*, Vol. 3, No. 3, September

Klobuchar, J. A. (1987) "Ionospheric Time-Delay Algorithm for Single Frequency GPS Users" *IEEE Transactions on Aerospace and Electronic Systems*, Vol. AES-23, No.3, pp. 325-331

Lachapelle, G., M. E. Cannon, G. Lu, and B. Loncarevic (1996) "Shipborne GPS Attitude Determination During MMST-93" *IEEE Journal of Oceanic Engineering*, Vol. 21, No. 1, pp. 100-105

Lachapelle, G. and M. E. Cannon (2002) *HEADRT+^{TM} Version 2.0 Operator's Manual*, Department of Geomatics Engineering, University of Calgary

Lemay, M., F. Michaud, and J.-M. Valin (2004) "Autonomous Initialization of Robot Formations" *IEEE International Conference on Robotics and Automation*, pp. 3018-3023

Lim, H.-M.., B. Newstrom, C. Shankwitz, and M. Donath (1999) "A Heads Up Display based on a DGPS and Real Time Accessible Geo-Spatial Database for Low Visibility Driving" *Proceedings of the ION GPS-99*, Nashville, TN, 14-17 September, pp. 469-477

Liu, J. (2003a) "Implementation and Analysis of GPS Ambiguity Resolution Strategies in Single and Multiple Reference Station Scenarios" MSc Thesis, UCGE Reports Number 20168, Department of Geomatics Engineering, University of Calgary

Liu, J. (2003b) *Flykin+^{TM} Version 1.0 Operating Manual*, Positioning, Location, and Navigation Group, Department of Geomatics Engineering, University of Calgary

Luo, N. (2001) "Precise Relative Positioning of Multiple Moving Platforms using GPS Carrier Phase Observables" PhD Thesis, UCGE Reports Number 20147, Department of Geomatics Engineering, University of Calgary

Michaud, F., D. Létourneau, M. Guilbert, and J.-M. Valin (2002) "Dynamic Robot Formations Using Directional Visual Perception" *Proceedings of the 2002 IEEE/RSJ International Conference on Intelligent Robots and Systems*, Lausanne, Switzerland, 20 September – 5 October, Vol 3, pp. 2740-2745

Nayak, R. A. (2000) "Reliable and Continuous Urban Navigation Using Multiple GPS Antennas and a Low Cost IMU" MSc Thesis, UCGE Reports Number 20144, Department of Geomatics Engineering, University of Calgary

NovAtel Inc. (2003a) "DL-4 Data Logger" http://www.novatel.ca/Documents/Papers/DL-4_Brochure.pdf, accessed Nov 27, 2003

NovAtel Inc. (2003b) "GPS 700" http://www.novatel.ca/Documents/Papers/GPS700.pdf, accessed Nov 27, 2003

Olynik, M. (2002) "Temporal Characteristics of GPS Error Sources and Their Impact on Relative Positioning" MSc Thesis, UCGE Reports Number 20162, Department of Geomatics Engineering, University of Calgary

Parkinson, B. and P. Enge (1995) "Differential GPS" in *Global Positioning System: Theory and Applications Volume II*, ed. B. Parkinson and J. Spilker Jr., American Institute of Aeronautics and Astronautics Inc., Washington DC

Petovello, M. (2003) "Real-Time Integration of a Tactical Grade IMU and GPS for High Accuracy Positioning and Navigation" PhD Thesis, UCGE Reports Number 20173, Department of Geomatics Engineering, University of Calgary

Ray, J. (2000) "Mitigation of GPS Code and Carrier Phase Multipath Effects Using a Multi-Antenna System" PhD Thesis, UCGE Reports Number 20136, Department of Geomatics Engineering, University of Calgary

Roberts, B. and L. Vallot (1990) "Vision Aided Inertial Navigation" *Position Location and Navigation Symposium 1990*, Las Vegas, NV, 20-23 March 1990, pp. 347-352

Saastamoinen, J. (1973) "Contribution to the Theory of Atmospheric Refraction" *Bulletin Geodesique*, 107, pp. 13-34.

Salychev, O. S., V. V. Vornov, M. E. Cannon, R. Nayak and G. Lachapelle (2000) "Low Cost INS/GPS Integration: Concepts and Testing" *Proceedings of the ION NTM-2000*, Anaheim CA, 26-28 January, pp. 98-105

Schwarz, K. P. (1999) "Fundamentals of Geodesy" ENGO 421 Course Lecture Notes, Department of Geomatics Engineering, University of Calgary

SICK Inc. (2003) "Sick Product Information – LMS 200-30106 (1015850)" http://www.sickusa.com/live/master/datasheet.asp?PN=1015850&FAM=Measurement, accessed Nov 27, 2003

Smart, R. G., M. E. Cannon, A. Howard, and R. E. Mann (2004) "Can We Design Cars to Prevent Road Rage?" Accepted to the *International Journal of Vehicle Information and Communication Systems*, (in press)

Sony Electronics Inc. (2002) "Sony Business Solutions and Systems" http://bssc.sel.sony.com/Professional/webapp/ModelInfo?id=22716, accessed Nov 27, 2003

Stephen, J. (2000) "Development of a Multi-Sensor GNSS Based Vehicle Navigation System" MSc Thesis, UCGE Reports Number 20140, Department of Geomatics Engineering, University of Calgary

Stephen, J. and G. Lachapelle (2000) "Development of a GNSS-Based Multi-Sensor Vehicle Navigation System" *Proceedings of the ION NTM-2000*, Anaheim, CA, 26-28 January, pp. 268-278

University Technologies International (UTI Inc.) (2002) "NDLTM: Navigation Development Library^{TM}" http://www.uti.ca/ndl.pdf, accessed Sept 9, 2004

U. S. Department of Transportation (US DoT) (2002) "Traffic Flow Theory: A State of the Art Report" Turner-Fairbank Highway Research Center, pp. 3.1-3.28 and 4.1-4.39

Vexilar Inc. (2003) "Vexilar – How SONAR works" http://www.vexilar.com/help/tips/tip011.html, accessed Jan 4, 2005.

Wang, C. (2003) "Development of a Low-Cost GPS-Based Attitude Determination System" M.Sc. thesis, UCGE Report No. 20175, Department of Geomatics Engineering, University of Calgary

Wei, M. and K. P. Schwarz (1990) "Testing a Decentralized Filter for GPS/INS Integration" *Proceedings of the IEEE Position, Location, and Navigation Symposium 1990*, Las Vegas, NV, March, pp. 429-435

Wu, Chin-Sheng (1996) "Navigation and Obstacle Avoidance of the Camera Guided Patrolling Vehicle" *30th Annual International Carnahan Conference on Security Technology*, 2-4 October, pp. 30-32

Appendix A: Matrices for the Robot Test Main Kalman Filter

Here, the matrix forms for important components of the main Kalman filter are discussed, as mentioned in section 4.3.

A.1 State Vector

The state vector is given as:

$$X = \begin{bmatrix} \text{Distance} \\ \text{Azimuth} \\ \text{Pitch} \\ \text{Angle} \\ \text{Double Differenced Ambiguity}_i \end{bmatrix} = \begin{bmatrix} d \\ a \\ p \\ a_{total} \\ \Delta\nabla N_i \end{bmatrix}. \tag{A.1}$$

A.2 Transition Matrix

All parameters are unrelated to other parameters from one epoch to the next. Therefore, the transition matrix is identity.

$$\Phi = \begin{bmatrix} 1 & 0 & 0 & 0 & 0 \\ 0 & 1 & 0 & 0 & 0 \\ 0 & 0 & 1 & 0 & 0 \\ 0 & 0 & 0 & 1 & 0 \\ 0 & 0 & 0 & 0 & 1 \end{bmatrix} \tag{A.2}$$

A.3 Design Matrices

A.3.1 Camera Observations

For the set of camera observations,

$$\ell_{camera} = \begin{bmatrix} \text{Camera Distance} \\ \text{Camera Angle} \end{bmatrix} = \begin{bmatrix} d_{camera} \\ a_{camera} \end{bmatrix} \tag{A.3}$$

the corresponding design matrix is simply:

$$H_{camera} = \begin{bmatrix} 1 & 0 & 0 & 0 & 0 \\ 0 & 0 & 0 & 1 & 0 \end{bmatrix} \tag{A.4}$$

A.3.2 Laser Observations

For the set of laser observations,

$$\ell_{laser} = \begin{bmatrix} \text{Laser Distance} \\ \text{Laser Angle} \end{bmatrix} = \begin{bmatrix} d_{laser} \\ a_{laser} \end{bmatrix} \tag{A.5}$$

the corresponding design matrix is simply:

$$H_{Laser} = \begin{bmatrix} 1 & 0 & 0 & 0 & 0 \\ 0 & 0 & 0 & 1 & 0 \end{bmatrix} \tag{A.6}$$

A.3.3 Double Differenced PseudoRange Observations

For the double differenced pseudorange observations, the equations are slightly more complicated. Recall from section 4.3:

$$\nabla \Delta P = -(\bar{u}^i - \bar{u}^j) \bullet (T\vec{b}_{12}) + \nabla \Delta \varepsilon_P \tag{A.7}$$

with

$$T = \begin{bmatrix} -\sin(\phi)\cos(\lambda) & -\sin(\lambda) & \cos(\phi)\cos(\lambda) \\ -\sin(\phi)\sin(\lambda) & \cos(\lambda) & \cos(\phi)\sin(\lambda) \\ \cos(\phi) & 0 & \sin(\phi) \end{bmatrix} \tag{A.8}$$

being constant, and

$$\bar{b}_{12} = \begin{bmatrix} d\cos(a)\cos(p) \\ d\sin(a)\cos(p) \\ d\sin(p) \end{bmatrix} \tag{A.9}$$

Therefore,

$$\frac{\partial \nabla \Delta P}{\partial d} = -(\bar{u}^i - \bar{u}^j) \bullet (T \begin{bmatrix} \cos(a)\cos(p) \\ \sin(a)\cos(p) \\ \sin(p) \end{bmatrix}) \tag{A.10}$$

$$\frac{\partial \nabla \Delta P}{\partial a} = -(\bar{u}^i - \bar{u}^j) \bullet (T \begin{bmatrix} -d\sin(a)\cos(p) \\ d\cos(a)\cos(p) \\ 0 \end{bmatrix}) \tag{A.11}$$

$$\frac{\partial \nabla \Delta P}{\partial a} = -(\bar{u}^i - \bar{u}^j) \bullet (T \begin{bmatrix} -d\cos(a)\sin(p) \\ -d\sin(a)\sin(p) \\ d\cos(p) \end{bmatrix}) \tag{A.12}$$

Substituting these equations, each row of the design matrix for pseudorange observations is:

$$H_{\Delta \nabla P} = \begin{bmatrix} (A.10) & (A.11) & (A.12) & 0 & 0 \end{bmatrix} \tag{A.13}$$

A.3.4 Double Differenced Carrier Phase Observations

For double differenced carrier phase observations, recall from section 4.3:

$$\nabla\Delta\Phi = (-(\bar{u}^i - \bar{u}^j) \bullet (T\vec{b}_{12})) + \lambda\nabla\Delta N + \nabla\Delta\varepsilon_\Phi \tag{A.14}$$

with

$$T = \begin{bmatrix} -\sin(\phi)\cos(\lambda) & -\sin(\lambda) & \cos(\phi)\cos(\lambda) \\ -\sin(\phi)\sin(\lambda) & \cos(\lambda) & \cos(\phi)\sin(\lambda) \\ \cos(\phi) & 0 & \sin(\phi) \end{bmatrix} \tag{A.15}$$

being constant, and

$$\vec{b}_{12} = \begin{bmatrix} d\cos(a)\cos(p) \\ d\sin(a)\cos(p) \\ d\sin(p) \end{bmatrix} \tag{A.16}$$

Therefore

$$\frac{\partial\nabla\Delta\Phi}{\partial d} = -(\bar{u}^i - \bar{u}^j) \bullet (T \begin{bmatrix} \cos(a)\cos(p) \\ \sin(a)\cos(p) \\ \sin(p) \end{bmatrix}) \tag{A.17}$$

$$\frac{\partial\nabla\Delta\Phi}{\partial a} = -(\bar{u}^i - \bar{u}^j) \bullet (T \begin{bmatrix} -d\sin(a)\cos(p) \\ d\cos(a)\cos(p) \\ 0 \end{bmatrix}) \tag{A.18}$$

$$\frac{\partial\nabla\Delta\Phi}{\partial p} = -(\bar{u}^i - \bar{u}^j) \bullet (T \begin{bmatrix} -d\cos(a)\sin(p) \\ -d\sin(a)\sin(p) \\ d\cos(p) \end{bmatrix}) \tag{A.19}$$

The derivative of the ith observation with respect to the ith double differenced ambiguity is the wavelength, λ. The derivative with respect to all other double differenced ambiguities is zero.

Substituting these equations, each row of the design matrix for double differenced carrier phase observations is:

$$H_{\Delta\nabla\Phi} = \begin{bmatrix} (A.17) & (A.18) & (A.19) & 0 & \lambda \end{bmatrix} \tag{A.20}$$

A.3.5 Pitch Constraint

A pitch constraint pseudo-observation directly observes the pitch parameter. Therefore, the design matrix for this observation is simply:

$$H_{Pitch} = \begin{bmatrix} 0 & 0 & 1 & 0 & 0 \end{bmatrix} \tag{A.21}$$

Appendix B: Matrices for the Robot Test Secondary Kalman Filter

Here, the matrix forms for important components of the secondary Kalman filter are discussed, as mentioned in section 4.3.

B.1 State Vector

The state vector is given as:

$$X = \begin{bmatrix} \text{latitude} \\ \text{longitude} \\ \text{height} \\ \text{clock offset} \\ \text{north velocity} \\ \text{east velocity} \\ \text{up velocity} \\ \text{clock drift} \end{bmatrix} = \begin{bmatrix} \phi \\ \lambda \\ h \\ dt \\ v_N \\ v_E \\ v_U \\ dt \end{bmatrix} \tag{B.1}$$

B.2 Transition Matrix

Latitude, longitude, and height depend on their own previous values as well as those of the velocity. The velocity parameters simply depend on their own previous values.

A general math principle shows that a circular arc length is equal to the radius of curvature multiplied by the angle swept out in radians.

$$\Delta\phi(\text{m}) = R_\phi \Delta\phi(\text{rad})$$
$$\Delta\lambda(\text{m}) = R_\lambda \Delta\lambda(\text{rad}) \tag{B.2}$$

Since

$$\Delta\phi(m) = v_N \Delta t$$
$$\Delta\lambda(m) = v_E \Delta t$$

(B.3)

therefore

$$v_N \Delta t = R_\varphi (\phi_2 - \phi_1)$$
$$v_E \Delta t = R_\lambda (\lambda_2 - \lambda_1)$$

(B.4)

$$\phi_2 = \phi_1 + v_N \Delta t / R_\phi$$
$$\lambda_2 = \lambda_1 + v_E \Delta t / R_\lambda$$

(B.5)

The radii of curvature for latitude and longitude are as follows (Schwarz 1999):

$$R_\phi = M + h$$
$$R_\lambda = (N + h) * \cos(\phi)$$

(B.6)

where

$$M = \frac{(1 - e^2)a}{(1 - e^2 \sin^2 \phi)^{3/2}}$$

$$N = \frac{a}{(1 - e^2 \sin^2 \phi)^{1/2}}$$

(B.7)

Height and clock offset are linearly related to upwards velocity and clock drift, respectively, by a factor of time. Using this information, and Equation B.5, the transition matrix is as follows:

$$\Phi = \begin{bmatrix} 1 & 0 & 0 & 0 & \dfrac{\Delta t}{R_\phi} & 0 & 0 & 0 \\ 0 & 1 & 0 & 0 & 0 & \dfrac{\Delta t}{R_\lambda} & 0 & 0 \\ 0 & 0 & 1 & 0 & 0 & 0 & \Delta t & 0 \\ 0 & 0 & 0 & 1 & 0 & 0 & 0 & \Delta t \\ 0 & 0 & 0 & 0 & 1 & 0 & 0 & 0 \\ 0 & 0 & 0 & 0 & 0 & 1 & 0 & 0 \\ 0 & 0 & 0 & 0 & 0 & 0 & 1 & 0 \\ 0 & 0 & 0 & 0 & 0 & 0 & 0 & 1 \end{bmatrix} \tag{B.8}$$

B.3 Design Matrices

B.3.1 Undifferenced Pseudorange Observations

Recall the pseudorange observation equation from section 2.1.1:

$$P = \rho + d\rho + c(dt - dT) + d_{trop} + d_{iono} + \epsilon_P \tag{B.9}$$

All parts of this equation are modelled out except for the geometric range, which is a function of the receiver position and satellite position, and the receiver clock offset. The geometric range can be written as follows:

$$\rho = \sqrt{(x - x^s)^2 + (y - y^s)^2 + (z - z^s)^2} \tag{B.10}$$

Partial derivatives of the pseudorange with respect to latitude, longitude, and height, are more clearly written using the product rule, as partial derivatives with respect to receiver x, y, and z coordinates multiplied with the partial derivatives of those coordinates with the latitude longitude, and height. The resulting equations are as follows:

$$\frac{\partial P}{\partial \phi} = \frac{\partial P}{\partial x} * \frac{\partial x}{\partial \phi} + \frac{\partial P}{\partial y} * \frac{\partial y}{\partial \phi} + \frac{\partial P}{\partial z} * \frac{\partial z}{\partial \phi}$$

$$= \frac{x - x^s}{\rho} * (-(M + h)\sin\phi\cos\lambda)$$

$$+ \frac{y - y^s}{\rho} * (-(M + h)\sin\phi\sin\lambda) \qquad (B.11)$$

$$+ \frac{z - z^s}{\rho} * ((M + h)\cos\phi)$$

$$\frac{\partial P}{\partial \lambda} = \frac{\partial P}{\partial x} * \frac{\partial x}{\partial \lambda} + \frac{\partial P}{\partial y} * \frac{\partial y}{\partial \lambda} + \frac{\partial P}{\partial z} * \frac{\partial z}{\partial \lambda}$$

$$= \frac{x - x^s}{\rho} * (-(N + h)\cos\phi\sin\lambda) \qquad (B.12)$$

$$+ \frac{y - y^s}{\rho} * ((N + h)\cos\phi\cos\lambda)$$

$$\frac{\partial P}{\partial h} = \frac{\partial P}{\partial x} * \frac{\partial x}{\partial h} + \frac{\partial P}{\partial y} * \frac{\partial y}{\partial h} + \frac{\partial P}{\partial z} * \frac{\partial z}{\partial h}$$

$$= \frac{x - x^s}{\rho} * (\cos\phi\cos\lambda)$$

$$+ \frac{y - y^s}{\rho} * (\cos\phi\sin\lambda) \qquad (B.13)$$

$$+ \frac{z - z^s}{\rho} * (\sin\phi)$$

$$\frac{\partial P}{\partial dT} = -c \qquad (B.14)$$

with M and N defined above in Equation B.7.

Substituting these equations, each row of the design matrix for undifferenced pseudorange observations is:

$$H_P = \begin{bmatrix} (B.11) & (B.12) & (B.13) & (B.14) & 0 & 0 & 0 & 0 \end{bmatrix} \tag{B.15}$$

B.3.2 Undifferenced Doppler Observations

Recall the Doppler observation equation from section 2.2.1:

$$\dot{\Phi} = \dot{\rho} + d\dot{\rho} + c(d\dot{t} - d\dot{T}) + \dot{d}_{trop} - \dot{d}_{iono} + \dot{\varepsilon}_{\Phi} \tag{B.16}$$

All parts of this equation are modelled out except for the rate of change of geometric range and the receiver clock drift.

Partial derivatives of the Doppler with respect to position are fairly insignificant, and position is already well observed by the code measurements. Therefore these partial derivatives will not be discussed here.

Partial derivatives of the Doppler with respect to northward, eastward, and upward velocities are more clearly written using the product rule, as partial derivatives with respect to receiver x, y, and z velocities multiplied with the partial derivatives of those velocities with respect to northward, eastward, and upward velocities. The resulting equations are as follows:

$$\begin{aligned}
\frac{\partial \dot{\Phi}}{\partial v_N} &= \frac{\partial \dot{\Phi}}{\partial v_x} * \frac{\partial v_x}{\partial v_N} + \frac{\partial \dot{\Phi}}{\partial v_y} * \frac{\partial v_y}{\partial v_N} + \frac{\partial \dot{\Phi}}{\partial v_z} * \frac{\partial v_z}{\partial v_N} \\
&= \frac{x - x^s}{\rho} * (-\sin\phi\cos\lambda) \\
&\quad + \frac{y - y^s}{\rho} * (-\sin\phi\sin\lambda) \\
&\quad + \frac{z - z^s}{\rho} * (\cos\phi)
\end{aligned} \tag{B.17}$$

$$\frac{\partial\dot{\Phi}}{\partial v_E} = \frac{\partial\dot{\Phi}}{\partial v_x}*\frac{\partial v_x}{\partial v_E} + \frac{\partial\dot{\Phi}}{\partial v_y}*\frac{\partial v_y}{\partial v_E} + \frac{\partial\dot{\Phi}}{\partial v_z}*\frac{\partial v_z}{\partial v_E}$$

$$= \frac{x-x^s}{\rho}*(-\sin\lambda) \tag{B.18}$$

$$+ \frac{y-y^s}{\rho}*(\cos\lambda)$$

$$\frac{\partial\dot{\Phi}}{\partial v_U} = \frac{\partial\dot{\Phi}}{\partial v_x}*\frac{\partial v_x}{\partial v_U} + \frac{\partial\dot{\Phi}}{\partial v_y}*\frac{\partial v_y}{\partial v_U} + \frac{\partial\dot{\Phi}}{\partial v_z}*\frac{\partial v_z}{\partial v_U}$$

$$= \frac{x-x^s}{\rho\lambda_{L1}}*(\cos\phi\cos\lambda) \tag{B.19}$$

$$+ \frac{y-y^s}{\rho}*(\cos\phi\sin\lambda)$$

$$+ \frac{z-z^s}{\rho}*(\sin\phi)$$

$$\frac{\partial\dot{\Phi}}{\partial d\dot{T}} = -c \tag{B.20}$$

Substituting these equations, each row of the design matrix for undifferenced Doppler observations is:

$$H_{\dot{\Phi}} = \begin{bmatrix} 0 & 0 & 0 & 0 & (B.17) & (B.18) & (B.19) & (B.20) \end{bmatrix} \tag{B.21}$$